HOKKAIDO UNIVERSITY

Title	Geochemical and microstructural approaches for high resolution reconstruction of paleoclimate and paleoecology using giant clam shells
Author(s)	駒越, 太郎
Degree Grantor	北海道大学
Degree Name	博士(理学)
Dissertation Number	甲第13314号
Issue Date	2018-09-25
DOI	https://doi.org/10.14943/doctoral.k13314
Doc URL	https://hdl.handle.net/2115/71908
Type	doctoral thesis
File Information	Taro_Komagoe.pdf

Hokkaido University Collection of Scholarly and Academic Papers : HUSCAP

博士学位論文

Geochemical and microstructural approaches for high resolution reconstruction of paleoclimate and paleoecology using giant clam shells
（シャコガイ殻を用いた高解像度古気候・古生態復元への地球化学および微細構造的アプローチ）

駒越　太郎

北海道大学大学院理学院

自然史科学専攻

平成 30 年 9 月

Geochemical and microstructural approaches for high resolution reconstruction of paleoclimate and paleoecology using giant clam shells

（シャコガイ殻を用いた高解像度古気候・古生態復元への地球化学および微細構造的アプローチ）

要旨

人類の観測記録以前の気候変動を知るために，海底堆積物の底生有孔虫や石筍，氷床コア，樹木年輪や古文書などが過去の気候を復元する古環境指標として用いられてきた．熱帯・亜熱帯の海洋表層の環境を復元するための古環境指標として，造礁サンゴ骨格や二枚貝の殻が強力なツールとして注目されてきた．二枚貝の殻，造礁サンゴの骨格などは炭酸カルシウムからなり，その酸素同位体比は古水温計として利用されてきた．また，微量元素濃度は古水温計や湧昇，過去の日射量の指標として用いることができる．二枚貝は炭酸カルシウムの殻の断面に成長線（年輪，日輪など）を刻みながら付加成長をするため，成長線の形成周期がわかれば成長線に沿った化学分析の結果に日付を入れられる．また，二枚貝殻に刻まれる微細構造である成長線は二枚貝の生物としての応答とともに生息環境の影響を記録している[Kennish and Olsson, 1975]．インド洋，太平洋の熱帯亜熱帯の珊瑚礁に広く分布する二枚貝シャコガイ科は，外套膜に褐虫藻が共生しているため成長が早く，殻に日輪・年輪を刻みながら数十年にわたり成長する[Watanabe *et al*., 2004]．熱帯亜熱帯域の海洋表層環境の復元に際し，シャコガイ殻の酸素・炭素同位体比そして微量元素分析から得られる古環境情報は，他の古環境間接指標と比較して，日から数十年の高い時間解像度という特徴がある．また，シャコガイ殻は始新世以降に化石として産出し[Harzhauser *et al*., 2008]，緻密な殻を持つため保存状態の良い化石が入手しやすい[Watanabe *et al*., 2004]．シャコガイ殻を用いたこれまでの古環境研究は，シャコガイ殻の化学組成と環境情報の比較したキャリブレーションが主であり，シャコガイ殻の高時間解像度を生かして具体的な気象を復元した研究は数少ない（例えば約 3 千年前の日射量を復元した Hori *et al*., 2015 など）．

本研究では，シャコガイ殻の地球化学分析および成長線解析を行い，高時間解像度でなければ復元の難しかった日から季節単位の気象現象（台風など）の復元とシャコガイ殻の成長に与える影響を検証することを目的とした．また，現生試料から得た知見を用いて，気候のバックグラウンドが異なる中新世，更新世，完新世の化石シャコガイ殻から，短期間に生じる気象現象と殻の成長に基づくシャコガイの古生態の復元に取り組んだ．

（事例 1）沖ノ鳥島産シラナミガイの地球化学分析と成長線解析から明らかになった台風の痕跡

2013 年に行われた IPCC 第 5 次評価報告書によると，将来巨大な熱帯低気圧の発生が増えることが予測されている[IPCC, 2013]．また，21 世紀末には台風の強度が増加し，今まで以上の強風が吹くことが予想されている[Tsuboki *et al*., 2015]．その結果，風害と波浪害が今まで以上に深刻化することが懸念される．長期的な台風の将来予測のためには過去の台風の履歴を復元することが必要である．過去の台風の復元研究は Paleotempestrogy と呼ばれ，これまでオーストラリアや大西洋などにおいてオーバーウォッシュ湖沼堆積物[Liu and Fearn, 1987]やビーチリッジ[Nott, 2011]から数十年から数百年単位での台風の頻度や強度が復元されている．また，中国において過去の文献記録から 11 世紀以降千年間の台風の頻度を復元している[Liu *et al*., 2001]．しかし有史以前の地質時代における台風を復元することは難しく，高時間解像度の古環境指標が求められる．そこで本研究では日本に接近する多くの台風の進路に位置する日本最南端の島，沖ノ鳥島から採取されたシャコガイ（シラナミガイ）殻の地球化学分析と成長線解析を行い台風の記録と比較した．

沖ノ鳥島に台風が接近した時，シャコガイ殻のバリウムカルシウム比（Ba/Ca）には正のピークが見られ，成長線の幅は減少し，酸素同位体比（$\delta^{18}O$）は水温の低下を示した（図 2 網掛け）．海山である沖ノ鳥島近海は台風に伴い表層水が流されることで湧昇が発生し栄養塩型の鉛直分布を持つバリウムが表層に運ばれる．台風後に生じるプランクトンブルームも関連してシャコガイ殻の Ba/Ca のピークが生じた可能性がある．これらのシャコガイ殻の地球化学的および微細構造的な痕跡は生息域への台風の接近を記録しており過去の台風記録計として期待出来る．

（事例 2）喜界島化石シャコガイから読み解く更新世-完新世の気候変遷

更新世は地球規模の寒冷化が顕著になる 258.8 万年前からヤンガードリアス期（1.29～1.17 万年前）の終わりまでとされている．氷期―間氷期の気候変動が明瞭になる時代であり，Dansgaard-Oeschger サイクルが示すように短周期で，急激な気温の上昇下降が生じており，人類の発展や現在の生態系の形成に影響を与えてきた．鹿児島県大島郡の喜界島は隆起サンゴ礁からなり，過去 12 万年の間日本最速の隆起速度をもつ[Ota & Omura, 1992].この特徴により同一地点で後期更新世から完新世の化石シャコガイ殻試料や化石サンゴ骨格試料を連続して入手可能である．特に，後期更新世の海洋同位体ステージ 3（MIS 3）は現在よりも 30 ｍ以上海水準が低く[Sasaki *et al*., 2004]，当時のサンゴ礁を観察できるのは，隆起速度の速いパプアニューギニアのヒュオン半島や喜界島に限られている．喜界島は北西太平洋と東シナ海に面しており台風やモンスーン気候などに大きな影響を受けている.喜界島は更新世から完新世における東アジアの海洋環境および気候変動の解明を目指す海洋地質学的研究において重要な位置にある．本研究では喜界島において後期更新世および完新世の化石シャコガイ殻を採取し高時間解像度での気象現象の復元を行った．

各化石シャコガイ殻試料は SEM および X 線回折で続成を評価し保存状態が良いことが判明した．完新世の化石試料の年代は暦年校正で，3924±49 年前および 7220±45 年前であった．また，後期更新世の化石試料の年代は，5 万 5 千年前(55 ka)と判明した．55ka の化石試料の酸素同位体比から復元した海水温は現在の喜界島周辺の海水温より平均で 4 ℃低いことがわかった．55ka の化石試料の成長線はよく保存されており，成長線幅は酸素同位体比と逆相関し化石試料の成長は水温に依存している．この化石試料の成長傾向は現生試料と類似していた．また，夏季に台風が喜界島に接近した時，現生試料の成長線幅は急激に減少した．そこで沖ノ鳥島での検証に基づき 55ka の化石試料から台風の復元を試みた．化石試料は現生試料と同様に夏季に急激な成長線幅の減少や Ba/Ca のピークを生じ，台風の存在が示唆された．造礁サンゴ骨格で Ba/Ca は陸域の河川流入の間接指標となることから[McCulloch *et al*., 2003]，シャコガイ殻の Ba/Ca も同様に台風に伴う陸域からのバリウムの流入が反映されている可能性がある．また，55 ka の化石試料に記録された台

風の頻度は現生試料よりも小さかった. また両者には台風が接近する季節にも違いがあった

（事例 3）Miocene の化石シャコガイ 高時間解像度の環境情報と ENSO 様数年周期変動復元

シャコガイの殻は緻密なアラゴナイトからなり，特に厚く発達する殻内層は化石となっても保存状態が良い. 約 10Ma のインドネシアジャワ島産化石シャコガイ殻の地球化学分析，成長縞解析を行った. 中新世は 2303 万～533 万 3000 年前（23.03-5.333Ma），新第三紀の最初の時代にあたり 1500 万年前（15Ma）を過ぎると再び寒冷化が進み，アジア地域のモンスーン気候が顕著となった(Zachos *et al*., 2001). 10Ma ごろには，現在とほぼ同様の大陸配置となった. この後期中新世の気候変動を季節以上の時間解像度で明らかにした例は少ない.

化石シャコガイ殻試料は SEM および X 線回折で保存状態の良い試料を選出し，殻の微細構造もよく保存されていることが明らかになった. 殻の酸素同位体比や成長線幅には年周期がみられ，成長線を用いて地球科学分析の結果に時間軸を入れることができた. さらに，殻の酸素同位体比には有意な数周年変動が認められ，現在のエルニーニョ南方振動に類似した変動が観察された. 殻の酸素同位体比のアノマリーをとり，その値が負にシフトする時には，現在のラニーニャ様時と同様に年間の水温差が小さくなり，降水量が増加していたことが示唆された.

以上，本研究でシャコガイ殻を用いた高時間解像度の地球科学分析および成長線解析より，シャコガイ殻に台風の痕跡が残されることを明らかにし過去の台風を復元できる可能性を示した. また、化石シャコガイの保存性を確認し、後期更新世及び後期中新世の気候変動を高時間分解能で指摘できた。

Contents

Chapter 1: **Giant clam shell as a high temporal resolution paleo environment proxy**

Paleo environment proxies such as foraminifera tests in sediment core, speleothem, ice core, tree rings, and historical documents have been used for reconstructing paleo climate changes prior to instrumental records. In surface tropical surface ocean, coral skeletons and bivalve shells have used as powerful tools for reconstructing tropical climate with high temporal resolution (Fig. 1-1). Bio genetic carbonate such coral skeletons and bivalve's shells consist of calcium carbonate and oxygen isotopes and trace elements have been widely used as the sea surface temperature (SST), upwelling, and insorration and so on. Bivalve shells had growth lines such as annual ring and daily growth ring, thus we can estimate the date for geochemical analysis in the shell specimen. In addition, the growth increments in the bivalve shell reflects surrounding environment and its growth patterns [Kennish and Olsson, 1975]. The giant clam (Tridacnidae) is widely distributed over the coral reefs in Indo – Pacific oceans and forms the largest shells among all bivalves [Rosewater, 1965]. Symbiont algae (zooxanthellae) in their hypertrophied mantle enable rapid growth, e.g., approximately 15 mm/year in a *Tridacna gigas* inner shell layer [*Watanabe et al*., 2004]. Tridacna shell has a fast growth rate and large daily growth increment (Fig. 1-2). Therefore, Tridacna $\delta^{18}O_{shell}$ provides high-resolution paleotemperature reconstruction on decadal to century timescales [*Watanabe and Oba*, 1999]. In addition, because giant clam has dense and thick shell, it is easily to get well preserved fossil sample [Watanabe *et al*., 2004]. Giant clam fossil appeared from Eocene, thus we can expect high temporal paleo environment reconstruction using giant clam shell (Fig.1-3). The studies about paleo environment reconstruction using giant clam shell mainly have focused the calibration such as comparing geochemical signals and instrumental environment records. The aim of this studies was to inspect the possibility of reconstructing short time period climate events, such as typhoon using geochemical and microstructure signals in the giant clam shell. Besides, we applied the method of modern shell specimen to the fossil shell specimens and tried to reconstruct the short-term climate changes in late Miocene, late Pleistocene, and Holocene when had different climate backgrounds.

References

Beerling, D. J., and D. L. Royer (2011), Convergent Cenozoic CO2 history, *Nat. Geosci.*, *4*(7), 418–420, doi:10.1038/ngeo1186.

Harzhauser, M., O. Mandic, W. E. Piller, M. Reuter, and A. Kroh (2008), TRACING BACK THE ORIGIN OF THE INDO-PACIFIC MOLLUSC FAUNA : BASAL TRIDACNINAE FROM THE OLIGOCENE AND MIOCENE OF THE SULTANATE OF, , *51*(1992), 199–213, doi:10.1111/j.1475-4983.2007.00742.x.

Kennish, M. J., & Olsson, R. K. (1975). Effect of thermal discharges on the microstructural growth of *Mercenaria mercenaria.* Environmental Geology, 1(1), 41–64. https://doi.org/10.1007/BF02426940

Rosewater, J. (1965). The family Tridacnidae in the Indo-Pacific. Indo-Pacific Mollusca, 1, 347–396.

Watanabe, T., & Oba, T. (1999). Daily reconstruction of water temperature from oxygen isotopic ratios of a modern Tridacna shell using a freezing microtome sampling technique. Journal of Geophysical Research, 104(C9), 20,667–20,674. https://doi.org/10.1029/1999JC900097

Watanabe, T., A. Suzuki, H. Kawahata, H. Kan, and S. Ogawa (2004), A 60-year isotopic record from a mid-Holocene fossil giant clam (Tridacna gigas) in the Ryukyu

Islands: Physiological and paleoclimatic implications, *Palaeogeogr. Palaeoclimatol. Palaeoecol.*, *212*(3–4), 343–354, doi:10.1016/j.palaeo.2004.07.001.

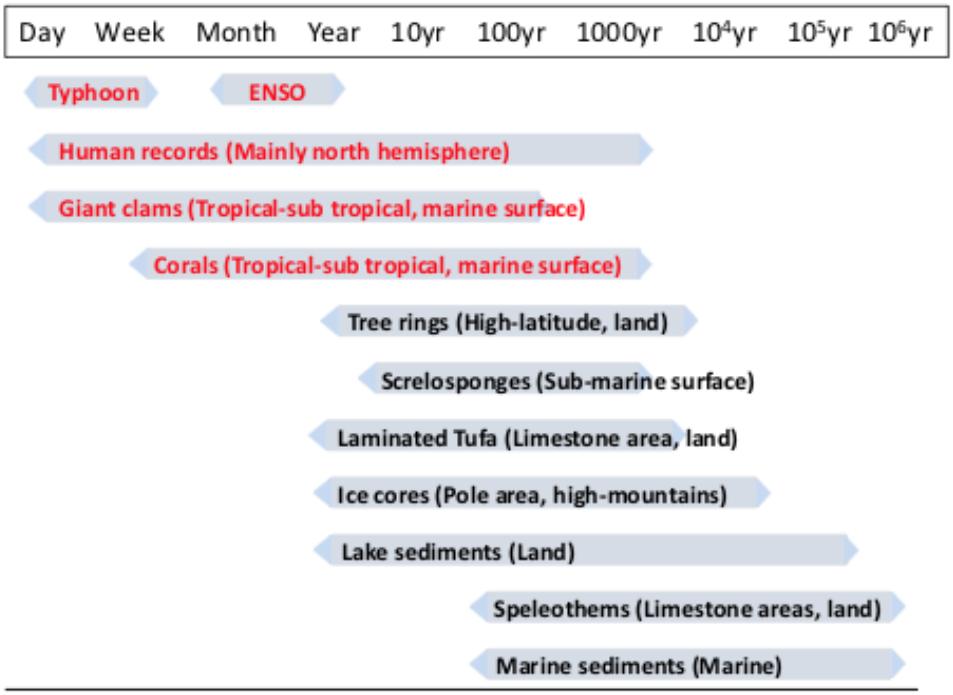

Figure 1.1： Paleoenvironmental recorders with various temporal resolutions. (modified from Watanabe, (2002a))

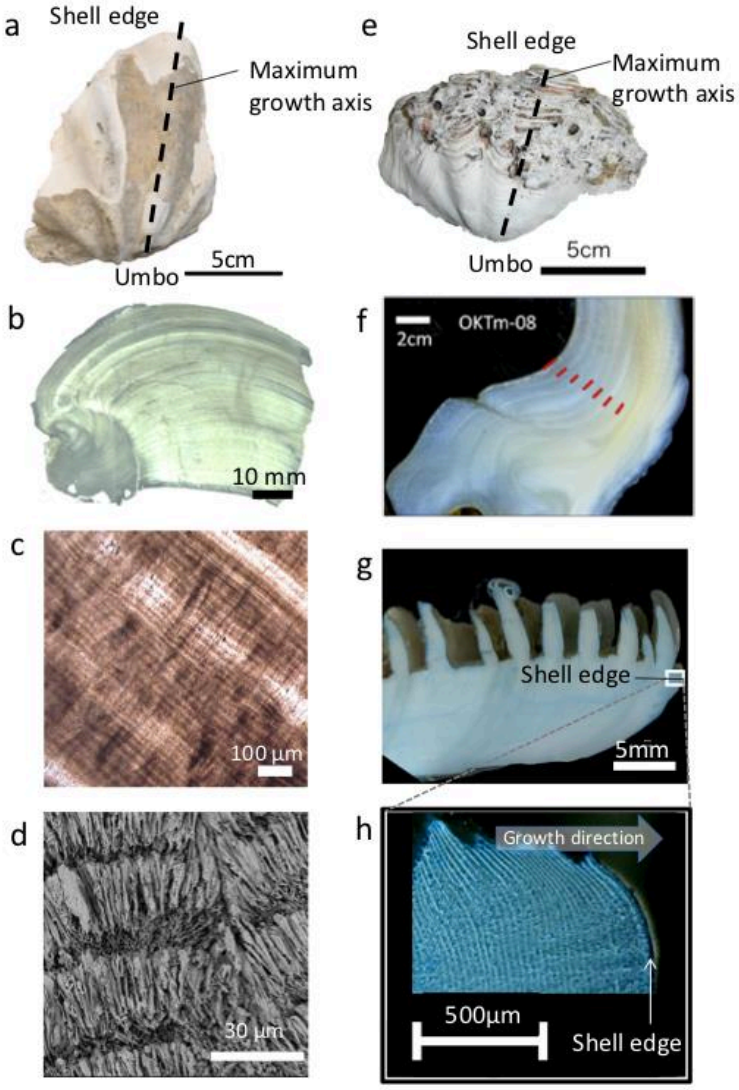

Figure 1–2: Giant clam shell and its growth increment.

a) to d): Late Miocene *Tridacna gigas* fossil, b) shell thin section of a), c) enraged image of b), Scanning electron microscope (SEM) image of a).

e) to h): modern *Tridacna maxima*, f) the shell section of e) red lines showed annual growth lines. g) The shell section stained with Mutvei's solution to observe micro growth increments, h) enraged image of g),

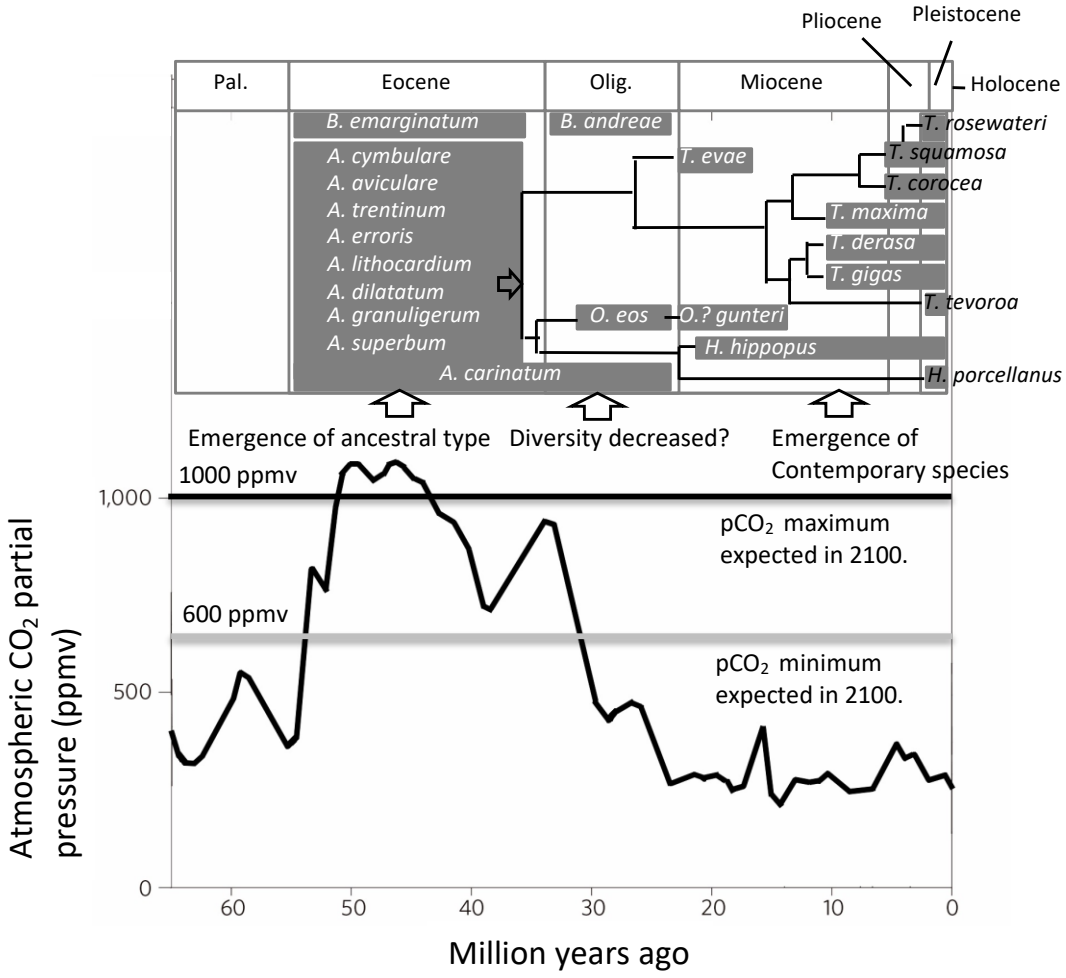

Figure 1-3. The fossil record of the Tridacnid species and atmospheric CO2 partial pressure of the Cenozoic.When ancestral type of Tridacnid appeared, the atmospheric CO_2 partial pressure was higher than pCO2 minimum expected in 2100. Modified from Beerling and Royer (2011), and Harzhauser *et al*. (2008).

Chapter 2: **Methods for paleo environment reconstruction studies using giant clam shell**

2.1 Sample preparation

The soft tissues of the modern shell specimens were removed immediately after collection. After that, the shell specimen was washed with distilled water and dried. The shell specimen was put into a Polyester Solidifier (p-resin, Geoscience Materials Nichika) or covered with epoxy bonding agent (quick weld, J-B weld) to prevent breakage of the shell outer layer structure during cutting (Figure 2.1). The shell was cut in two 10-mm-thick sections with a stonecutter (blade thickness 0.5 mm, ISOMET 100, Buehler) along the maximum growth axis (Figure 2.1). One shell section was for geochemical analysis and the other was for sclerochronological analysis (Figure 2.1). When thin section needed, the shell was cut into 5 mm-thick section. The sections were polished with #800, #2000, and #8000 polishing powder. The sections were ultrasonically rinsed (ultra-sonic bath, SND corp. US-207) in deionized water for 15 minutes between the three rounds of polishing.

2.2 Evaluation of diagenetic alternation in fossil giant clam shell samples

It is necessary to evaluate diagenetic alternation in the fossil shell specimens before geochemical analysis. Diagenetic alternation in the shell, such as precipitation of calcite or secondary aragonite to the pristine aragonite microstructure in the shell is thought to be the cause of inaccuracy in the paleo environment proxies (McGregor and Gagan, 2003; Hendy *et al*., 2007; Sayani *et al*., 2011; Water *et al*., 2015). To evaluate the

diagenetic alternation in the biogenic carbonate samples, X-ray diffraction (XRD) and scanning electron microscope (SEM) is generally used for determination of mineral phases and for determination of secondary carbonate deposition or dissolution respectively (McGregor *et al*., 2002; Reuter *et al*., 2005; McGregor and Abram, 2008; Sayani *et al*. 2011; Watanabe *et al*., 2004; Watanabe *et al*., 2011; Faylona *et al*., 2011; Warter *et al*., 2015; Warter and Müller, 2017) (Fig. 2.2). Using staining method for identification of diagenetic alternation in biogenetic carbonate samples in the field work is the simple first step in the determining whether the sample is suitable for paleo environment proxies. Hutchinson (1974) introduced a mineral phases determination flow chart of carbonate mineral species by staining method (Fig. 2.3). Both Feigl's solution method (Feigl, 1934) and Meigen's solution method (Meigen, 1901) are known to selectively dye aragonite among calcium carbonate. Feigl's solution is made by placing 1 g Ag2SO4 in 100 ml of % wt % MnSO4 water solution, boil it, cooling it, and filter the suspension with filter paper. Then add 1-2 drops of NaOH and after 1-2 hour filter again the solution with filter paper and store in light shielded bottle (Aoyagi, 1975; Kato *et al*., 2001). When using this staining solution, the surface of aragonite is stained black, but calcite is not stained (Htchinson, 1974) (Fig. 2.4). On the other hand, Meigen's solution can be used as a staining solution by adjusting cobalt nitrate (II) to distilled water to a concentration of 10 % by weight (Suzuki *et al*., 1993, Kato *et al*., 2001). When suing this staining solution, the aragonite surface is stained purple, but the calcite is not stained (Suzuki *et al*., 1993, Kato *et al*., 2001) (Fig.2.5).

Feigl's staining method is easy to prepare and has the advantage of being able to carry out the reaction at room temperature, and it can easily distinguish aragonite and calcite by bringing it to the field work site. Although Meigen's solution staining method requires keeping the temperature at 70 ℃ during reaction, a thin firm of fine particles is formed on the aragonite, thus it is possible to evaluate more detailed diagenetic alternation. This staining method is considered to be useful also when observing with SEM observation.

2.3 Sclerochronological methodology

To emphasize the growth increments, one shell section was immersed in Mutvei's solution [*Schöne et al*., 2005]. Increments were clearly observed after 15 min of etching in Mutvei's solution (500 ml acetic acid 1%, 500 ml glutaraldehyde 25%, and 0.1 g of alcian blue powder) at 37-40 °C (Figure 1.O g, h). The other methods to emphasize the growth increment are making thin section of the shell and peel method (Figure 2.6). Photographs of the shell section were taken under a digital microscope (KEYENCE VHX - 2000), and the increment thickness in the outer layer was measured using the image processing software ImageJ [*Rasband, W.S*., 1997-2015.]. The increments were measured in the recent (edge; collected date) to old direction along the growth axis, corresponding to the geochemical analysis transect on the other section. By comparing composite photographs of geochemical and sclerochronological analysis shell sections, we can determine the calendar date for the geochemical analysis results.

2.4 Stable Isotope Analysis

Powder samples for isotope analysis were taken from the pair of shell sections. Each sample was obtained from the parallel to the growth increments using a hand drill (HP-200S, Toyo associates Co., Ltd., Japan) with a 0.4-mm drill bit (model BS1201, Minitor Co. Ltd., Japan) (Figure 2.6). The sampling grooves were taken discretely. Hand drill sampling provided an average width of 400 μm providing 20 - 40 μg powder samples for isotope analysis. The microsampling stage provided an average width of 300 μm, length of 1000 μm, and ~200 μm depth groove providing 200~300 μg powder samples for isotope analysis. The 20- to 40-μg powder samples were reacted with 100% phosphoric acid at 70 °C in a carbonate preparation device (Kiel IV Carbonate preparation device), and the produced CO_2 was analyzed using a stable isotope ratio mass spectrometer (Thermo Scientific MAT 253). Isotopic values ($\delta^{18}O$ and $\delta^{13}C$) were one-point calibrated against National Bureau of Standards (NBS) 19 and reported in standard δ notation relative to Vienna Pee Dee belemnite (VPDB) and confirmed the calibration using NBS 18. The standard deviations (1σ) for 22 replicate measurements of NBS 19 are 0.03‰ and 0.02‰ for $\delta^{18}O$ and $\delta^{13}C$ as external long-term reproducibility throughout this study, respectively.

2.5 Analysis of trace elements in the shell

Barium and calcium concentrations were analyzed by Laser Ablation Inductively Coupled Plasma Mass Spectrometry (LA-ICP-MS) (Agilent 7700 ICP-MS coupled with New Wave Research NWR193 laser ablation system: 193 nm ArF excimer laser (pulse width <5 ns)) along the same sampling line used for isotopic analysis sampling. The laser conditions were below; irradiance 0.82 GW/cm^2, repetition rate 10 Hz, and 40 second of laser duration. The sample surface was cleaned by 5 seconds of pre-ablation. The shell sample was ablated using a 100-μm laser spot, and each spot was adjacent to its neighbor, without overlap. There were 2 to 6 growth increments in each ablated spot. The calibration of the signal intensity to the Ba/Ca ratio was performed using glass standard materials: NIST 612 standard grass distributed by the National Institute of Standard and Technology [*Shirai et al*., 2008]. ^{43}Ca was used as an internal standard, and ^{138}Ba was expressed in terms of its molar ratio to ^{43}Ca. The analytical error for the Ba/Ca ratio (relative standard deviation) was within 3.86 % (n = 42, 1σ NIST612) as external long-term reproducibility throughout this study. After isotopic and Ba/Ca ratio analysis, the sampling grooves and spots on the shell section were compared to the growth increment positions by overlaying photographs of the sections. I also measured Strontium Calcium ratio (Sr/Ca), Magnesium Calcium ratio (Mg/Ca), and Ba/Ca with an Inductively Coupled Plasma Optical Emission Spectrophotometer (ICP-OES) installed at Hokkaido University. Approximately 132 ± 15 μg of giant clam powder sample was dissolved in 4 mL of HNO_3. The sample solution for the measurement of trace elements was prepared via serial dilution with 2% HNO3 for a Ca concentration of ca. 9 ppm. Analytical precision of the

Sr/Ca, Mg/Ca, and Ba/Ca determinations were 0.06, 0.4, and 5.5 RSD (%, n = 23, 1σ, JCt-1) respectively.

2.6 References

McGregor, H. V., and M. K. Gagan (2003), Diagenesis and geochemistry of Porites corals from Papua New Guinea: Implications for paleoclimate reconstruction, *Geochim. Cosmochim. Acta*, *67*(12), 2147–2156, doi:10.1016/S0016-7037(02)01050-5.

Hendy, E. J., M. K. Gagan, J. M. Lough, M. McCulloch, and P. B. deMenocal (2007), Impact of skeletal dissolution and secondary aragonite on trace element and isotopic climate proxies in Porites corals, *Paleoceanography*, *22*(4), 1–10, doi:10.1029/2007PA001462.

Sayani, H. R., K. M. Cobb, A. L. Cohen, W. C. Elliott, I. S. Nurhati, R. B. Dunbar, K. A. Rose, and L. K. Zaunbrecher (2011), Effects of diagenesis on paleoclimate reconstructions from modern and young fossil corals, *Geochim. Cosmochim. Acta*, *75*(21), 6361–6373, doi:10.1016/j.gca.2011.08.026.

Warter, V., W. Muller, F. P. Wesselingh, J. A. Todd, and W. Renema (2015), Late miocene seasonal to subdecadal climate variability in the indo-west pacific (east kalimantan , indonesia) preserved in giant clams, *Palaios*, *30*, 66–82, doi:10.2110/palo.2013.061.

Reuter, M., T. C. Brachert, and K. F. Kroeger (2005), Diagenesis of growth bands in fossil scleractinian corals : identification and modes of preservation, , 146–159, doi:10.1007/s10347-005-0064-7.

McGregor, H. V., and N. J. Abram (2008), Images of diagenetic textures in Porites corals from Papua New Guinea and Indonesia, *Geochemistry, Geophys. Geosystems*, *9*(10), 1–17, doi:10.1029/2008GC002093.

Warter, V., and W. Müller (2017), Daily growth and tidal rhythms in Miocene and modern giant clams revealed via ultra-high resolution LA-ICPMS analysis — A novel methodological approach towards improved sclerochemistry, *Palaeogeogr. Palaeoclimatol. Palaeoecol.*, *465*, 362–375, doi:10.1016/j.palaeo.2016.03.019.

Hutchinson C. S. (1974): Laboratory Handbook of Petrographic Techniques, John Wiley & Sons, New York, 527.

Feigl, F. (1934): Mineral. Petrog. Mitt. 45, 447-56.

Meigen, W. (1901): Eine einfache Reaktion zue unterscheidung von aragonit und kalkspath Zentralblatt fur Mineralogie, Geologie und Palaeontologie. 577–578.

Suzuki S., Tago Y. & Hikida Y. (1993): Using Meigen's Staining for aragonite –Calcite identification in fossil molluscan shells under the scanning electron microscope, The Journal of the Geological Society of Japan, 99, 1-8.

Kato, K., H. Wada, and K. Fujioka (2003), The application of chemical staining to separate calcite and aragonite minerals for micro-scale isotopic analyses, *Geochem. J.*, *37*(2), 291–297, doi:10.2343/geochemj.37.291.

Kato, K.,and H. Wada (2001), Calcite-aragonite mineral separation using staining method for micro-scale isotopic analyses, *Geosci. Repts. Shizuoka Univ.*, *28* (July, 2001), 25-31

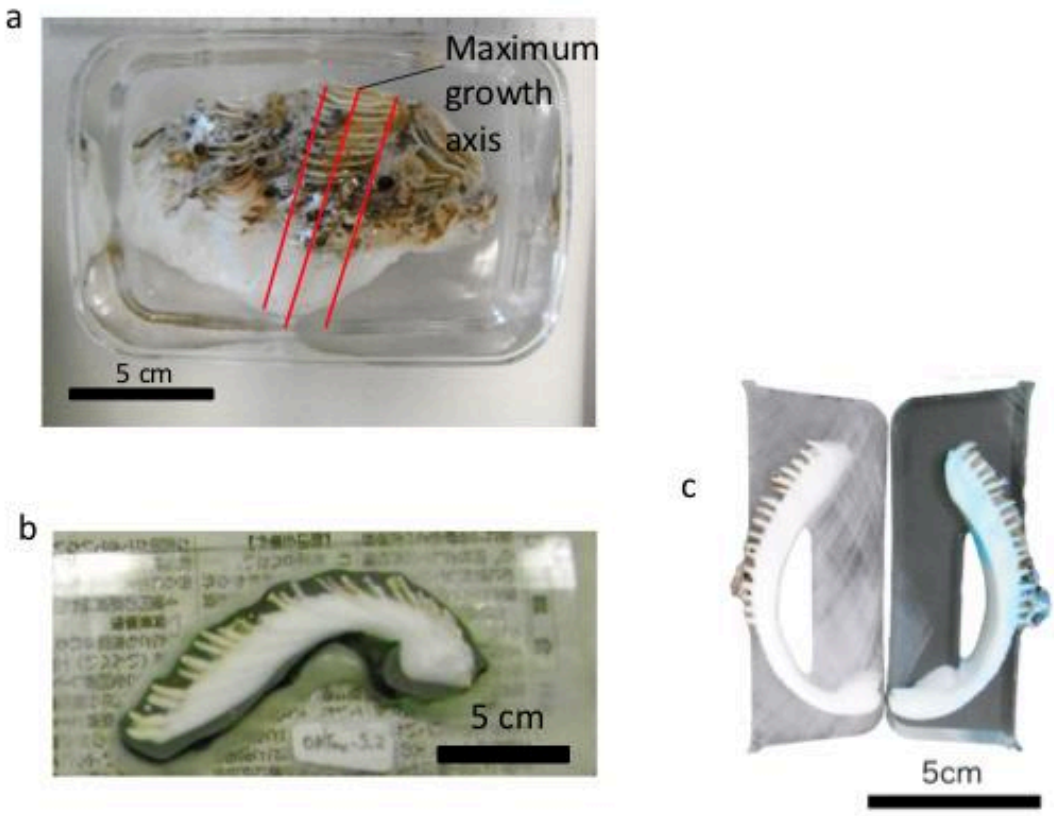

Figure 2.1
Giant clam shell sample cutting preparation.
(a) The shell specimen was put into a Polyester Solidifier (p-resin, Geoscience Materials Nichika). Red lines indicate cutting lines. (b) The shell section which covered with epoxy bonding agent (quick weld, J-B weld). (c) The shell sections.

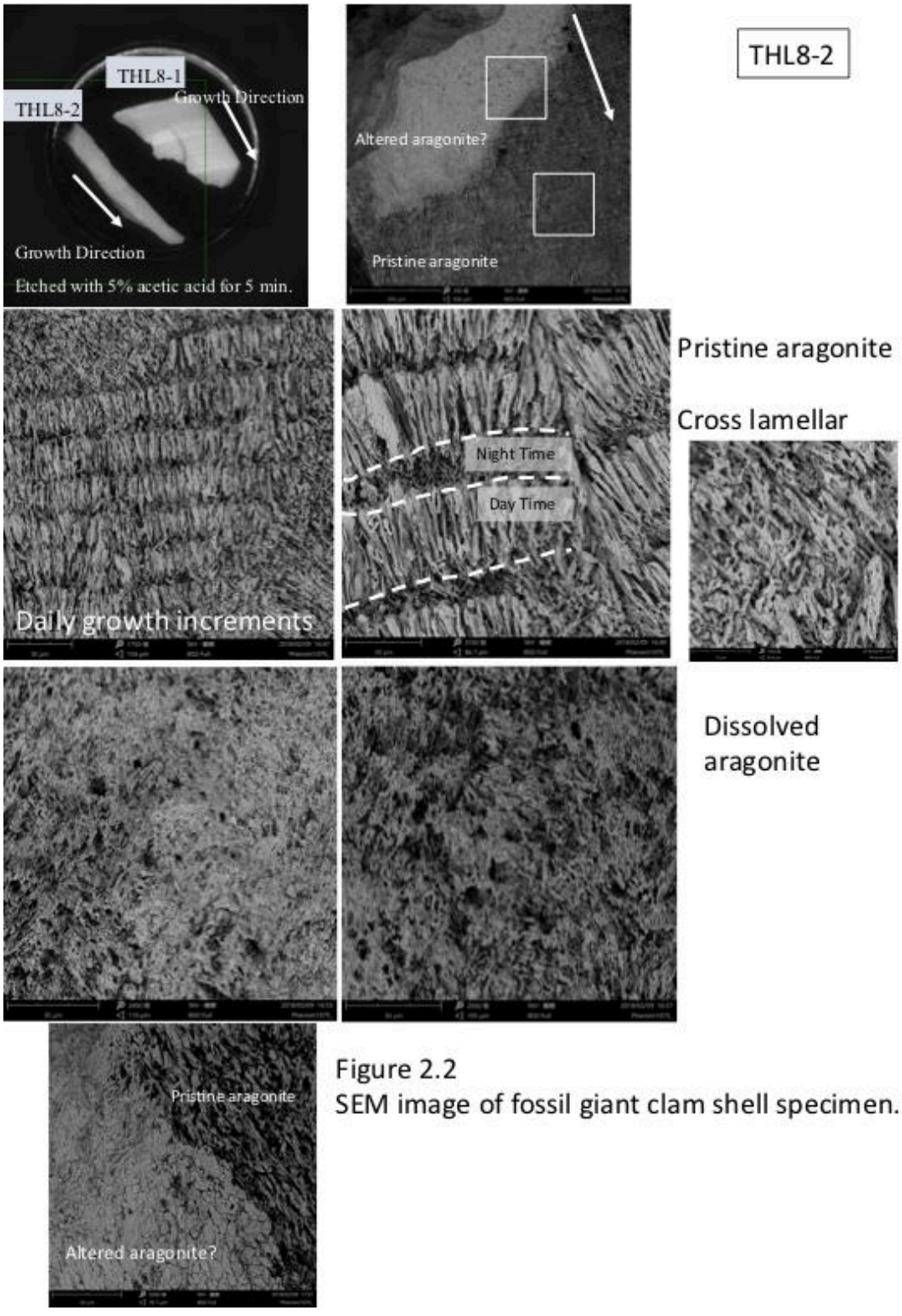

Figure 2.2
SEM image of fossil giant clam shell specimen.

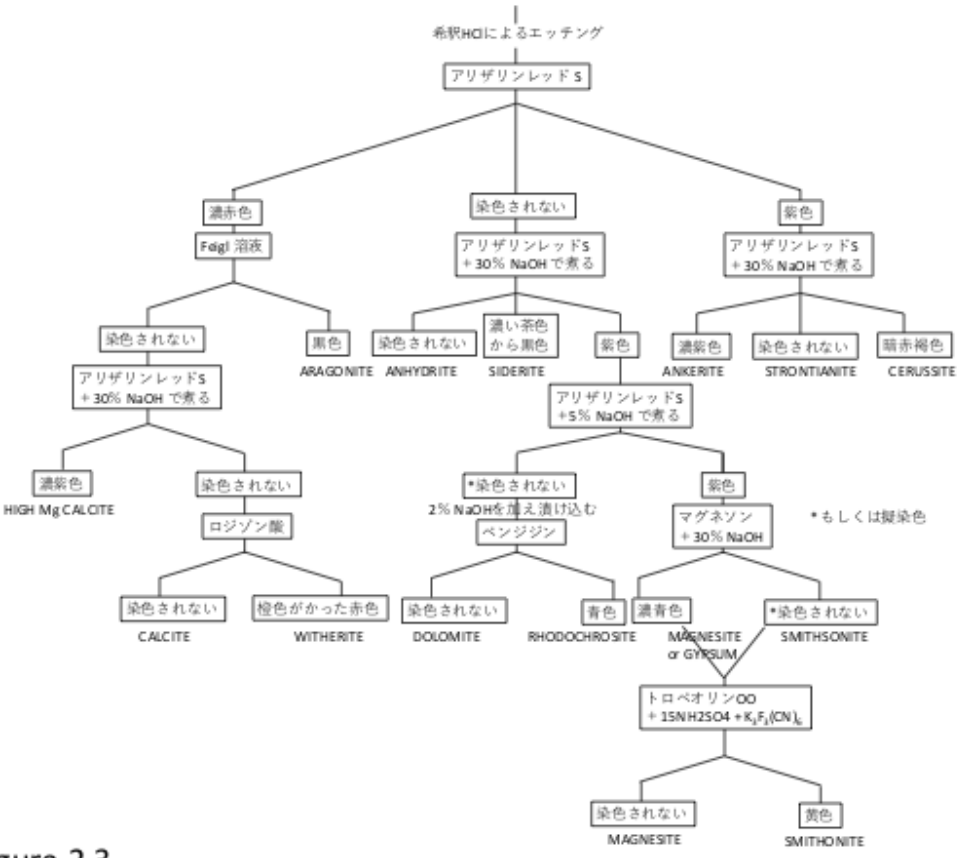

Figure 2.3
Flow chart of carbonate minerals species separation (after Warne 1962).

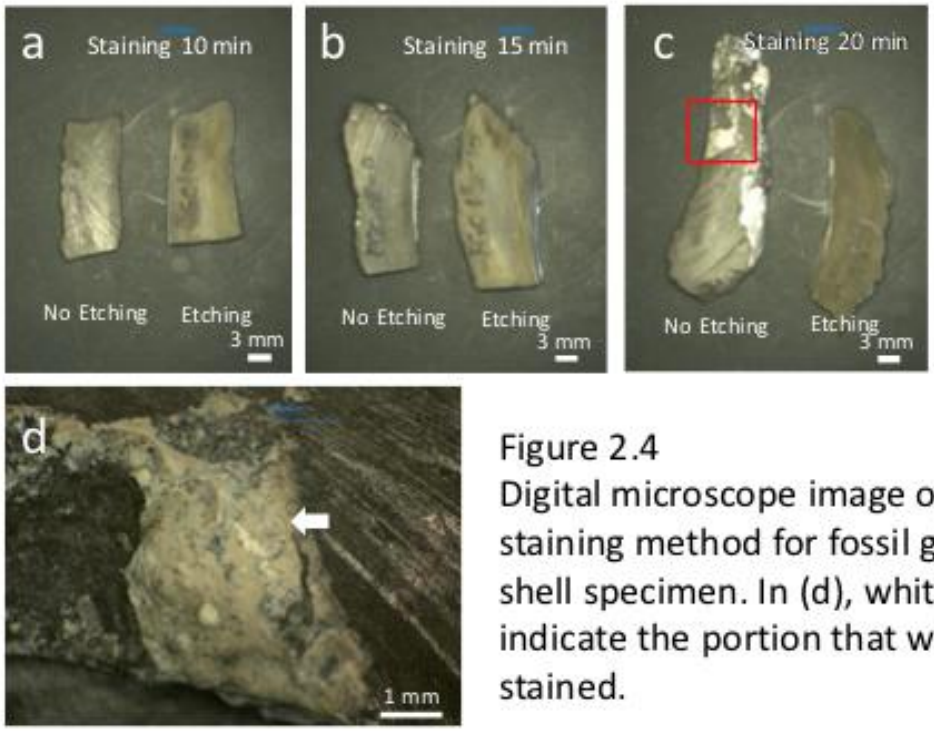

Figure 2.4
Digital microscope image of Feigl's staining method for fossil giant clam shell specimen. In (d), white allow indicate the portion that were not stained.

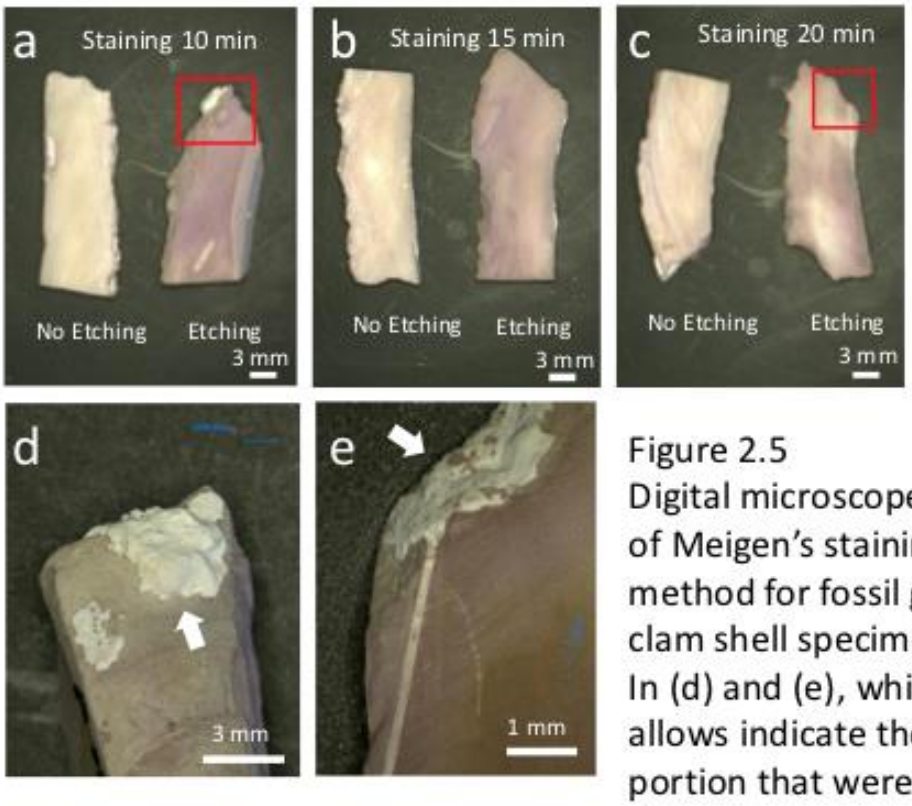

Figure 2.5
Digital microscope image of Meigen's staining method for fossil giant clam shell specimen. In (d) and (e), white allows indicate the portion that were not stained.

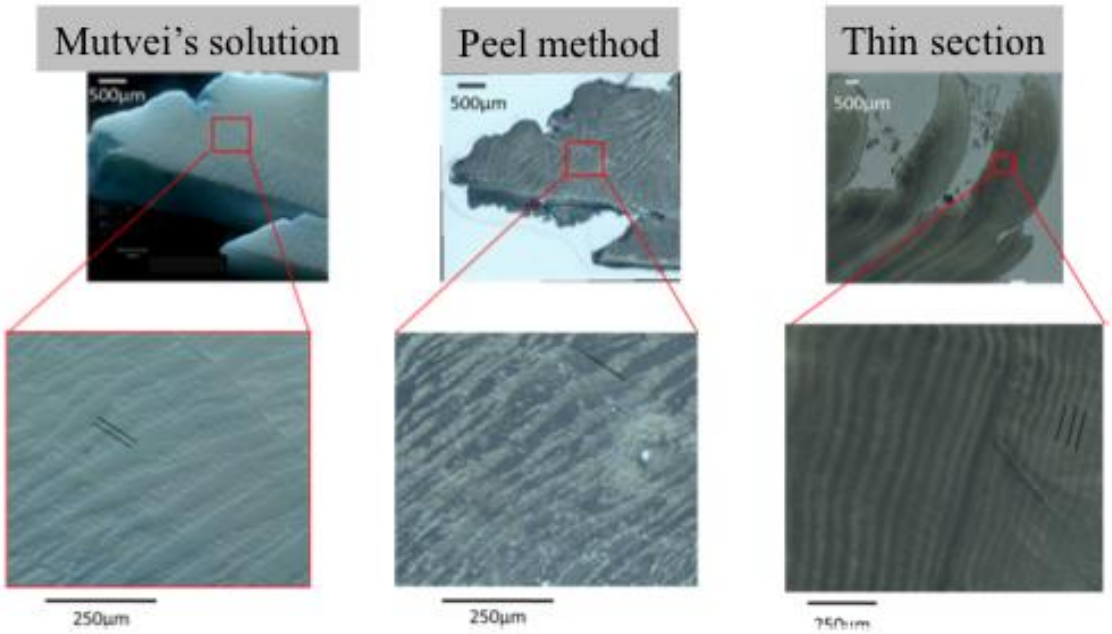

Figure 2.6
Comparison of sclerochronologucal methodology
Black lines show dairy growth lines.

(a)

(b)

Figure 2.7
(a) Hand drill and stereo-microscope,
(b) micro sampling stage for shell sample

Chapter 3: **Geochemical and microstructural signals in giant clam Tridacna maxima recorded typhoon events at Okinotori Island, Japan**

Abstract

To validate the usability of the giant clam shell as a recorder of short-term environmental changes such as typhoons, we collected a live *Tridacna maxima* from Okinotori Island, Japan on June 15, 2006. Growth increment thickness, stable isotope ratio ($\delta^{18}O_{shell}$, $\delta^{13}C_{shell}$) and the barium/calcium ratio (Ba/Ca) in the *Tridacna maxima* shell sample were measured and compared to Okinotori Island instrumental environmental data. In the outer layer of the shell sample, there were 365 ± 6 growth increments per year, as estimated by the $\delta^{18}O_{shell}$ profile compared with sea surface temperature (SST). The growth increments in the specimen were formed daily, and thus, we can determine the date of the sampling points of $\delta^{18}O_{shell}$, $\delta^{13}C_{shell}$ and the Ba/Ca ratio by counting growth increments. After typhoons approach, there is a decrease in increment thickness and some disturbed growth increments. The positive peaks in the shell Ba/Ca ratio and $\delta^{18}O_{shell}$ corresponded to lower SST caused by typhoons. These results indicated that the microstructural and geochemical record in *Tridacna maxima* shells could be useful for detecting past typhoon events.

1 Introduction

In recent years, with global warming of the climate, there is concern that the frequency of major tropical cyclones such as typhoons, hurricanes or cyclones will increase [*IPCC*,

2013]. The passage of major tropical cyclones is a weather phenomenon that occurs in a few days but sometimes causes great damage to human society. Clarifying the frequency of tropical cyclones in an era warmer than the present age would provide important information for predicting the frequency of tropical cyclones caused by global warming. Paleotempestology has sought to develop tropical cyclone activities over a large range of timescales, from daily to millennial-scale reconstructions [*Muller et al.*, 2017]. The more commonly used archives for past tropical cyclone activities include (1) historical documentary record, such as official histories, gazettes, newspaper, and civilian writings like travel logbooks, diaries, poems etc. [*Fan and Liu*, 2008]; (2) speleothem [*Frappier*, 2008; *Haig et al.*, 2014], coral-ring [*Hetzinger et al.*, 2008; *Kilbourne et al*., 2011; *Kilbourne et al.*, 2011], and tree-ring archives [*Li et al.*, 2011]; (3) beach ridges [*Nott et al.*, 2009; *Forsyth et al.*, 2010; *Nott*, 2011a; *Nott and Forsyth*, 2012]; and (4) coastal lacustrine, lagoonal, and marsh overwash deposits [*Horton et al.*, 2009; *Woodruff et al.*, 2009; *Williams*, 2012]. However, there are no daily records before human history in historical documents, and it is difficult to clarify individual typhoons due to the insufficient time resolution of these past tropical cyclone archives. Therefore, a proxy to clarify the occurrence of typhoons with high temporal resolution is important for high-resolution paleotempestology applications.

The giant clam (Tridacnidae) is widely distributed over the coral reefs in Indo – Pacific oceans and forms the largest shells among all bivalves [Rosewater, 1965]. Symbiont algae (zooxanthellae) in their hypertrophied mantle enable rapid growth, e.g., approximately 15 mm/year in a *Tridacna gigas* inner shell layer [*Watanabe et al*., 2004]. Annual and

daily growth increments were recognizable in the shells of *T. gigas*, *T. maxima*, *T. squamosa* and *Hippopus hippopus* [*Bonham* 1965; *Pannella and MacClintock* 1968; *Aharon and Chappell* 1986; *Patzöld et al*. 1991; *Watanabe and Oba* 1999; *Watanabe et al*. 2004; *Aubert* al., 2009; *Sano et al*., 2012 *Duprey et al*. 2014; *Warter et al*., 2015]. Counting daily growth increments provides us exact deposition dates for daily increments. This attribute also allows precise dating for geochemical analysis data from a Tridacna shell [*Watanabe and Oba*, 1999; *Aubert et al.,* 2009; *Duprey et al*., 2014]. Growth pattern analysis is useful for reconstruction of past environments with daily resolution [Upwelling: *Aubert et al*., 2009; Cyclone: *Schwartzmann et al*., 2011]. In addition, Tridacnidae precipitates a dense aragonite shell resistant to diagenetic alternation. Growth increments are well preserved in a fossil shell specimen and give accurate paleoenvironmental records [*Aharon and Chappell* 1986; *Watanabe et al*., 2004; *Ayling et al*., 2015; *Warter et al*., 2015; *Warter and Müller*, 2016].

The oxygen-stable isotope ratios ($\delta^{18}O$) of a biogenic carbonate-including bivalve shell is a function of both sea surface temperature (SST) and the oxygen isotopic composition of the surrounding seawater ($\delta^{18}O_{sw}$) [Epstein *et al*., 1953; Grossman and Ku, 1986]. The $\delta^{18}O$ of biogenic carbonates sometimes deflects from the isotopic equilibrium with surrounding sea water; this is called the "vital effect" [Urey *et al*., 1952; Horibe and Oba, 1972, e.g., coral skeleton]. However, Tridacna shells calcify essentially in isotopic equilibrium with surrounding seawater [e.g., Aharon, 1983; Watanabe and Oba, 1999]. $\delta^{18}O$ of bivalve shell ($\delta^{18}O_{shell}$) is sometimes affected by ontogenetic growth [e.g., *Goodwin et al*., 2003]. However, Tridacna shell has a fast growth rate and large daily

growth increment. Therefore, Tridacna $\delta^{18}O_{shell}$ provides high-resolution paleotemperature reconstruction on decadal to century timescales [*Watanabe and Oba*, 1999]. In addition, previous studies have suggested that Tridacnidae shell is secreted in isotopic equilibrium with seawater [*Aharon and Chappell* 1986; *Jones et al*. 1986; *Romanek and Grossman* 1989; *Aharon*, 1991; *Watanabe and Oba* 1999: *Duprey et al*., 2014]. The earlier study of *Romanek and Grossman* [1989] revealed that the $\delta^{18}O_{shell}$ profile of the giant clam *Tridacna maxima* recorded seasonal SST periods. *T. maxima* has the widest distribution in the Indo-Pacific Ocean in *Tridacnidae* [*Moir*, 1985] and generally occurs in geological and archaeological fossil assemblages [Faylona *et al*., 2011].

Barium has a nutrient-like distribution in the ocean, and the coralline barium /calcium ratio (Ba/Ca) has been used as record of upwelling events in the tropical ocean [*Lea et al*., 1989]. In bivalve species, common mussel (*Mytilus edulis*) calcite shell Ba/Ca profiles appear to show seasonal peaks in Ba associated with changes in particulate Ba, dissolved Ba or phytoplankton productivity [*Gillikin et al*., 2006]. Similarly, Ba/Ca peaks in the inner shell layer of *T. gigas* appear to reflect the timing and amplitude of chlorophyll peaks associated with phytoplankton blooms [*Elliot et al*., 2009].

In this study, we measured growth increment width, $\delta^{18}O_{shell}$, and Ba/Ca in *Tridacna maxima* from Okinotori Island, a site in the open ocean in the tropical western Pacific. Okinotori Island is very isolated from any sources of anthropogenic contamination, and the island is in the path of typhoons approaching Japan (Figure 1). From 1993-1998, 46 of 157 typhoons passed within a radius of 500 km from the island [JAMSTEC].

According to Japan Metrological Agency's classification of typhoon zone, 500 to 800 km radius typhoon is called major typhoon and there is possibility of blowing wind speed of 15m/s or more. *T. maxima* from Okinotori Island is thus appropriate for an investigation of whether the giant clam can be used as a record of abrupt environment changes. The aim of this study was to validate whether the shell of *T. maxima* in Okinotori Island, Japan could record daily- to weekly-scale environmental events such as typhoons.

2 Materials and Methods

2.1 Okinotori Island and *Tridacna maxima* sample

Okinotori Island (20° 25′N, 136° 05′E) is the southernmost island (an atoll) in Japan and is isolated from islands with human inhabitants (Figure 1). Thus, there are few terrestrial and artificial effects on its coral reefs. According to general seasonal Sea Surface Temperature (SST) variation for Okinotori Island (statistics processed for April 1993 to February 2001) reported in Nakano *et al*. [2001], SST in Okinotori Island monotonously rises through April to June and reaches up to 29.5 °C in July. SST in Okinotori Island exceeds 29 °C from June to September. After that, SST decreases gradually from October to February. The average amplitude of annual SST changes in Okinotori Island is 4.8 °C [Nakano *et al*., 2011]. A living *Tridacna maxima* specimen was collected at 2 m depth in the coral reef of Okinotori Island on 15th June 2006, during the cruise KH-06-2 of the Research Vessel (R/V) *Hakuhoumaru*. We caught few *Tridacna maxima* specimen from the island and we used the youngest shell specimen with fast growth rate to detect the geochemical and sclerochronological signals during typhoon approaches. The shell was

12.8 cm long and 8.6 cm tall (umbo-edge) (Figure 2. a). All *Tridacnidae* in Okinotori Island are *T. maxima* [*Yoneyama et al*., 2006].

2.2 Sample preparation

The soft tissues of the *T. maxima* specimen were removed immediately after collection. The shell was put into a Polyester Solidifier (p-resin, Geoscience Materials Nichika) to prevent breakage of the shell outer layer structure during cutting. The shell was cut in two 10-mm-thick sections with a stonecutter (blade thickness 0.5 mm), along the maximum growth axis (Figure 2. a, b). One shell section was for geochemical analysis and the other was for sclerochronological analysis (Figure 2. b, c, d). The sections were polished with #800, #2000, and #8000 polishing powder. The sections were ultrasonically rinsed (ultra-sonic bath, SND corp. US-207) in deionized water for 15 minutes between the three rounds of polishing.

2.3 Sclerochronological methodology

To emphasize the growth increments, one shell section was immersed in Mutvei's solution [*Schöne et al*., 2005]. Increments were clearly observed after 15 min of etching in Mutvei's solution (500 ml acetic acid 1%, 500 ml glutaraldehyde 25%, and 0.1 g of alcian blue powder) at 37-40 °C (Figure 2. d). Photographs of the shell section were taken under a digital microscope (KEYENCE VHX - 2000), and the increment thickness in the outer layer was measured using the image processing software ImageJ [*Rasband, W.S*., 1997-2015.]. The increments were measured in the recent (edge; collected date) to old

direction along the growth axis, corresponding to the geochemical analysis transect on the other section (Figure 2d). By comparing composite photographs of geochemical and sclerochronological analysis shell sections, we can determine the calendar date for the geochemical analysis results.

2.4 Stable Isotope Analysis

Powder samples for isotope analysis were taken from the pair of shell sections (Figure 2c). Each sample was obtained from the parallel to the growth increments using a hand drill (HP-200S, Toyo associates Co., Ltd., Japan) with a 0.4-mm drill bit (model BS1201, Minitor Co. Ltd., Japan) (Figure 2d). The sampling grooves were taken discretely and had an average width of 400 μm, providing 20 - 40 μg powder samples for isotope analysis. Each sampling groove contained 8 - 36 increments depending on shell growth rates (Figure 2 c). The 20- to 40-μg powder samples were reacted with 100% phosphoric acid at 70 °C in a carbonate preparation device (Kiel IV Carbonate preparation device), and the produced CO_2 was analyzed using a stable isotope ratio mass spectrometer (Thermo Scientific MAT 253). Isotopic values ($\delta^{18}O$ and $\delta^{13}C$) were one-point calibrated against National Bureau of Standards (NBS) 19 and reported in standard δ notation relative to Vienna Pee Dee belemnite (VPDB) and confirmed the calibration using NBS 18. The standard deviations (1σ) for 22 replicate measurements of NBS 19 are 0.03‰ and 0.02‰ for $\delta^{18}O$ and $\delta^{13}C$ as external long-term reproducibility throughout this study, respectively.

2.5 Analysis of the Barium / Calcium Ratio

Barium and calcium concentrations were analyzed by Laser Ablation Inductively Coupled Plasma Mass Spectrometry (LA-ICP-MS) (Agilent 7700 ICP-MS coupled with New Wave Research NWR193 laser ablation system: 193 nm ArF excimer laser (pulse width <5 ns)) along the same sampling line used for isotopic analysis sampling (Figure 2c). The laser conditions were below; irradiance 0.82 GW/cm^2, repetition rate 10 Hz, and 40 second of laser duration. The sample surface was cleaned by 5 seconds of pre-ablation. The shell sample was ablated using a 100-μm laser spot, and each spot was adjacent to its neighbor, without overlap. There were 2 to 6 growth increments in each ablated spot. The calibration of the signal intensity to the Ba/Ca ratio was performed using glass standard materials: NIST 612 standard grass distributed by the National Institute of Standard and Technology [*Shirai et al*., 2008]. ^{43}Ca was used as an internal standard, and ^{138}Ba was expressed in terms of its molar ratio to ^{43}Ca. The analytical error for the Ba/Ca ratio (relative standard deviation) was within 3.86 % (n = 42, 1σ NIST612) as external long-term reproducibility throughout this study. After isotopic and Ba/Ca ratio analysis, the sampling grooves and spots on the shell section were compared to the growth increment positions by overlaying photographs of the sections.

2.6 Environmental Data

The SST in Okinotori Island was observed by the Japan Agency for Marine–Earth Science and Technology (JAMSTEC; SST data available at the JAMSTEC Okinotori Island Web site, http://www.jamstec.go.jp/j/database/okitori/index.html). The SST was

measured in 40-minute intervals at an automatic observatory in Okinotori Island. These datasets were converted into daily averages to compare to the temporal resolution of the isotope analysis. The data on temporal chlorophyll-a concentrations (8-day binned data available at NASA's Ocean Color Web, http:// oceancolor.gsfc.nasa.gov/) were obtained from a 9 km by 9 km pixel containing Okinotori Island in SeaWiFS (Sea-viewing Wide Field-of-view Sensor) [McClain *et al*., 2004] by Yamazaki *et al.* (2011). The outgoing long-wave radiation (OLR) is the intensity of infrared emission from ocean, land or cloud surfaces, which decreases with cloud cover. Cloud surfaces emit relatively short-wave radiation, reflecting the cooling temperature altitude. In contrast, warming surfaces emit long-wave radiation. In the tropical zone, low OLR values show active convective activity and much rainfall. OLR can be used as an indicator of high sunlight-like OLR in strong sunlight [*Shupe and Intrieri*, 2004]. Typhoons that passed over Okinotori Island were defined from the past position of typhoons in a weather chart (Japan Meteorological Agency), and the wind speed at Okinotori Island was observed by JAMSTEC (wind speed data available at http://www.jamstec.go.jp/j/database/okitori/index.html).

3 Results

3.1 Sclerochronological record and Chronology for *T. maxima*

The growth increments in the shell section appeared under microscopic observation as a pair of less-etched white lines (growth lines) and deeply etched blue bands (growth increments) when stained with Mutvei's solution (Figure 2d). There were 937 increments observed in the shell section (5-time replication counting error was within ±1.3 % of increments number). The thicknesses of the increments ranged from 6.16 to 59.9 μm, and

the average thickness was 25.2 μm. Bivalves sometimes form irregular growth increment patterns called “growth breaks” [*Kennish*, 1980]. There is a distinct growth break characterized by a deep V–shaped notch in the outer shell layer at the 230th growth increment counted from the shell edge and the growth break continued to the measurement part (Figure 2c, d). In addition, there are growth breaks in which width suddenly decreased appearing at the 98th, 122nd, 241st, 411th, 617th, 795th, 831st, and 858th growth increments (Figure 3 arrow marks).

To assign calendar dates to the isotope ratios and Ba/Ca ratio, the age model was established using the number of growth increments (Figure 3). The growth increments in *Tridacna maxima* shells are formed daily, i.e., they are a “daily growth increment” [Duprey *et al*., 2014]. We determined the date of sampling spots for $\delta^{18}O$, $\delta^{13}C$ and the Ba/Ca ratio by counting growth increments from the shell edge (collected on 15th June 2006) toward each center of sampling spot (Figure 3). The shell $\delta^{18}O$ minima were at the 108th, 455th, and 886th increments and assigned as 28th February 2006, 18th March 2005 and 12th January 2004 (Figure 3, vertical lines). For shell $\delta^{18}O$, we assigned the calendar date to each isotope ratio and the Ba/Ca ratio.

To confirm the accuracy of daily growth increment counting, we counted the number of growth increments between the shell $\delta^{18}O$ maxima (Figure 3c). The number of days between the SST minimum and the next year SST minimum were 124 days during period A (15th June 2006 to 12th February 2006; Figure 3 A), 343 days during period B (12th February 2006 to 7th March 2005; Figure 3 B) and 428 days during period C (7th March 2005 to 5th January 2004; Figure 3 C). The number of growth increments between the

shell $\delta^{18}O$ maxima were 108 during period A, 348 during period B and 432 during period C (Figure 3). When $\delta^{18}O_{shell}$ maxima correspond to the date of SST minima, the number of days and the number of growth increments coincide. The differences between the number of days and growth increments (day - increments) were 16 in period A, -5 in period B and -4 in period C (Figure 3). Consequently, the number of increments between the shell $\delta^{18}O$ maxima almost corresponded with the number of days within increments counting error.

To validate the daily growth increment-based chronology, we established another chronology using the relationship between 16.6-day average SST and $\delta^{18}O_{shell}$. The resolution of the micro sampling for $\delta^{18}O_{shell}$ analysis was approximately 400 μm, and there were 8 to 36 growth increments in the sampling grooves. On average, each $\delta^{18}O_{shell}$ datum reflected the 16.6-day average SST and $\delta^{18}O_{sw}$. We calculated the 16.6-day average SST from daily instrumental SST. The dates of the 16.6-day average SST minima in each year were 23rd January 2006, 13th March 2005, and 7th January 2004, respectively. There was no significant difference in SST minima between the 1-day average SST and 16.6-day average SST except for 2006. As time control points, maxima of the $\delta^{18}O_{shell}$ were tied to the minima of the 16.6-day average SST. For 16.6-day average SST-based chronology, the dates and the number growth increments during each SST minima were as follows. From 15th June 2006 (collected date) to 23rd January 2006 (143 days), the number of growth increments was 107. From 23rd June 2006 to 13th March 2005 (315 days), the number of growth increments was 347. From 13th March 2005 to 7th January 2004 (432 days), the number of the growth increments was 431. Thus, using

the 16.6-day average SST-based chronology, the differences between the number of days and the growth increments were 36, -32, and 1, respectively. Therefore, the chronology based on daily growth increments was more accurate than the age model established from the chronology using SST and $\delta^{18}O_{shell}$.

These results showed that the growth increments in our specimen formed growth increments on a daily basis and confirmed the accuracy of a daily growth increment-based chronology.

3.2 Stable isotope ratios in Okinotori *T. maxima*

The shell $\delta^{18}O$ ratios of the *T. maxima* shell ranged from -1.81 to -0.38‰ with an average of -1.25‰ (n = 57) (Figure 3d). Lower $\delta^{18}O$ values in biogenic carbonates are normally associated with warmer and/or wetter conditions. The shell $\delta^{18}O$ ratios and SST were correlated with SST ($r = 0.62$, $p < 0.001$) from 21 November 2003 to 5 June 2006. The $\delta^{13}C$ ratios of the *T. maxima* shell ranged from 0.40 to 1.23‰ with an average of 0.81‰ (n = 57) (Figure 3c). The $\delta^{13}C$ ratios decreased during the period of lower SST (winter or typhoon season, e.g., 2004, 2005) (Figure 3c, 3e).

3.3 Ba/Ca in Okinotori *T. maxima*

The Ba/Ca ratios of the *T. maxima* shell ranged from 0.53 to 3.06 μmol/mol, with an average of 0.79 μmol/mol (n = 245) (Figure 3a). The Ba/Ca profile showed sharp positive peaks. The Ba/Ca peaks appeared (Figure 4, 2004: 19th April, 7th June, 29th August;

2005: 30th March, 27th April, 18th June, 27th July, 8th October). The highest peak (3.07 μmol/mol) was in August - September 2004 when four typhoons passed across Okinotori Island in succession. However, there was also a Ba/Ca peak at 19th April and the end of March 2005, even though no typhoon approached (Figure 4a, 4e).

4 Discussion

4.1 Shell growth increments and chronology

Comparison of SST records and $\delta^{18}O_{shell}$ confirms that the growth increments in *Tridacna maxima* were daily growth increments and confirms the accuracy of the daily growth increment-based chronology. The two error factors for calendar date were uncertainty of the peak position of $\delta^{18}O_{shell}$ and formation of the growth increment. The difference in the chronology on a daily growth increment basis was large in period A. Since low SST continued in the winter of 2006, the date for the $\delta^{18}O_{shell}$ maximum may not coincide with the date of minimum water temperature. In addition, abrupt SST decreases on 12th February 2006 may have caused thermal stress to the specimen, and the specimen stopped or decreased growth, causing a growth break (14th February 2006) (Figure 3b). The *Tridacna maxima* specimen stopped growth and did not make a growth increment when the specimen was exposed to thermal stress. However, in periods B and C, the remainder (number of days – that of increments) showed more growth increments than the number of days between SST minima (5 and 4, respectively) (Figure 3). These disagreements were within counting error (±1.3 % of increments number). *Duprey et al*. [2014] suggested *T. maxima* sometimes made complex daily growth increments (sub-daily

growth increments) and it might be related to sub-daily rhythms in shell deposition itself related to sub-daily shell gaping behavior in *T. maxima*. Therefore, our specimen could also make complex growth increments and it might cause of over counting of growth increments. Although there was some uncertainty in of counting the growth increments, we could assign dates to geochemical analysis data using a daily growth increment-based chronology with 12.9%, 1.5%, and 0.9% counting error in periods A, B and C respectively (Figure 3).

4.2 Shell stable oxygen isotope ratios

In this study, the $\delta^{18}O_{sw}$ in Okinotori Island is unknown, therefore we assumed that $\delta^{18}O_{sw}$ was 0 ‰ and used the aragonitic shell bivalves relationship: T (°C) = 21.8 − 4.69 * ($\delta^{18}O$ − $\delta^{18}O_{sw}$) [Grossman and Ku, 1986] for reconstruntinon of Okinimnotori Island SST. The instrumental SST and reconstructed SST differed. Causes of the differences are considered below.

First, insufficient sampling resolution of $\delta^{18}O_{shell}$ is a likely contributing factor. In March 2005, a reconstructed SST minimum (25.7 °C) was approximately 3 °C higher than the instrumental SST minimum (22.86 °C). In March 2005, the growth increment thickness suddenly fell below 20 μm for 26 days (23rd February 2005 to 21st March 2005) with SST decrease (Figure 3b, e). The sampling point of maximum $\delta^{18}O_{shell}$ in 2005 included growth lines corresponding to 5th March to 25th March 2005. The average instrumental SST from 5th March to 25th March 2005 was 24.28 °C. Therefore, the disagreement

between the reconstructed SST and instrumental SST in March 2005, was caused by a decreasing growth rate and reduction in the temporal resolution of $\delta^{18}O_{shell}$.

Second, the higher oxygen isotope ratios of sea water may cause the difference. The reconstructed SST minimum in February 2006 (23.6 °C), corresponded with the instrumental SST minimum in February 2006 (23.48 °C). However, from April to June 2006, the reconstructed SST was 1 °C higher than the instrumental SST. In this period, high OLR indicated that insolation promoted evaporation of sea water. The evaporation might lead to higher oxygen isotope ratios of sea water. Third, thermal stress to the giant clam might cause the differences. In January 2004, the reconstructed SST minimum (24.9 °C) almost corresponded with the instrumental SST minimum (24.11 °C). However, from October 2004 to February 2005, the reconstructed SST maximum (29.2 °C) was approximately 3 °C lower than the instrumental SST maximum (32.28 °C). After three typhoons from 25th August 2004 to 7th September 2004, the instrumental SST increased 6.06 °C during the period from 7th September 2004 to 20th October 2004. This SST increase (6.06 °C) was higher than the annual average SST amplitude (4.8 °C), and the SST reached 32.38 °C on 20th October 2004. In addition, the SST above 30 °C might stress the giant clam specimen [*Andréfouët et al.*, 2013]. Instrumental SST above 30 °C continued from 26th September 2004 to 16th December 2004. Indeed, the growth increment thickness fell below 30 μm from 16th November 2004 to 22nd December 2004 (Figure 3b). The continuous high SST might hinder the growth of giant clam specimens. However, the decrease in growth caused by thermal stress was not a sufficient reason for the disagreement between the reconstructed SST and instrument SST at that time. The

two $\delta^{18}O_{shell}$ values around November to December 2004, reflected SST from 2nd November 2004 to 13th November 2004 and from 17th November 2004 to 6th December 2004, respectively (Figure 3 d, e). The average SST from 2nd November 2004 to 13th November 2004 was 31.89 °C, and the average SST from 17th November 2004 to 6th December 2004 was 30.77 °C. The disagreement between the reconstructed and instrumental SST in October 2004, was not completely explained by the reduction in the temporal resolution of $\delta^{18}O_{shell}$ with shell growth decrease.

Consequently, $\delta^{18}O_{shell}$ reflected annual SST fluctuation, while the reconstructed SST from $\delta^{18}O_{shell}$ is affected by the sampling resolution of the shell growth.

4.3 Synchronous geochemical and microstructural signals in the giant clam shell with approaching typhoons

The World Meteorological Organization (WMO) category of typhoons passing above Okinotori Island are shown as black circles (category 5: maximum wind speed above 33 m/s) and gray circles (category 3: maximum wind speed from18 to 24 m/s; category 4: maximum wind speed from25 to 32 m/s) above the SST profile (Figure 3, 4). We distinguished the typhoons affected to the specimen habitat using the WMO category and whether the typhoons were within more than 500 km from Okinotori Island. We compared the time series of $\delta^{18}O_{shell}$, Ba/Ca, and increment thickness of the giant clam specimen to metrological data (Figure 3, 4). The shell Ba/Ca and $\delta^{18}O_{shell}$ profiles showed abrupt changes during periods of typhoons approach (Figure 3, 4). In addition,

there was a decrease in increment thickness and some disturbed growth increments after typhoon approach. The shell Ba/Ca and $\delta^{18}O_{shell}$ had positive peaks and decreasing increment thickness when SST suddenly decreased in May 2004.

4.3.1 Growth increments and growth breaks -

Hippopus hippopus (Tridacnidae; Linné, 1758) closes its valves and decrease its shell growth during an intense upwelling event [*Aubert et al*., 2009] and cyclone [*Schwartzman et al*., 2011]. In addition, *Aubert et al*. [2009] suggested that abrupt SST decrease caused a decrease in growth increment thickness. Our specimen (*Tridacna maxima*) can also close its valves and decrease its shell growth when typhoon approaches. Indeed, there was a decrease in growth increment thickness during typhoon periods (Figure 3b, 4b). Cold upwelling water and strong waves caused by typhoons could stress the shell specimen. Shell growth quickly returned to normal after the typhoons (Figure 3b, 4b).

The specimen had nine growth breaks in its growth increments (see section 3.1). Previous studies revealed that the growth increment pattern of several bivalve species relates to environmental changes. For example, a growth break in hard-shell clams (*Mercenaria mercenaria*) is classified as a Freeze-shock break, Heat-shock break, Thermal-shock break, Abrasion break, Spawning break, Neap-tide break or Storm break via its microgrowth patterns [*Kennish and Olsson*, 1975]. However, sclerochronology studies of giant clam are scarce [*Aubert et al*., 2009; *Schwartzman et al*., 2011]. Daily growth increments for giant clams would be a paleoenvironmental proxy with high temporal resolution. In our results, the *T. maxima* shell specimen had some growth breaks (arrows

in Figure 2, Figure 3b, and Figure 4b). In particular, the distinct growth break around November 2005, characterized by a V-shape notch, was observed from the shell scute surface to the shell outer layer (white arrow in Figure 2d, Figure 3c, and Figure 4b). On 3rd September 2005, the most powerful typhoon passed through the meteorological observation in Okinotori Island during 1993 - 2013. Another distinct break characterized by a notch in the shell outer layer corresponded to September 2004, when continuous typhoons passed the island (Figure 4e). These growth breaks suggest that typhoons can disturb the giant clam specimen habitat; simultaneously decreasing SST would be a stress for the specimen.

Environmental factors but also ontogenetic factors cause growth breaks. For instance, a spawning break could be a factor for growth breaks. *Kubo and Iwai* [2006] reported that *T. maxima* reaches sexual maturity at approximately 120 mm of shell length or 500,000 mm^3 volume. Furthermore, *T. maxima* in Okinawa Island in southern Japan increases gonad development in spring [*Kubo and Iwai*, 2006]. Although the timing of gonadal development of *T. maxima* in Okinotori Island is unknown, our *T. maxima* specimen shell length was 12.8 mm. Thus, the specimen likely reached sexual maturity, and reproduction may cause the growth breaks in the spring of each year (Figure 4b). It is possible to differentiate spring growth breaks (mainly seasonal spawning) and fall breaks (mainly typhoons) from its seasonality.

4.3.2 $\delta^{18}O_{shell}$ and SST decrease with the typhoon

The instrumental SST rapidly decreased after typhoons approached Okinotori Island (Figure 3e, 4e, Table 1). The base of Okinotori Island is a seamount from the deep sea (approximately 2500 m) that causes upwelling [*Genin and Boehlert*, 1985]. Heavy winds due to tropical cyclones also causes upwelling [*Price, 1981*]. Consequently, typhoons approaching Okinotori Island cause upwelling and decreasing SST in the Okinotori Island reef. In addition, typhoon precipitation also causes decreased SST.

The $\delta^{18}O_{shell}$ reflected SST changes caused by typhoons (summary in Table 1).

For example, huge typhoons approached Okinotori Island on 29th August 2005 and especially 3rd September 2005 (maximum wind speed 72 m/s) (Figure 4e). The instrumental SST decreased 3.08 °C from 1st September 2005 (29.31 °C) to 7th September 2005 (after two typhoons, 26.23 °C), and the SST increased 2.56 °C to 15th September 2005 (28.79 °C) (Figure 4e). The reconstructed SST from $\delta^{18}O_{shell}$ correspondingly decreased 2.2 °C at that time (Figure 4d).

There was a sharp decline in the SST with of 2.70 °C from 20th May 2004 (29.86 °C) to 24th May 2004 (27.41 °C) without typhoon (Figure 4e). The reconstructed SST from $\delta^{18}O_{shell}$ correspondingly decreased 1.5 °C at that time (Figure 4d).

The reconstructed SST changes were sometimes smaller than the instrumental SST changes when typhoons approached. On 15th July 2005 when the typhoon approached, the instrumental SST decreased 2.17 °C from 14th July (30.28 °C) to 16th July (28.11 °C) (Figure 4e). However, the reconstructed SST from $\delta^{18}O_{shell}$ decreased 0.8 °C (Figure 4d).

The OLR decreased when the typhoons approached, suggesting the development of cumulonimbus. The cumulonimbus caused precipitation, and $\delta^{18}O_{sw}$ decreased. Rainfall

led to low $\delta^{18}O_{shell}$, and the reconstructed SST changes were consequently smaller than the instrumental SST changes, reflecting the combined effects of low $\delta^{18}O$ rainwater and high $\delta^{18}O_{shell}$ due to cooler SSTs. When typhoons approached Okinotori Island, as in September 2004 and September 2005, there were lags between the minima of the instrumental SST and the maxima for $\delta^{18}O_{shell}$ (Figure 4d, 4e, Table 1). These lags could result from the different geographical locations of the observatory and specimen. Because the location of the specimen was separated from the channel of the Okinotori Island reef, it might have delayed the SST decrease due to typhoons. Additionally, the insufficient sampling resolution could not reconstruct the minima of decreasing SST in the typhoon periods exactly.

Consequently, $\delta^{18}O_{shell}$ reflected SST decreases due to typhoons and the higher resolution $\delta^{18}O_{shell}$ may clearly reflect the SST changes caused by the typhoons.

4.3.3 Ba/Ca in *T. maxima*

Ba/Ca peaks in the *T. maxima* shell specimen appeared when a typhoon approached Okinotori Island (Figure 4a, e). *Elliot et al*. [2009] suggested that the amplitude and timing of Ba/Ca peaks in the inner layer of the *Tridacna gigas* shell reflected the increase in chlorophyll concentration associated with phytoplankton blooms. Previous studies have suggested that Ba concentration in the bivalve shell reflects the concentration of dissolved or particulate Ba in ambient sea water [*Lazareth et al*., 2003; *Vander Putten et al*., 2000] and Ba-rich phytoplankton ingested by the shell specimen [*Stecher et al*., 1996].

However, in the Tridacna shell, the exact mechanisms of Ba concentration in the shell have not been defined.

To investigate the mechanisms of Ba concentration in the Tridacna shell, we compare the Ba/Ca peaks and meteorological data. We compared the timing of the chlorophyll concentration near Okinotori Island with the Ba/Ca peaks in the shell specimen to estimate the effect of phytoplankton ingestion on the Ba/Ca peaks (Figure 4). The Ba/Ca peaks in the shell coincided with the chlorophyll peaks in April 2004, in June 2004, in September 2004, in March 2005, in April 2005, from September to November in 2005, and from April to May in 2006 (Figure 3a, 3g 4a, 4g). *Yamazaki et al*., [2011] reported that vertical mixing carried nutrients from deeper water to sea surface of Okinotori Island. Thus, the chlorophyll concentration increased during the period of the low SST and in typhoon seasons, which indicated the timing of vertical mixing and phytoplankton bloom. The Ba/Ca peaks in June 2004, March 2005, and October 2005 did not coincide with typhoons but corresponded with chlorophyll peaks and SST decreases (Figure 4a, 4e, 4g). The period of the Ba/Ca peaks did not always correspond to chlorophyll peaks. The Ba/Ca peak in June 2005, July 2005, and August 2005 when the typhoons approached Okinotori Island did not coincide with chlorophyll concentration (Figure 4a, 4g). Chlorophyll data consisted of the 8-day average of the satellite observation, and thus, the amplitude and the timing of chlorophyll concentration might be underestimated because developed cumulonimbus which estimated by low OLR values in these periods prevented satellite observation. In addition, shell Ba/Ca may be controlled not only by not ingestion of phytoplankton but also by variation in dissolved Ba in seawater. The vertical distribution

of oceanic Ba is similar to that of nutrients [e.g., *Lea et al*., 1989; *Monnin et al*., 1999]. Upwelling due to typhoons could bring Ba-rich deep sea water to the surface of the Okinotori Island reef. *Yamazaki et al*. [2011] measured coral skel*et al* Ba/Ca in *Porites lobata* from Okinotori Island during the same period as this study, suggesting that coral Ba/Ca peaks and oceanic chlorophyll peaks appeared in typhoon season and winter with the supply of nitrate from deep sea water. In addition, the coral Ba/Ca ranged from 5 to 14 μmmol/mol and averaged 6.6 μmmol/mol [*Yamzaki et al*., 2011], with different amplitude and values from the *Tridacna maxima* shell Ba/Ca (0.53 to 3.06 μmol/mol, averaged 0.79 μmol) in this study. Because Ba in the coral skeleton reflects seawater-dissolved Ba, with a partition coefficient of $D_{Ba} = [Ba/Ca]_{shell}/[Ba/Ca]_{water} \approx 1$ [*Lea et al*., 1989; *Alibert et al*., 2003], D_{Ba} in *T. maxima* might be smaller than coral D_{Ba}. Comparing the Ba/Ca results in this study to those in *Yamazaki et al*. (2011), the *T. maxima* shell Ba/Ca peaks did not appear in winter (Figure 4a, S2). The coral skel*et al* Ba/Ca peaks in winter were relatively smaller than the Ba/Ca peaks in the summer typhoon season. Thus, Ba/Ca peaks in winter did not appear in the *T. maxima* shell due to small D_{Ba}. However, Ba/Ca peaks in *T. maxima* clearly appeared in each typhoon period because the shell specimen had high temporal resolution records. Our sampling resolution (100μm spot: 2 to 6 day) was sufficient to detect the typhoons. The range of shell Ba/Ca peaks suggested the influence of typhoons continued for 12.9 day (min. 8 day and max. 21day) (Figure 4). Ba/Ca peaks in the *T. maxima* specimen shell could be affected by the upwelling of Ba-rich seawater and its ingestion by phytoplankton, which bloomed due to this upwelling.

In summary, it is expected that the shell Ba/Ca peaks, the decrease in growth increment thickness, and the increase in oxygen isotope ratio of the *T. maxima* shell in Okinotori Island will occur as follows, regarding typhoons. During a typhoon, the giant clam closes its shell, the growth of the shell decreases, the growth increment thickness decreases, and sometimes, growth breaks with a sharp decrease in thickness appeared.

Okinotori Island is an atoll on the seamount, and thus, surface seawater was mixed with cold water from below the thermocline by the typhoon, and cold deep sea water upwelled. As a result, cold deep sea water increases $\delta^{18}O_{shell}$. Since deep seawater has more Ba than surface sea water, Ba was captured from the surrounding seawater in the calcium carbonate of the shell, increasing Ba/Ca in the shell when shell growth recovered from typhoon stress. In addition, deep sea water transported by upwelling due to a typhoon and vertical mixing in winter was abundant in nutrients, sometimes causing plankton blooms (chlorophyll concentration in sea water increases). The giant clam ingested these phytoplankton, and thus, significant Ba was taken up in the shell. Moreover, when the stress of environmental factors such as abrupt SST decreases and ecological stresses such as spawning time occur, the growth increment thickness decreases, and Ba/Ca peaks may occur.

5 Conclusions

We presented seasonal variations in $\delta^{18}O_{shell}$, $\delta^{13}C_{shell}$, Ba/Ca, and growth increment thicknesses in the *Tridacna maxima* shell from Okinotori Island. By counting the daily growth increments in the shell, it is possible to determine the exact date for geochemical analysis. In addition, $\delta^{18}O_{shell}$ reflected seasonal variations in SST. When typhoons

approached Okinotori Island, the growth increment thickness decreased, $\delta^{18}O_{shell}$ increased, and the Ba/Ca showed positive peaks. The increment thickness of the *T. maxima* decreased with typhoon stress. Although, similar patterns in growth and geochemistry that occur in spring are attributed to seasonal spawning behavior rather than typhoons which are restricted to summer and fall occurrence. An increase in $\delta^{18}O_{shell}$ during typhoons reflected a decrease in SST due to the typhoon. High resolution sampling for stable isotope analysis will improve the reconstruction of SST changes during typhoon periods. Positive peaks for Ba/Ca in the shell are considered to reflect upwelling and plankton blooms resulting from typhoons. Although the cause of the Ba/Ca peaks varies by region, these results suggest that by combining the growth increments and $\delta^{18}O_{shell}$, these signals will be a useful tool to reconstruct past typhoons using giant clam shell fossils.

Acknowledgments, Samples, and Data

Sampling of Okinotori giant clam occurred with the help of the crew on the R/V *Hakuhoumaru* KH-06-2. Sections of the shell specimen were prepared with the technical support of Tsuzumi Miyaji, Hidehiko Nomura, and Kousuke Nakamura. We acknowledge Tomohisa Irino for performing stable isotope measurement and Shirai laboratory members for conducting trace element analysis. The environmental data set was provided by Chika Sakata, M.S. 2006.

We really thank the helpful comments of Associate Editor, two reviewers, and Ankur Desai, Editor of Journal of Geophysical Research-Biogeosciences.

This study was supported by JSPS KAHENHI Grant Number JP 25257207, and 15H03742.

All data from the *Tridacna maxima* specimen available in the supplemental information. The SST and the wind speed data in Okinotori Island were available in JAMSTEC Okinotori Island web site - Section 5.4 data directory (http://www.jamstec.go.jp/j/database/okitori/index.html). The weather charts in Japan were available in Japan Meteorological Agency web site (http://www.data.jma.go.jp/fcd/yoho/hibiten/index.html). The data on temporal chlorophyll-a concentrations (8-day binned data available at NASA's Ocean Color Web, http://oceancolor.gsfc.nasa.gov/) were obtained from a 9 km by 9 km pixel containing Okinotori Island in SeaWiFS (Sea-viewing Wide Field-of-view Sensor). The OLR data in Okinotori Island were obtained from The International Research Institute for Climate and Society Data library web site (Data library: NOAA NCEP CPC GLOBAL daily olr: Daily OLR 135E 20N: http://iridl.ldeo.columbia.edu/SOURCES/.NOAA/.NCEP/.CPC/.GLOBAL/.daily/.olr/) [*Liebmann and Smith*, 1996].

References

Aharon, P. (1983), 140,000-yr isotope climatic record from raised coral reefs in New Guinea, *Nature*, *304*(5928), 720–723.

Aharon, P. (1991), Recorders of reef environment histories: stable isotopes in corals, giant clams, and calcareous algae, *Coral Reefs*, *10*, 71–90, doi:10.1007/bf00571826.

Aharon, P., and J. Chappell (1986), Oxygen isotopes, sea level changes and the temperature history of a coral reef environment in New Guinea over the last 105 years, *Palaeogeogr. Palaeoclimatol. Palaeoecol.*, *56*(3–4), 337–379, doi:10.1016/0031-0182(86)90101-X.

Alibert, C., L. Kinsley, S. J. Fallon, M. T. McCulloch, R. Berkelmans, and F. McAllister (2003), Source of trace element variability in Great Barrier Reef corals affected by the Burdekin flood plumes, *Geochim. Cosmochim. Acta*, *67*(2), 231–246, doi:10.1016/S0016-7037(02)01055-4.

Andréfouët, S., S. Van Wynsberge, N. Gaertner-Mazouni, C. Menkes, A. Gilbert, and G. Remoissenet (2013), Climate variability and massive mortalities challenge giant clam conservation and management efforts in French Polynesia atolls, *Biol. Conserv.*, *160*, 190–199, doi:10.1016/j.biocon.2013.01.017

Aubert, A., C. Lazareth, G. Cabioch, H. Boucher, T. Yamada, Y. Iryu, and R. Farman (2009), The tropical giant clam *Hippopus hippopus* shell, a new archive of environmental conditions as revealed by sclerochronological and $\delta^{18}O$ profiles, *Coral Reefs*, *28*(4), 989–998, doi:10.1007/s00338-009-0538-0.

Ayling, B. F., J. Chappell, M. K. Gagan, and M. T. McCulloch (2015), ENSO variability during MIS 11 (424–374 ka) from Tridacna gigas at Huon Peninsula, Papua New Guinea, *Earth Planet. Sci. Lett.*, *431*, 236–246, doi:10.1016/j.epsl.2015.09.037.

Bonham, K. (1965), Growth Rate of Giant Clam Tridacna gigas at Bikini Atoll as Revealed by Radioautography, *Sci. New Ser.*, *149*(3681), 300–302.

Duprey, N., C. E. Lazareth, C. Dupouy, J. Butscher, R. Farman, C. Maes, and G. Cabioch (2014), Calibration of seawater temperature and $\delta^{18}O$ seawater signals in Tridacna maxima's δ 18Oshell record based on in situ data, *Coral Reefs*, *34*(2), 437–450, doi:10.1007/s00338-014-1245-z.

Elliot, M., K. Welsh, C. Chilcott, M. McCulloch, J. Chappell, and B. Ayling (2009), Profiles of trace elements and stable isotopes derived from giant long-lived Tridacna gigas bivalves: Potential applications in paleoclimate studies, *Palaeogeogr. Palaeoclimatol. Palaeoecol.*, *280*(1–2), 132–142, doi:10.1016/j.palaeo.2009.06.007.

Epstein, S., R. Buchsbaum, H. a Lowenstam, and H. C. Urey (1953), Revised Carbonate-Water Isotopic Temeprature Scale, *Geol. Soc. Am. Bull.*, *64*, 1315–1325, doi:10.1130/0016-7606(1953)64.

Fan, D., and K. Liu (2008), Perspectives on the linkage between typhoon activity and global warming from recent research advances in paleotempestology, *Chinese Sci. Bull.*, *53*(19), 2907–2922.

Forsyth, A. J., J. Nott, and M. D. Bateman (2010), Beach ridge plain evidence of a variable late-Holocene tropical cyclone climate, North Queensland, Australia, *Palaeogeogr. Palaeoclimatol. Palaeoecol.*, *297*(3–4), 707–716, doi:10.1016/j.palaeo.2010.09.024.

Frappier, A. B. (2008), A stepwise screening system to select storm-sensitive stalagmites: Taking a targeted approach to speleothem sampling methodology, *Quat. Int.*, *187*(1), 25–39, doi:10.1016/j.quaint.2007.09.042.

Genin, A., and G. W. Boehlert (1985), Dynamics of temperature and chlorophyll structures above a seamount: An oceanic experiment, *J. Mar. Res.*, *43*(4), 907, doi:10.1357/002224085788453868.

Gillikin, D. P., F. Dehairs, A. Lorrain, D. Steenmans, W. Baeyens, and L. André (2006), Barium uptake into the shells of the common mussel (Mytilus edulis) and the potential for estuarine paleo-chemistry reconstruction, *Geochim. Cosmochim. Acta*, *70*(2), 395–407, doi:10.1016/j.gca.2005.09.015.

Goodwin, D. H., B. R. Schöne, D. L. Dettman, D. H. Goodwin, and B. R. Scho (2003), Resolution and Fidelity of Oxygen Isotopes as Paleotemperature Proxies in Bivalve Mollusk Shells : Models and Observations Resolution and Fidelity of Oxygen Isotopes as Paleotemperature Proxies in Bivalve Mollusk Shells : Models and Observations, , *18*(2), 110–125.

Grace, M., P. G. Faylona, C. E. Lazareth, A. Sémah, S. Caquineau, H. Boucher, W. P. Ronquillo, H. Varagnat, and B. Cedex (2011), Preliminary Study on the Preservation of Giant Clam (Tridacnidae) Shells from the Balobok Rockshelter Archaeological, , *26*(6), 888–901, doi:10.1002/gea.20377.

Grossman, E. L., and T. L. Ku (1986), Oxygen and carbon isotope fractionation in biogenic aragonite: temperature effects., *Chem. Geol.*, *59*, 59–74.

Haig, J., J. Nott, and G.-J. Reichart (2014), Australian tropical cyclone activity lower than at any time over the past 550-1,500 years., *Nature*, *505*(7485), 667–71, doi:10.1038/nature12882.

Hetzinger, S., M. Pfeiffer, W. C. Dullo, N. Keenlyside, M. Latif, and J. Zinke (2008), Caribbean coral tracks Atlantic Multidecadal Oscillation and past hurricane activity, *Geology*, *36*(1), 11–14, doi:10.1130/G24321A.1.

Horibe, Y., and T. Oba (1972), Temperature scales of aragonite-water and calcite-water system, Fossils, 23/24, 69-79

Horton, B. P., V. Rossi, and A. D. Hawkes (2009), The sedimentary record of the 2005 hurricane season from the Mississippi and Alabama coastlines, *Quat. Int.*, *195*(1–2), 15–30, doi:10.1016/j.quaint.2008.03.004.

Iwao, N., Junichi, K., Hidetoshi, F., Hirohumi and Hirohumi, Y. (2002), Marine Weather Observation at Oki-no-tori Sima, Meteorological Society of Japan, 49(7), 569-579

Jones, D. S., D. F. Williams, and C. S. Romanek (1986), Life History of Symbiont-Bearing Giant Clams from Stable Isotope Profiles, , *231*(4733), 46–48.

Kennish M. J., and Olsson, R. K., 1975, Effect of thermal discharges on the microstructural growth of *Mercenaria mercenaria,* Environ. Geol. 1:41-64.

Kilbourne, K. H., R. P. Moyer, T. M. Quinn, and A. G. Grottoli (2011), Testing coral-based tropical cyclone reconstructions: An example from Puerto Rico, *Palaeogeogr. Palaeoclimatol. Palaeoecol.*, *307*(1–4), 90–97, doi:10.1016/j.palaeo.2011.04.027.

Klumpp, D. W. (1992), Nutrition of the giant clam Tridacna gigas (L.) I. Contribution of filter feeding and photosynthates to respiration and growth, *J. Exp. Mar. Bio. Ecol.*, *155*, 105–122, doi:10.1016/0022-0981(92)90030-E.

Komagoe, T., T., Watanabe, K., Shirai, A., Yamazaki, and M. Uemasu, High temporal resolution analysis for palaeo environments using giant clam shells: Elongate giant

clam *Tridacna maxima* shell reveals typhoon events Okinotori Island, Japan, Kaiyo extra, 56, 80-93

Kubo, H. and K., Iwai (2006), Seasonal fluctuation on gonadal maturation of *Tridacna maxima*, Annual Report of Okinawa Fishery and Ocean Research Center, 68: 211–214.

Lazareth, C. E., E. Vander Putten, L. André, and F. Dehairs (2003), High-resolution trace element profiles in shells of the mangrove bivalve Isognomon ephippium: A record of environmental spatio-temporal variations?, *Estuar. Coast. Shelf Sci.*, *57*(5–6), 1103–1114, doi:10.1016/S0272-7714(03)00013-1.

Lea, D. W., G. T. Shen, and E. A. Boyle (1989), Coralline barium records temporal variability in equatorial Pacific upwelling, *Nature*, *340*, 373–376, doi:10.1038/340373a0.

Li, Z. H., N. Labbé, S. G. Driese, and H. D. Grissino-Mayer (2011), Micro-scale analysis of tree-ring δ18O and δ13C on α-cellulose spline reveals high-resolution intra-annual climate variability and tropical cyclone activity, *Chem. Geol.*, *284*(1–2), 138–147, doi:10.1016/j.chemgeo.2011.02.015.

McClain, C. R., G. C. Feldman, and S. B. Hooker (2004), An overview of the SeaWiFS project and strategies for producing a climate research quality global ocean bio-optical time series, *Deep Sea Res. Part II Top. Stud. Oceanogr.*, *51*(1–3), 5–42, doi:10.1016/j.dsr2.2003.11.001.

Moir, B. G. (1985), Review of Trdacnid Ecology and Some Possible Implications for Archaeological Research, *Asian Perspect.*

Monnin, C., C. Jeandel, T. Cattaldo, and F. Dehairs (1999), The marine barite saturation state of the world ' s oceans, , 253–261.

Muller, J., J. M. Collins, S. Gibson, and L. Paxton (2017), Recent Advances in the Emerging Field of Paleotempestology, in *Hurricanes and Climate Change*, pp. 1–33, Springer.

Nakano, I., H. Fujimori, and J. Kimura (2001), Marine Weather Observation at Oki-no-Tori Sima, *JAMSTECR*, 43, 143-152.

Nott, J. (2011), A 6000 year tropical cyclone record from Western Australia, *Quat. Sci. Rev.*, *30*(5–6), 713–722, doi:10.1016/j.quascirev.2010.12.004.

Nott, J., and A. Forsyth (2012), Punctuated global tropical cyclone activity over the past 5,000 years, *Geophys. Res. Lett.*, *39*(14), 1–5, doi:10.1029/2012GL052236.

Nott, J., S. Smithers, K. Walsh, and E. Rhodes (2009), Sand beach ridges record 6000 year history of extreme tropical cyclone activity in northeastern Australia, *Quat. Sci. Rev.*, *28*(15–16), 1511–1520, doi:10.1016/j.quascirev.2009.02.014.

Okai, T., A. Suzuki, S. Terashima, M. Inoue, M. Nohara, H. Kawahata, and N. Imai (2004), Collaborative analysis of GSJ/AIST geochemical reference materials JCp-1 (Coral) and JCt-1 (Giant Clam), *Chikyukagaku (Geochemistry)*, *38*, 281–286.

Pätzold, J., J. . Heinrichs, K. Wolschendorf, and G. Wefer (1991), Correlation of stable oxygen isotope temperature record with light attenuation profiles in reef-dwelling Tridacna shells, *Coral Reefs*, *10*, 65–69, doi:10.1007/bf00571825.

Price, J. F. (1981), Upper Ocean Response to a Hurricane, *J. Phys. Oceanogr.*, *11*(2), 153–175, doi:10.1175/1520-0485(1981)011<0153:UORTAH>2.0.CO;2.

Putten, E. Vander, F. Dehairs, E. Keppens, and W. Baeyens (2000), High resolution distribution of trace elements in the calcite shell layer of modern Mytilus edulis: Environmental and biological controls, *Geochim. Cosmochim. Acta*, *64*(6), 997–1011, doi:10.1016/S0016-7037(99)00380-4.

Romanek, C. S., and E. L. Grossman (1989), Stable isotope profiles of Tridacna maxima as environmental indicators, *Palaios*, 402–413.

Rosewater, J. (1965), *The family Tridacnidae in the indo-pacific*, Department of Mollusks, Academy of Natural Sciences of Philadelphia.

Sano, Y., S. Kobayashi, K. Shirai, N. Takahata, K. Matsumoto, T. Watanabe, K. Sowa, and K. Iwai (2012), Past daily light cycle recorded in the strontium/calcium ratios of giant clam shells, *Nat. Commun.*, *3*, 761, doi:10.1038/ncomms1763.

Schone, B. R., E. Dunca, J. Fiebig, and M. Pfeiffer (2005), Mutvei's solution: An ideal agent for resolving microgrowth structures of biogenic carbonates, *Palaeogeogr. Palaeoclimatol. Palaeoecol.*, *228*(1–2), 149–166, doi:DOI 10.1016/j.palaeo.2005.03.054.

Schwartzmann, C., G. Durrieu, M. Sow, P. Ciret, C. E. Lazareth, and J.-C. Massabuau (2011), In situ giant clam growth rate behavior in relation to temperature: A one-year coupled study of high-frequency noninvasive valvometry and sclerochronology, *Limnol. Oceanogr.*, *56*(5), 1940–1951, doi:10.4319/lo.2011.56.5.1940.

Shirai, K., T. Kawashima, K. Sowa, T. Watanabe, T. Nakaniori, N. Takahata, H. Arnakawa, and Y. Sano (2008), Minor and trace element incorporation into

branching coral Acropora nobilis skeleton, *Geochim. Cosmochim. Acta*, *72*(22), 5386–5400, doi:DOI 10.1016/j.gca.2008.07.026.

Shupe, M. D., and J. M. Intrieri (2004), Cloud radiative forcing of the Arctic surface: The influence of cloud properties, surface albedo, and solar zenith angle, *J. Clim.*, *17*(3), 616–628, doi:10.1175/1520-0442(2004)017<0616:CRFOTA>2.0.CO;2.

Stecher, H. A., D. E. Krantz, C. J. Lord, G. W. Luther, and K. W. Bock (1996), Profiles of strontium and barium in Mercenaria mercenaria and Spisula solidissima shells, *Geochim. Cosmochim. Acta*, *60*(18), 3445–3456, doi:10.1016/0016-7037(96)00179-2.

Toratani, M. (2008), Primary production enhancement by typhoon Ketsana in 2003 in western North Pacific, in *Asia-Pacific Remote Sensing*, p. 715013, International Society for Optics and Photonics.

Urey, H. C., H. A. Lowenstam, S. Epstein, and C. R. McKinney (1951), Measurement of Paleotemperatures and Temperatures and the Southeastern United States, *Bull. Geol. Soc. Am.*, *62*(April), 399–416.

Warter, V., and W. Müller (2017), Daily growth and tidal rhythms in Miocene and modern giant clams revealed via ultra-high resolution LA-ICPMS analysis—A novel methodological approach towards improved sclerochemistry, *Palaeogeogr. Palaeoclimatol. Palaeoecol.*, *465*, 362–375.

Warter, V., W. Muller, F. P. Wesselingh, J. A. Todd, and W. Renema (2015), Late miocene seasonal to subdecadal climate variability in the indo-west pacific (east

kalimantan , indonesia) preserved in giant clams, *Palaios*, *30*, 66–82, doi:10.2110/palo.2013.061.

Watanabe, T., and T. Oba (1999), Daily reconstruction of water temperature from oxygen isotopic ratios of a modern Tridacna shell using a freezing microtome sampling technique, *JGR-Oceans*, *104*(C9), 20,667, doi:10.1029/1999jc900097.

Watanabe, T., A. Suzuki, H. Kawahata, H. Kan, and S. Ogawa (2004), A 60-year isotopic record from a mid-Holocene fossil giant clam (Tridacna gigas) in the Ryukyu Islands: Physiological and paleoclimatic implications, *Palaeogeogr. Palaeoclimatol. Palaeoecol.*, *212*(3–4), 343–354, doi:10.1016/j.palaeo.2004.07.001.

Williams, H. F. L. (2012), Magnitude of Hurricane Ike storm surge sedimentation: Implications for coastal marsh aggradation, *Earth Surf. Process. Landforms*, *37*(8), 901–906, doi:10.1002/esp.3252.

Woodruff, J. D., J. P. Donnelly, and A. Okusu (2009), Exploring typhoon variability over the mid-to-late Holocene: evidence of extreme coastal flooding from Kamikoshiki, Japan, *Quat. Sci. Rev.*, *28*(17–18), 1774–1785, doi:10.1016/j.quascirev.2009.02.005.

Yamazaki, A., T. Watanabe, N. O. Ogawa, N. Ohkouchi, K. Shirai, M. Toratani, and M. Uematsu (2011), Seasonal variations in the nitrogen isotope composition of Okinotori coral in the tropical western Pacific: A new proxy for marine nitrate dynamics, *J. Geophys. Res.*, *116*(G4), G04005, doi:10.1029/2011JG001697.

Yoneyama, S., K., Seno, H., Maeda, A., Okada, and T., Hayashibara (2006), Marine animals on the coral reefs of Okino-torishima, Tokyo Metropolitan Research on Fisheries Science, 1, 73-85

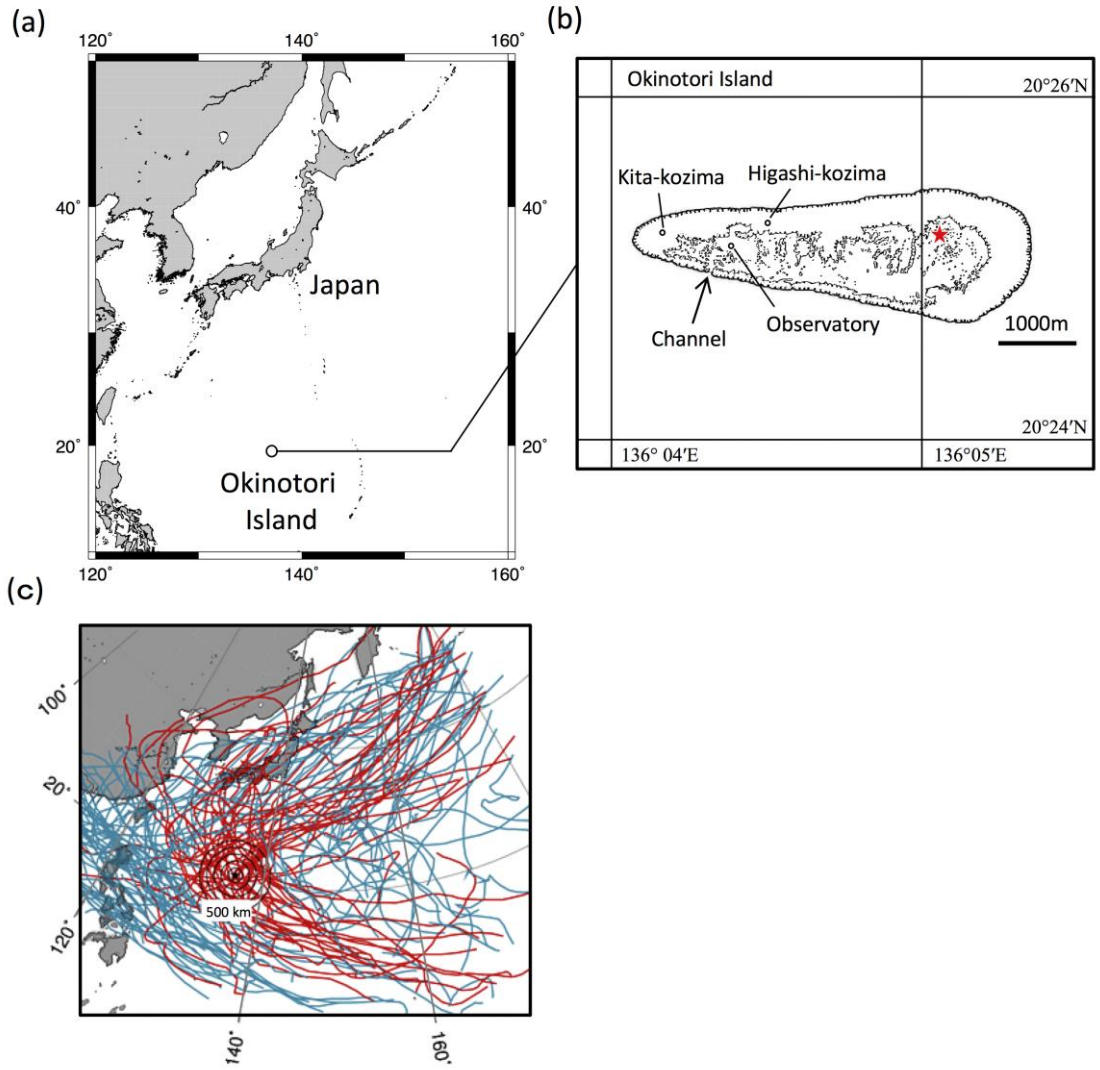

Figure 1. (a) Location of Okinotori Island (black circle; 20°25′N, 136°05′E). (b) Okinotori (20°25′N, 136°05′E) and sampling point (star), and (c) trajectory of typhoons 1993 – 1998 (Modified from Iwao *et al*., 2002). Okinotori Island locates passage of typhoons approach Japan. 46 (red) of 157 (blue) typhoons passed in radius of 500km from Okinotori Island.

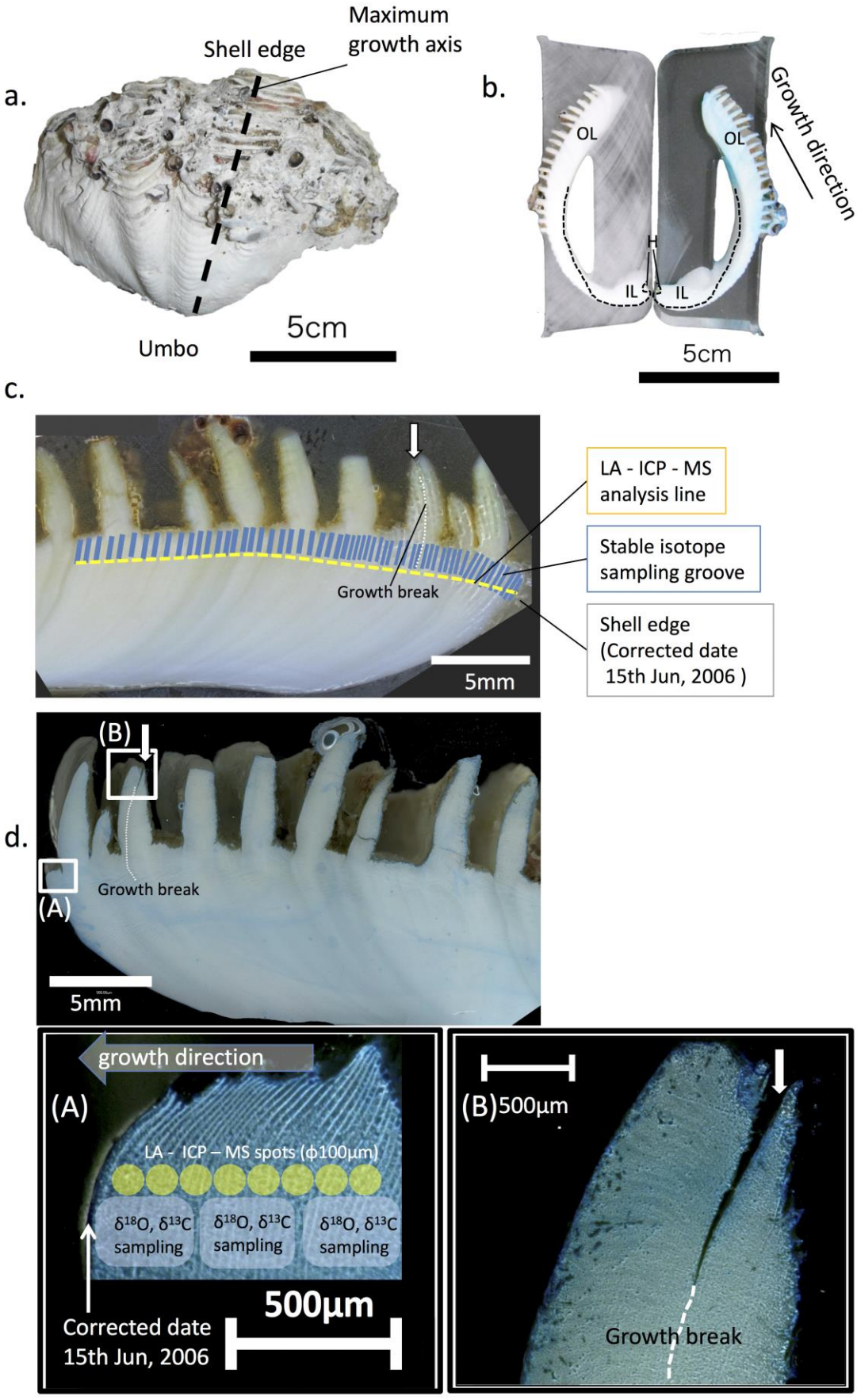
a.
Maximum growth axis
Shell edge
Umbo
5cm
b.
OL
OL
Growth direction
H
IL
IL
5cm
c.
Growth break
5mm
LA - ICP - MS analysis line
Stable isotope sampling groove
Shell edge (Corrected date 15th Jun, 2006)
d.
(B)
(A)
Growth break
5mm
growth direction
(A)
LA - ICP – MS spots (ϕ100μm)
δ18O, δ13C sampling
δ18O, δ13C sampling
δ18O, δ13C sampling
500μm
Corrected date 15th Jun, 2006
(B)500μm
Growth break

Figure 2. The shell samples of *Tridacna maxima specimen*. (a) The whole *Tridacna maxima* valve. The dotted line shows maximum growth axis. (b) Thick shell sections from maximum growth axis. The left one is for geochemical analysis and the right one is for sclerochronological analysis, outer layer (OL), inner layer (IL), hinge area (H), (c) sampling design for geochemical analysis, and (d) microscopic image of the shell microgrowth lines. (A) is enlarge image of the shell edge and shows sampling design for geochemical analysis in another shell section and (B) is enlarge image of the growth break in the shell ornamentation. The growth break continued to sampling line.

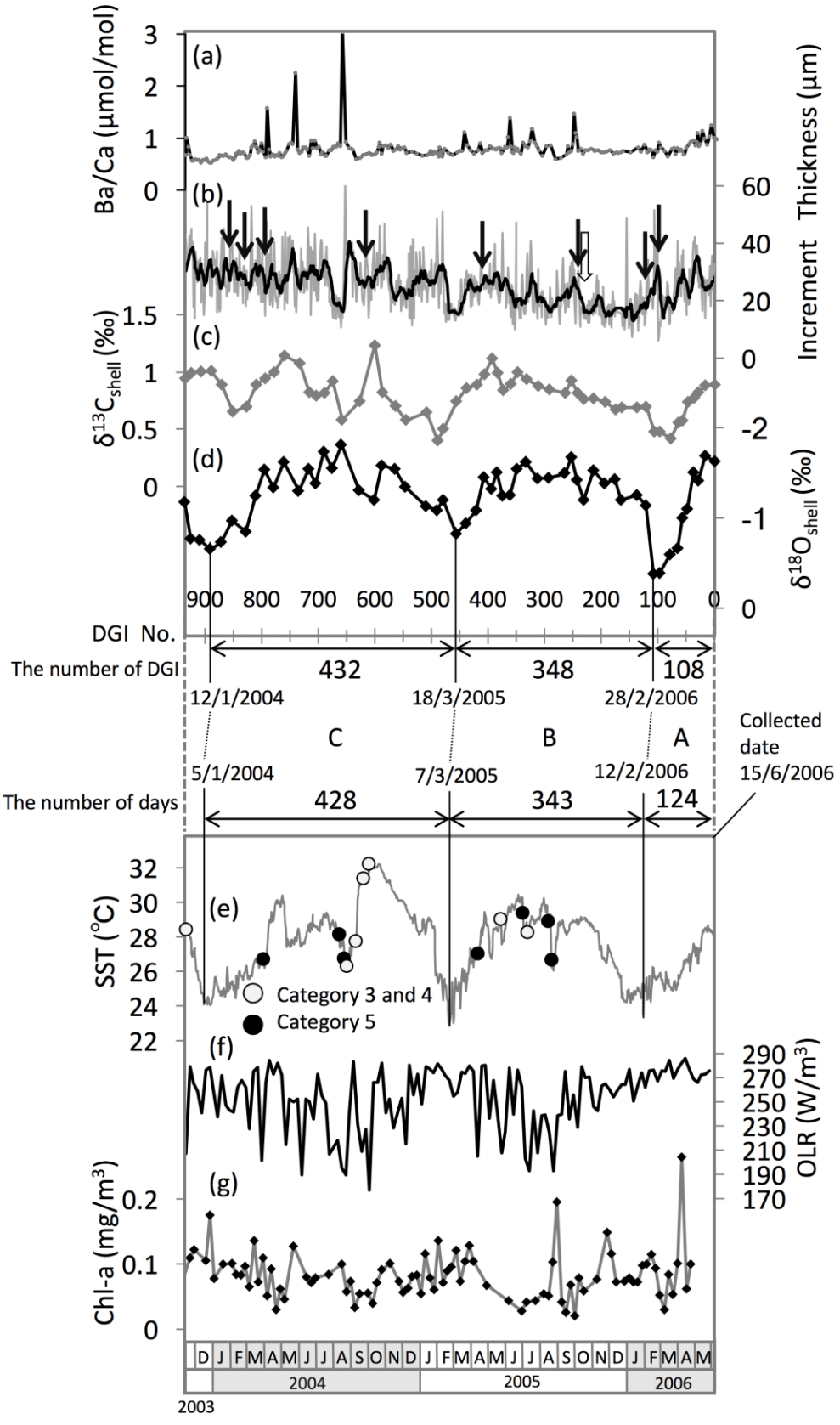
(a)
(b)
(c)
(d)
(e)
(f)
(g)
Ba/Ca (µmol/mol)
Increment Thickness (µm)
δ13Cshell (‰)
δ18Oshell (‰)
SST (°C)
OLR (W/m3)
Chl-a (mg/m3)
DGI No.
The number of DGI
432
348
108
12/1/2004
18/3/2005
28/2/2006
C
B
A
Collected date 15/6/2006
5/1/2004
7/3/2005
12/2/2006
The number of days
428
343
124
Category 3 and 4
Category 5
D J F M A M J J A S O N D J F M A M J J A S O N D J F M A M
2004
2005
2006
2003

Figure 3. The time series of the geochemical and sclerochronological profiles in the *Tridacna maxima* shell and the environmental data of Okinotori Island.

(a) Ba/Ca ratio in the shell, (b) growth increment thickness in the shell (thin line: row plots, solid line: 10-day average plots). Black and white arrows show growth breaks and white one is distinct growth break (see Fig.2), (c) carbon isotope ratio in the shell ($\delta^{13}C_{shell}$), and (d) oxygen isotope ratio in the shell ($\delta^{18}O_{shell}$). The $\delta^{18}O$ y-axis is reversed for better comparison with the instrumental SST data. The numbers below the profile are the number of DGI (DGI: daily growth increments) between $\delta^{18}O_{shell}$ minima to the other minima. (e) Daily sea surface temperature (SST) from the observatory of Japan Agency for Marine-Earth Science and Technology (JAMSTEC). The numbers above the profile are the number of the days between SST minima to the other minima. Category of the typhoons passing above Okinotori Island was shown as black circles (category 5: maximum wind speed larger than 33 m/s) and gray circles (category 3: maximum wind speed 18 to 24 m/s, category 4: maximum wind speed 25 to 32 m/s) above the SST profile. Maximum wind speed is 10-minute average of wind speed, (f) weekly outgoing long-wave radiation (OLR) from satellite data of NOAA, and (g) Chl-a concentration calculated from 8-day composite image of Sea WiFS.

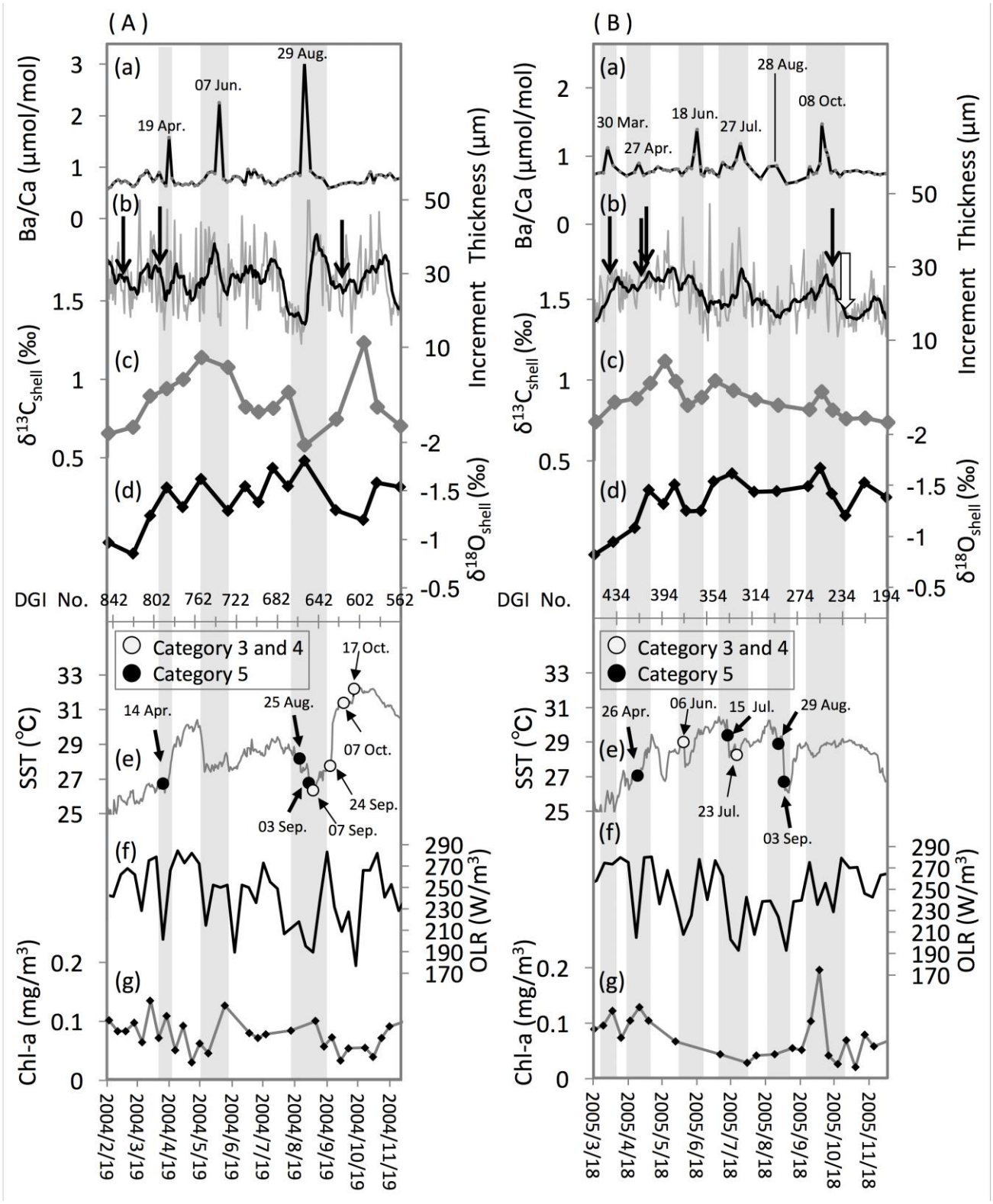
(A)
(B)
(a)
(b)
(c)
(d)
(e)
(f)
(g)
Ba/Ca (μmol/mol)
Increment Thickness (μm)
δ13Cshell (‰)
δ18Oshell (‰)
DGI No.
842 802 762 722 682 642 602 562
434 394 354 314 274 234 194
19 Apr.
07 Jun.
29 Aug.
30 Mar.
27 Apr.
18 Jun.
27 Jul.
28 Aug.
08 Oct.
Category 3 and 4
Category 5
SST (°C)
14 Apr.
25 Aug.
17 Oct.
07 Oct.
24 Sep.
03 Sep.
07 Sep.
26 Apr.
06 Jun.
15 Jul.
29 Aug.
23 Jul.
03 Sep.
OLR (W/m3)
Chl-a (mg/m3)
2004/2/19
2004/3/19
2004/4/19
2004/5/19
2004/6/19
2004/7/19
2004/8/19
2004/9/19
2004/10/19
2004/11/19
2005/3/18
2005/4/18
2005/5/18
2005/6/18
2005/7/18
2005/8/18
2005/9/18
2005/10/18
2005/11/18

Figure 4. Enlarge images of typhoon periods described in Figure 3. (A) 2004 and (B) 2005

typhoon periods respectively. (a) Ba/Ca ratio in the shell, vertical lines show the Ba/Ca peaks. (b) Growth increment thickness in the shell (thin line: row plots, solid line: 10-day average plots). Black and white arrows show growth breaks and white one is distinct growth break (see Fig.2), (c) carbon isotope ratio in the shell ($\delta^{13}C_{shell}$), and (d) oxygen isotope ratio in the shell ($\delta^{18}O_{shell}$). The $\delta^{18}O$ y-axis is reversed for better comparison with the instrumental SST data. (e) Daily sea surface temperature (SST), (f) weekly outgoing long-wave radiation (OLR) from satellite data of NOAA, and (g) Chl-a concentration calculated from 8-day composite image of Sea WiFS.

Year	2004		2005		
Typhoon date	No typhoon	25th Aug., 3rd Sep., and 7th Sep.	6th Jun	15th Jul., and 23rd Jul.	29th Aug., and 3rd Sep.
SST decrease periods (days)	20th to 24th May (5)	3rd Aug. to 7th Sep. (35)	6th Jun. to 16th Jul. (11)	15th Jul. to 30th Jul. (16)	1st Sep. to 14th Sep. (15)
Instrumental SST changes (℃)	2.45	3.09	1.3	2.17	3.08
Reconstructed SST period (days)	20th May to 15th Jun (26)	29th Aug. to 29th Sep. (31)	29th May to 8th Jun (10)	19th Jul. to 8th Aug. (20)	25th Sep. to 28th Oct. (33)
Reconstructed SST changes (℃)	1.5	2.8	1.2	0.8	2.2
$\delta^{18}O_{shell}$ changes (‰)	0.33	0.59	0.26	0.18	0.47

Table 1. The instrumental and reconstructed SST changes during typhoon period and SST decrease period.

SST decrease periods (days) indicate the SST decrease period due to the typhoons. Instrumental SST (℃) indicate the amplitude of instrumental SST changes during the typhoon period. Reconstructed SST periods (days) were decided using daily growth increment dating. Reconstructed SST (℃) and $\delta^{18}O_{shell}$ changes (‰) showed the amplitude of reconstructed SST and $\delta^{18}O_{shell}$ changes during the typhoon period respectively.

Chapter 4: **Late Pleistocene MIS 3 high temporal resolution climate reconstruction using giant clam fossils in Kikai Island, Japan**

1. Introduction

Pleistocene was 258.8 million years ago (Ma) to 0.0117 Ma and has been characterized by glacial-interglacial climates. Especially, Marine Isotope Stage 3 (MIS-3) has been characterized by short cycle and high amplitude climate changes known as Dansgaard-Oeschger cycles [Dansgaard *et al.*, 1993] . Besides, MIS-3 was the period of drastic changes in human history. For example, extinction of Neanderthal and immigration of Homo sapiens to Europe[Andel, 2002; d'Errico and Goñi, 2003]. For example, Ice core, and lake deposits have been used for reconstructing MIS-3 climate changes [Van Meerbeeck *et al.*, 2011; Swann *et al.*, 2005]. These paleo environments proxies have several dozen to hundred years resolution even so using high temporal resolution methods. On the other hand, coral skeleton and bivalve shell have daily to centennial temporal resolution climate information. Thus, we can evaluate the influence of climate changes for the human society using coral skeleton and bivalve shell.

Kikai island, Kagoshima, Japan is characterized by a high uplifted rate, which was estimated to be 1.7 m/kyr based on the altitude of the MIS-5e terrace on top of the island [Ota and Omura, 1992]. This characteristic allows us to obtain fossil coral or giant clam specimens from late Pleistocene to Holocene continuously. Especially, the sea level of MIS-3 was 30 m lower than that of today(Sasaki *et al.*, 2004), MIS-3 coral reefs is unique and limited in high uplift area such as Huon peninsula in Papua New guinea, and

Kikai island. In addition, Kikai island where locates between North-pacific and East China sea has been affected by monsoon and typhoon. Thus, Kikai island is an unique site for revealing the climate changes in Pleistocene to Holocene East Asia.

In this study, fossil and modern giant clam shell specimens were obtained from up rifted coral reefs in Kikai island to reconstruct MIS-3 short term climate changes.

2. Materials and Methods

2-1. Giant clam shell samples

The three fossil and one modern giant clam shell specimens were obtained from Kikai island (Figure 4-1). The soft tissues of modern specimen were removed immediately. The sample ages were datamined using radiocarbon date for Holocene samples and U/Th date of the coral fossil which was obtained from same stratigraphy (Nalkaya *et al*., 2016, Watanabe T. K. in preparation). The species of the fossil giant clam specimens were decided by shell form shows in Table 4-1. The shell was cut in two 5-mm-thick sections with a stonecutter (blade thickness 0.5 mm), along the maximum growth axis.

2-2. Evaluation of diagenetic alternation and dating in fossil samples

It is important to evaluate the fossil preservation when reconstruct paleo environment using fossil biogenetic carbonates. In fossil giant shell specimen, the pristine shell aragonite sometimes altered to calcite, and or secondly aragonite precipitation occurred [Faylona *et al.*, 2011] . For example, the concentration of trace element in the altered coral skeleton and giant clam shell did not preserve original values (Coral

skeleton: McGregor and Gagan, 2003, Giant clam shell: Warter *et al.*, 2015). Mineral phase of fossil specimens was checked using X-ray diffraction machine (MiniFlex II) in Hokkaido University Institute for the Advancement of Higher Education. In order to evaluate diagenetic alternation, the shell thin section observation by optical microscope and scanning electron microscope (SEM) observation were performed.

The sample ages were datamined using radiocarbon date (Yamagata university) for Holocene samples and U/Th date of the coral fossil which was obtained from same stratigraphy (Nalkaya *et al*., 2016, Watanabe T. K. in preparation). OxCal 4.21 (Ramsey *et al*., 2009) was used for calendar year calibration of 14C dating, and Marine 13 (Reimer *et al*., 2013) was used for calibration curve data.

2-3. Sclerochronological analysis of giant clam shell

The shell specimens were cut in two 5-mm-thick sections with a stonecutter (blade thickness 0.5 mm), along the maximum growth axis. One of the sections was polished to make thin section (~100 μm thickness) and took panoramic photos using digital microscope (KEYENCE VHX-2000). The growth increment thicknesses were measured using image processing software ImageJ [Abramoff *et al*., 2004].

2-4. Stable oxygen and carbon isotope ratios in giant clam shell

Another shell section was used for geochemical analysis. The shell samples were milled with 300 μm width using micro cross slide tables (KISO POWER TOOL

MFG.CO., LTD.) attached hand drill (HP-200S, Tokyo associates Co., Ltd., Japan） with dental drill bit (Fissher curva Shohu Co., Ltd., Japan). The 20 to 40 μg powder samples were reacted with 100% phosphoric acid at 70 °C in a carbonate preparation device (Kiel IV Carbonate preparation device), and the produced CO_2 was analyzed using a stable isotope ratio mass spectrometer (Thermo Scientific MAT 253) in Hokkaido University. Isotope ratios ($\delta^{18}O$ and $\delta^{13}C$) were one-point calibrated against National Bureau of Standards (NBS) 19 and reported in standard δ notation relative to Vienna Pee Dee belemnite (VPDB) and confirmed the calibration using NBS 18. The standard deviations (1σ) for 22 replicate measurements of NBS 19 are 0.12 ‰ and 0.04 ‰ for $\delta^{18}O$ and $\delta^{13}C$ as external long-term reproducibility throughout this study,

2-5. Trace elements in giant clam shell

MIS-3 fossil specimen's barium and calcium concentrations were analyzed by Laser Ablation Inductively Coupled Plasma Mass Spectrometry (LA-ICP-MS) (Agilent 7700 ICP-MS coupled with New Wave Research NWR193 laser ablation system: 193 nm ArF excimer laser (pulse width <5 ns)) along the same sampling line used for isotopic analysis sampling. The laser conditions were below; irradiance 0.82 GW/cm^2, repetition rate 10 Hz, and 40 second of laser duration. The sample surface was cleaned by 5 seconds of pre-ablation. The shell sample was ablated using a 100-μm laser spot, and each spot was 1 spot per 500μm along analytical line. The calibration of the signal intensity to the Ba/Ca ratio was performed using glass standard materials: NIST 612 standard grass

distributed by the National Institute of Standard and Technology [*Shirai et al*., 2008]. ^{43}Ca was used as an internal standard, and ^{138}Ba was expressed in terms of its molar ratio to ^{43}Ca. The analytical error for the Ba/Ca ratio (relative standard deviation) was within 3.86 % (n = 42, 1σ NIST612) as external long-term reproducibility throughout this study.

Barium calcium ratio in modern shell specimen was measured using Inductively Coupled Plasma Atomic Emission Spectrometry (ICP-AES; Thermo scientific iCAP6100) connected with ultrasonic nebulizer (DBA CETAC Technologies U-5000AT^{+}). The samples were same powder for stable isotope analysis. Each sample weighted within 115~128 μg and dissolved with 280 μl of 25 % nitric acid. Then, the samples solution diluted with milli-Q water to adjust 9 ppm of calcium concentration. The calibration of the signal intensity to the Ba/Ca ratio was performed using GSJ certified geochemical reference material JCt-1 Giant Clam (*Tridacna gigas*) [*Okai et al*., 2004].

2-6. Meteorological data and SST in Kikai island

Meteorological data in Kikai island from 2008 to 2015 was obtained from Japan Meteorological Agency web page (http://www.data.jma.go.jp/obd/stats/etrn/). Sea surface temperature (SST) surrounding Kikai island data set was obtained from Advanced Very High-Resolution Radiometer: (AVHRR)（IRI/LDEO Climate Data Library : http://iridl.ldeo.columbia.edu）.

3. Results

3-1. Preservation and dating of the fossil giant clam samples

In X-ray diffraction, there were no significant calcite peak (Fig. 4-2). In addition, there were no significant altered aragonite or dissolved aragonite with SEM observation. Moreover, modern and fossil shell thin section also had clear growth increments (Fig. 4-2). Thus, these fossil samples were suitable for geochemical analysis.

Two Holocene fossil samples (KFT-02 and KFT-03) were 7,220±45 and 3,924±49 years ago respectively with radiocarbon dating (2σ). $^{230}Th/^{234}U$ date of the coral fossil which was obtained from same stratigraphy with the late Pleistocene sample (KFT-01) was 55,794±195 years ago (Watanabe T. K. in preparation).

3-3. Sclerochronological result

The summary of giant clam shell sclerochronological results showed in Table 4-2. The growth increments in the shell thin section appeared under microscopic observation as a pair of dark and light-colored bands (Fig. 4-3). There were 2406 increments observed in the modern shell thin section (KSTm150613). The thickness of the increments in KSTm150613 ranged 6.77 to 83.32 μm, and the average thickness was 27.27 μm. There were almost clear growth increments, but also there were sometimes unclear growth increment such as translucent layer in shell edge for instance (Fig. 4-3).

In Holocene fossil samples KFT-02 and KFT-03, there was 1148 and 1300 increments observed in the shell thin sections respectively. The thickness of the increments in KFT-02 and KFT-03 ranged 5.47 to 113.82 μm and 8.44 to 96.91 μm, and the average thickness were 34.47 μm and 28.97 μm. In late Pleistocene MIS-3 fossil

sample KFT-01, there were 2683 increments observed. The thickness of the increments in KFT-01 ranged 6.79 to 98.83 μm, and the average thickness was 29.50 μm. There were 12 growth breaks in the shell outer layer.

3-4. Geochemical analyses in the shell specimens

The summary of giant clam shell stable oxygen and carbon isotope ratios ($\delta^{18}O_{shell}$ and $\delta^{13}C_{shell}$) showed in Table 4-3. $\delta^{18}O_{shell}$ in each modern and fossil sample showed clear annual cycles.

The Ba/Ca ratios of the modern KSTm150613 ranged from 1.17 to 255.35 μmol/mol, with an average of 4.60 μmol/mol (n = 138) (Fig. 4-6). The Ba/Ca ratios of the MIS-3 sample KFT-01 ranged from 1.33 to 93.29 μmol/mol, with an average of 5.51 μmol/mol (n = 138) (Fig. 4-6). Both modern and MIS-3 shell sample showed Ba/Ca peaks corresponded with $\delta^{18}O_{shell}$ maxima (Fig. 4-6).

3-5. Chronology for geochemical

Giant clam makes daily growth increments and it is a useful characteristic for chronology to the shell geochemical data (Duprey *et al*., 2014; Komagoe *et al*., 2018). However, giant clam sometimes does not make the growth increments daily basis (Komagoe *et al*., 2016) and it makes growth increments basis chronology difficult. The age model for modern KSTm150613 was established using the relationship between the $\delta^{18}O_{shell}$ profiles and SST (Fig. 4-5). As time control points, the maxima for the $\delta^{18}O_{shell}$ were tied to the minima for SST. In MIS-3 fossil samples, the number of growth

increments between the maxima for the $\delta^{18}O_{shell}$ were 324, 316, 296, 329, 219, 272, 243 and 251. In addition, the growth breaks in KFT-01 suggested the hiatus of the shell growth (Fig. 4-6). The age model for MIS-3 KFT-01 was established using the relationship between the $\delta^{18}O_{shell}$ profiles and SST minima which assumed as February 1 (Fig. 4-6). In modern Kikai island, the average SST minimum was almost Februaly (Fig. 4-7). To convert distances into dates, the growth rate was assumed to be constant during each of the tied points. Then, chronology for the growth increments were decided to compare growth increments and geochemical sampling points. The time series of the geochemical and sclerochronological profiles in the modern and fossil specimen were showed in Figure 4-7.

4. Discussion

4-1. Shell stable oxygen isotope ratios

To compare the modern monthly Kikai island SST and $\delta^{18}O_{shell}$ changes, reconstructed SST was calculated using he aragonitic shell bivalves relationship: equation $T\ (℃) = 21.8 - 4.69\ (\delta^{18}O - \delta 18O_{sw})$ [Grossman and Ku (1986)] (Fig. 4-7). The average annual amplitude of salinity in Kikai island was 34.48 ‰ (August) to 34.9 ‰ (February) and it was 0.18 ‰ changes in sea water $\delta^{18}O$ ($\delta^{18}O_{sw}$) [Kimura *et al*., 2000]. The 0.18 ‰ changes in $\delta^{18}O_{sw}$ consist with 0.7 ℃ SST changes, which is not so bigger changes than annual SST amplitude in Kikai island 8.2 ℃. Thus, in this study, the $\delta^{18}O_{sw}$ in Kikai island is unknown, therefore we assumed that $\delta^{18}O_{sw}$ was 0 ‰. The modern $\delta^{18}O_{shell}$ well corresponded with instrumental SST (r =0.96, p < 0.01) (Fig. 4-7). The modern

reconstructed SST showed minima in February and maxima in September to November similar to instrumental SST records (Fig. 4-7). On May, Jun, and November when precipitation gains, the reconstructed SST was higher than instrumental SST. Thus, it was considered that lighter value $\delta^{18}O_{sw}$ brought by precipitation affected the $\delta^{18}O_{shell}$ (Fig. 4-7). $\delta^{18}O_{shell}$ of MIS-3 KFT-01 showed clear seasonal cycles (Fig. 4-6). The number of $\delta^{18}O_{shell}$ in KFT-01 decreased because of reduction of later growth in life span of the specimen (Fig. 4-6). Watanabe and Oba (1998) showed that in the case of rough sampling intervals of analytical samples of giant clam shell, the amplitude of $\delta^{18}O_{shell}$ could not reflect SST minima or maxima. However, $\delta^{18}O_{shell}$ amplitude in KFT-01's later growth did not change, thus 300 μm sampling interval for KFT-01 was enough to reconstruct seasonal SST (Fig. 4-6).

Next, I calculated the 55 ka average monthly SST changes in Kikai island from $\delta^{18}O_{shell}$ in KFT-01. $\delta^{18}O_{shell}$ reflects SST and $\delta^{18}O_{sw}$, thus it is necessary to consider $\delta^{18}O_{sw}$ when reconstruct past SST. Lea *et al.*, (2002) reconstructed past 350 thousand years sea level and $\delta^{18}O_{sw}$ using planktonic foraminiferal shell $\delta^{18}O$ and magnesium calcium ratio in the sediment core and they showed $\delta^{18}O_{sw} = 0.55$ in 55 ka. Then, the 55 ka average monthly SST changes in Kikai island were reconstructed using Grossman and Ku (1986) equation (Fig. 4-8). The reconstructed 55 ka SST showed that average SST in 55 ka was 2.5 ºC lower and amplitude was 1.9 ºC smaller than that of modern Kikai island (Fig. 4-7). warm period (April to September)

The reconstructed 55 ka SST was much lower in cooling season (November to March) than warm period (April to September). In addition, SST maxima in 55ka appeared on

Jun which was 3 months earlier than that of today (Fog, 4-8). The 55ka SST profile showed short summer at that time. The average reconstructed 55ka SST minimum in February (19 ºC) was close to the limit SST of coral reef development (18 ºC) [Veron and Minchin, 1992]. Thus, MIS-3 55ka SST seasonality in Kikai island seemed to be close to the minimum SST of coral reef development.

4-2. Shell stable carbon isotope ratios

In order to clarify the seasonal variation of$\delta^{13}C_{shell}$ of the modern sample KSTm150613, the carbon isotope ratio was calculated as the average of each month. The $\delta^{13}C_{shell}$ in modern KSTm150613 decreased in rainy season Jun and July (Fig. 4-7). November has comparatively much precipitation however, the $\delta^{13}C_{shell}$ did not decreased. Thus, $\delta^{13}C_{shell}$ changes is not only because of precipitation. Watanabe *et al*., (2004) showed that carbon isotopic fractionation in giant clam is complex, the two possible sources of carbon for shell carbonates are dissolved inorganic carbon (DIC) in ambient seawater, and metabolic CO_2 passing through the respiration photosynthesis pathways, which includes symbiotic zooxanthellae within giant clam tissue. In the case of hermatypic corals skeleton, which have been studied much more than Tridacna, it has been suggested that carbon isotopic variations could be a useful proxy of insolation mediated by water depth, because insolation determines the photosynthetic activity of symbiotic zooxanthellae in corals [Grottoli, 2000]. Because giant clam also has symbiotic zooxanthellae in its tissue, its activity will be changed by insolation and $\delta^{13}C_{shell}$ will be a proxy of insolation. In this study, there was no instrumental record of insolation in Kikai island which is important

to investigate the cause of $\delta^{13}C_{shell}$ changes. DIC in Kikai island was also unknown. Kikai institute for coral reef science in Kikai island established in 2014 investigates water condition in Kikai island with monitoring water quality and installing data logger. It is expected that these environmental data will be compared with geochemical analysis such as carbon isotope ratio in giant clam shell. $\delta^{13}C_{shell}$ profile of KFT-01 had clear cycles and correlation with $\delta^{18}O_{shell}$ ($r = 0.83$, $p < 0.01$). Thus, it seemed that the $\delta^{13}C_{shell}$ of KFT-01 mainly derived from photosynthesis of symbiotic zooxanthellae caused by the seasonal fluctuation of irradiation.

4-3. Growth pattern comparison modern and MIS-3 giant clam

Growth increment thickness in modern KSTm150613 had correlation with ($r = 0.91$, $p < 0.01$) and SST ($r = 0.86$, $p < 0.01$) (Fig. 4-7). The seasonal changes of the growth increment thickness were 22.1 ± 5.8 μm in winter (January to March), and 29.0 ± 7.9 μm in summer (July to September). The maximum was on September and the minimum was on March. The growth increment thickness decreased gradually summer to winter (Fig.4-7). The translucent layer in the outer layer of KSTm150613 was estimated as on November, 2012, August to September, 2014, and April to Jun, 2015 (Fig. 4-5). The seasonal changes of the growth increment thickness of MIS-3 KFT-01 were 20.2 ± 7.6 μm in winter (January to March), and 40.1 ± 16.0 μm in summer (July to September). The maximum was on August to September and the minimum was on March (Fig.4-7). The standardized Growth Index (SGI) which was subtracted the decrease in growth increment width with age and converted to monthly average, showed that growth of MIS-

3 sample had been increased in a short period of summer when the water temperature rose (Fig. 4-7). In addition, there were growth breaks which showed the hiatus of the growth in winter and summer (Fig. 4-6). The growth breaks in winter looked like deep notched shape (Fig. 4-3), it seems to be winter ring when the giant clam stopped the growth in winter. The growth pattern of MIS-3 giant clam (Tridacna squamosa) was different from modern because SST and its amplitude of Kikai island at that time (MIS-3, 55ka) was lower than that of today. Thus, SST frequency was calculated from $\delta^{18}O_{shell}$ of MIS-3 sample (Fig. 4-8). Since the sampling interval of $\delta^{18}O_{shell}$ is constant (0.3 mm), the reconstructed SST with a high occurrence frequency indicates that the SST continued for a long period of time or that the giant clam grew more. The modern KSTm150613 grew evenly in the SST rage of 12 to 28 ℃ (Fig 4-8). The frequency of reconstructed SST decreased on the SST of 29 ℃ or more and 21 ℃ or less. In this SST rages, it indicated that growth of the sample slowed. Because the appearance frequency of the reconstructed SST of 23.4 ℃ or less decreased, it was considered that MIS-3 fossil sample slowed its growth in that SST range. Since the MIS-3 sample also had winter growth break and decline of the growth in winter, the MIS-3 sample might have taken a strategy of fast growing in the SST range suitable for growth. SST was important factor for giant clam survive. Watson *et al.*, (2012) showed that the survival rate of *Tridacna squamosa* fell to less than 20% in future anticipated global warming · acidified sea water temperature and carbon dioxide partial pressure. MIS-3 giant clams (*Tridacna squamosa*) in Kikai island adapted lower SST and *Tridacna squamosa* lives in Kikai island now. Giant clam fossil growth records in Kikai island where fossil giant clam from 100 thousand years ago to

modern are available will provide the information of adaptation and distribution of the giant clams.

4-4. Past typhoon reconstruction in modern and MIS-3

The Ba/Ca ratio of modern KSTm150613 had positive peaks in August to November and winter season (December and February) (Fig 4-6). The Ba/Ca ratio of MIS-3 KFT-01 had positive peaks in winter season and from April to November (Fig 4-6). The Ba / Ca ratio of the giant clam shell will be an indicator of plankton bloom by correlation the timing and fluctuation range of the peak with the chlorophyll concentration of surrounding surface seawater (Elliot *et al*., 2009). Komagoe *et al*., 2018 showed that after typhoon approach, there was a decrease in increment thickness and some disturbed growth increments and the positive peaks in the shell Ba/Ca ratio and δ18Oshell corresponded to lower sea surface temperature caused by typhoons. Modern KSTm150613 showed positive Ba/Ca and growth decrease in summer season corresponded to the approaching typhoons (Fig. 4-7). In order to evaluate the typhoon approaching in Kikai island detection from geochemical and sclerochronological signals, these signals and meteorological data were compared. The frequency of approaching typhoon was calculated by geochemical geochemical and sclerochronological signals in the giant clam specimens (Fig. 4-10). The modern reconstructed typhoon frequency detected 56% of instrumental typhoon records. The frequency was lower than actual records, but seasonality of the typhoons was almost reconstructed. As same process, MIS-3 (55ka) typhoon frequency was reconstructed (Fig. 4-9). The frequency of the

reconstructed typhoons in MIS-3 was about half and the seasonality was different from that of today (Fig. 4-9). The typhoon peak in MIS-3 was early summer (May) and $\delta^{18}O_{shell}$ of MIS-3 showed short summer period in Kikai island at that time (Fig. 4-6, 4-9). Driscoll *et al*., (2014) compared MIS-3 and Holocene El Nino Southern Oscillation (ENSO) using the deviation of $\delta^{18}O_{shell}$ in fossil giant clams shell from Huon Peninsula, Papua New Guinea and they showed that ENSO variability seen during the late twentieth century is rare but not unprecedented within glacial MIS-3 (34 ~ 60 ka) climates. Kikai island is located in high latitude compared to Papua New Guinea and there is not located in the Western Pacific Warm Pool (WPWP).

Typhoons approaching Japan today occur most frequently during the period from July to October. The typhoons occur in early spring at low latitudes and heads west towards the Philippines, but in the summer the typhoons occur in the higher latitude and there are many typhoons going around the Pacific high pressure to the north towards Japan (Japan Meteorological Agency). Reconstructed typhoon seasonality and short summer period in MIS-3 seems that MIS-3 has different strengths of westerly wind and Pacific high pressure, which determines typhoon path. By reconstructing the approach frequency and the timing of the typhoon from the MIS-3 or the Holocene fossil giant clam shell from Kikai island, it can be expected to clarify the transition of the typhoons approaching to Japan during the glacial period.

5. Summerly

・The fossil giant clam shell well preserved from diagenetic alternation.

・As a result of dating, fossil samples were 3942±83 BP, 7203±93 BP, and 55ka.

・Oxygen isotope ratio and growth line widths of the modern sample correlated with SST and showed seasonal variation.

・The reconstructed MIS-3 (55ka) SST in Kikai island was about 4℃ lower and showed short summer period.

・The growth pattern of the giant clam in MIS-3 was different from today and It seemed that the giant clam might have taken a strategy of growth at a stretch in a SST rage suitable for growth.

・ The reconstructed typhoon seasonality from modern giant clam shell reflected 56% of typhoons approached Kikai island and seasonality.

・Reconstructed typhoon seasonality and short summer period in MIS-3 seems that MIS-3 has different strengths of westerly wind and Pacific high pressure, which determines typhoon path.

6. Acknowledgement

In the research, I was able to collect fossil giant clam shell sample on corporation of many people in Kikai-town. In addition, I received the ideas from Dr. Sowa for improving the powder sampling methods. Mr. Hideo Nomura and Mr. Akira Nakamura of Hokkaido University Graduate School of Engineering Department of Thin section Engineering gave cooperation in the creation of shell thin sections. Dr. Kentaro Tanaka of the University of Tokyo Atmosphere and Ocean Research Institute and member of Dr. Shirai laboratory

helped LA-ICP-MS measurement and analysis. I would like to express my gratitude to the people involved in this research and CREES members.

References

Abramoff, M.D., Magalhaes, P.J., Ram, S.J. "Image Processing with ImageJ". Biophotonics International, volume 11, issue 7, pp. 36-42, 2004.

Andel, T. H. Van (2002), The Climate and Landscape of the Middle Part of the Weichselian Glaciation in Europe : The Stage 3 Project, , *8*, 2–8, doi:10.1006/qres.2001.2294.

Andréfouët, S., S. Van Wynsberge, L. Kabbadj, C. C. C. Wabnitz, C. Menkes, T. Tamata, M. Pahuatini, I. Tetairekie, I. Teaka, and T. A. H. Scha (2017), Adaptive management for the sustainable exploitation of lagoon resources in remote islands: lessons from a massive El Niño-induced giant clam bleaching event in the Tuamotu atolls (French Polynesia), *Environ. Conserv.*, 1–11.

Batenburg, S. J., G. J. Reichart, T. Jilbert, M. Janse, F. P. Wesselingh, and W. Renema (2011), Interannual climate variability in the Miocene: High resolution trace element and stable isotope ratios in giant clams, *Palaeogeogr. Palaeoclimatol. Palaeoecol.*, *306*(1–2), 75–81, doi:10.1016/j.palaeo.2011.03.031.

d'Errico, F., and M. F. S. Goñi (2003), Neandertal extinction and the millennial scale climatic variability of OIS 3, *Quat. Sci. Rev.*, *22*(8), 769–788.

Dansgaard, W. *et al*. (1993), Evidence for general instability of past climate from a 250-kyr ice-core record, *Nature*, *364*(6434), 218–220, doi:10.1038/364218a0.

Driscoll, R., M. Elliot, T. Russon, K. Welsh, Y. Yokoyama, and A. Tudhope (2014), ENSO reconstructions over the past 60 ka using giant clams (Tridacna sp.) from Papua New Guinea, *Geophys. Res. Lett.*, *41*(19), 6819–6825.

Duprey, N., C. E. Lazareth, C. Dupouy, J. Butscher, R. Farman, C. Maes, and G. Cabioch (2014), Calibration of seawater temperature and δ 18Oseawater signals in Tridacna maxima's δ 18Oshell record based on in situ data, *Coral Reefs*, *34*(2), 437–450, doi:10.1007/s00338-014-1245-z.

Elliot, M., K. Welsh, C. Chilcott, M. McCulloch, J. Chappell, and B. Ayling (2009), Profiles of trace elements and stable isotopes derived from giant long-lived Tridacna gigas bivalves: Potential applications in paleoclimate studies, *Palaeogeogr. Palaeoclimatol. Palaeoecol.*, *280*(1–2), 132–142, doi:10.1016/j.palaeo.2009.06.007.

Grace, M., P. G. Faylona, C. E. Lazareth, A. Sémah, S. Caquineau, H. Boucher, W. P. Ronquillo, H. Varagnat, and B. Cedex (2011), Preliminary Study on the Preservation of Giant Clam (Tridacnidae) Shells from the Balobok Rockshelter Archaeological, , *26*(6), 888–901, doi:10.1002/gea.20377.

Grossman, E. L., and T. L. Ku (1986), Oxygen and carbon isotope fractionation in biogenic aragonite: temperature effects., *Chem. Geol.*, *59*, 59–74.

Grottoli, A. G. (2000), Stable Carbon Isotopes (δ13C) in Coral Skeletons, *Oceanography*, *13*, 93–97.

Jochum, K. P., Weis, U., Stoll, B., Kuzmin, D., Tang, Q., Raczek, I., Jacob, D. E., Stracke, A., Birabaum, K., Frick, D. A., Günther, D., Enzweiler, J. (2011), Determination of

reference values for NIST SRM 610-617 glasses following ISO guidelines, Geostand. Geoanalytical *Res*., 35(4), 397–429, doi:10.1111/j.1751-908X.2011.00120.x.

Lea, D. W., P. A. Martin, D. K. Pak, and H. J. Spero (2002), Reconstructing a 350 ky history of sea level using planktonic Mg/Ca and oxygen isotope records from a Cocos Ridge core, *Quat. Sci. Rev.*, *21*(1–3), 283–293, doi:10.1016/S0277-3791(01)00081-6.

McGregor, H. V., and M. K. Gagan (2003), Diagenesis and geochemistry of Porites corals from Papua New Guinea: Implications for paleoclimate reconstruction, *Geochim. Cosmochim. Acta*, *67*(12), 2147–2156, doi:10.1016/S0016-7037(02)01050-5.

Van Meerbeeck, C. J. *et al*. (2011), The nature of MIS 3 stadial-interstadial transitions in Europe: New insights from model-data comparisons, *Quat. Sci. Rev.*, *30*(25–26), 3618–3637, doi:10.1016/j.quascirev.2011.08.002.

Ota, Y., and A. Omura (1992), Contrasting styles and rates of tectonic uplift of coral reef terraces in the Ryukyu and Daito Islands, southwestern Japan, *Quat. Int.*, *15*, 17–29.

Sasaki, K., A. Omura, K. Murakami, N. Sagawa, and T. Nakamori (2004), Interstadial coral reef terraces and relative sea-level changes during marine oxygen isotope stages 3-4, Kikai Island, central Ryukyus, Japan, *Quat. Int.*, *120*(1), 51–64, doi:10.1016/j.quaint.2004.01.006.

Swann, G. E. A., A. W. Mackay, M. J. Leng, and F. Demory (2005), Climatic change in Central Asia during MIS 3/2: A case study using biological responses from Lake

Baikal, *Glob. Planet. Change*, *46*(1–4 SPEC. ISS.), 235–253, doi:10.1016/j.gloplacha.2004.09.019.

Veron, J. E. N., and P. R. Minchin (1992), Correlations between sea surface temperature, circulation patterns and the distribution of hermatypic corals of Japan, *Cont. Shelf Res.*, *12*(7–8), 835–857, doi:10.1016/0278-4343(92)90047-N.

Warter, V., W. Mueller, F. P. Wesselingh, J. A. Todd, and W. Renema (2015), Late Miocene seasonal to subdecadal climate variability in the Indo-West Pacific (East Kalimantan, Indonesia) preserved in giant clams, *Palaios*, *30*(1), 66–82.

Watanabe, T., A. Suzuki, H. Kawahata, H. Kan, and S. Ogawa (2004), A 60-year isotopic record from a mid-Holocene fossil giant clam (Tridacna gigas) in the Ryukyu Islands: Physiological and paleoclimatic implications, *Palaeogeogr. Palaeoclimatol. Palaeoecol.*, *212*(3–4), 343–354, doi:10.1016/j.palaeo.2004.07.001.

Watson, S., P. C. Southgate, G. M. Miller, J. a Moorhead, and J. Knauer (2012), Ocean acidification and warming reduce juvenile survival of the fluted giant clam, Tridacna squamosa, *Molluscan Res.* , *32*(3), 177–180.

駒越太郎, 渡邊剛, 白井厚太朗, 山崎敦子, and 植松光夫 (2016), シャコガイ殻を用いた高時間解像度の環境解析: 沖ノ鳥島シラナミガイ殻に刻まれた台風の痕跡 (総特集 サンゴ礁科学研究: 喜界島サンゴ礁科学研究所設立記念号), *海洋. 号外= Kaiyo Mon. カラー版*, (56), 80–93.

山崎敦子, 渡邊剛, 岨康輝, 中地シュウ, 山野博哉, and 岩瀬文人 (2009), 高知県竜串湾に生息する造礁性サンゴ骨格を用いた温帯域の古環境復元, 日本サンゴ礁学会誌, *11*(1), 91–107.

渡邊剛 (2004), 生物源炭酸塩の同位体比及び微量元素を用いた熱帯域海洋表層の高解像度古環境解析に関する研究, 地球化学, *38*(1), 29–43.

渡邊剛, 大場忠道 (1998), 冷凍マイクロトーム法による現生シャコガイ殻の酸素同位体比分析より推定される詳細な水温変化, 地球化学, *32*(2), 87–95.

木山修, 山田努, 中森亨, and 井龍康文 (2000), 造礁サンゴ骨格の酸素同位体比から推定された完新世初期の海水温, 第四紀研究, *39*(1), 69–80.

Komagoe, T., T. Watanabe, K. Shirai, A. Yamazaki, and M. Uematu (2018), Geochemical and microstructural signals in giant clam Tridacna maxima recorded typhoon events at Okinotori Island, Japan, *J. Geophys. Res. Biogeosciences*. 123, (5), 1460-1474.

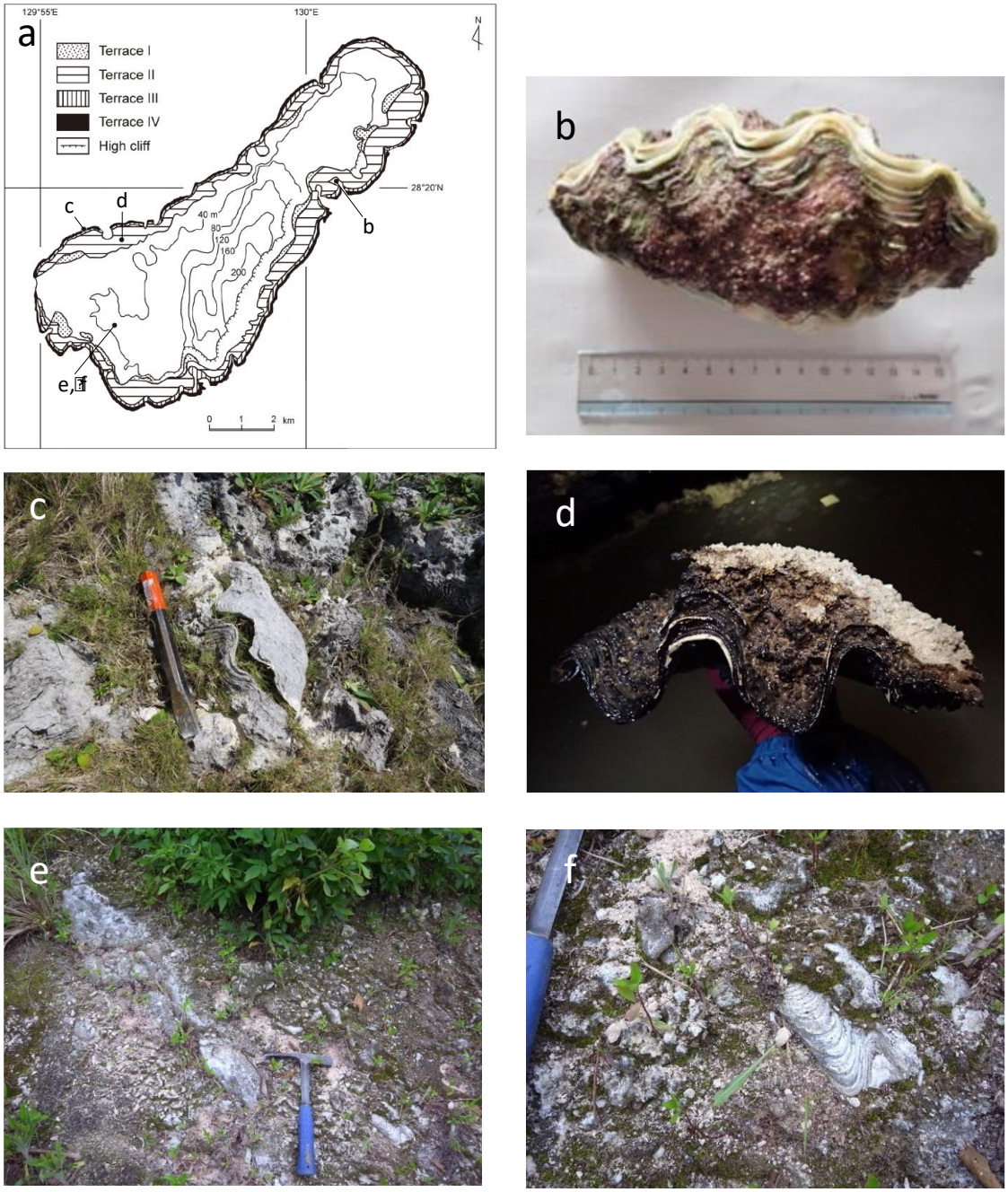

Figure 4-1giant clam samples and sampling place

(a) Distribution of harvested samples of Shigella crassa and the Holocene marine terraces of Kikai Island. (Based on Ota *et al*. 1978). The alphabet indicates the sampling place of each sample. (b) Current living silkworm (collected on Shion Road Nagahama Park on

13th June 2015). (c) Holocene shipwreck fossil stored in coral reef terraces. (d) Sakkogai fossil stored on the wall of the well. (e) Sakkogai fossil stored in the outcrop of Late Pleistocene. (f) (e) Expansion of the surroundings of the funnel. The rock formations consist of unconsolidated coral rudstone ~ floatstone, framestone, branches of *Acropora*, broken coral gravels.

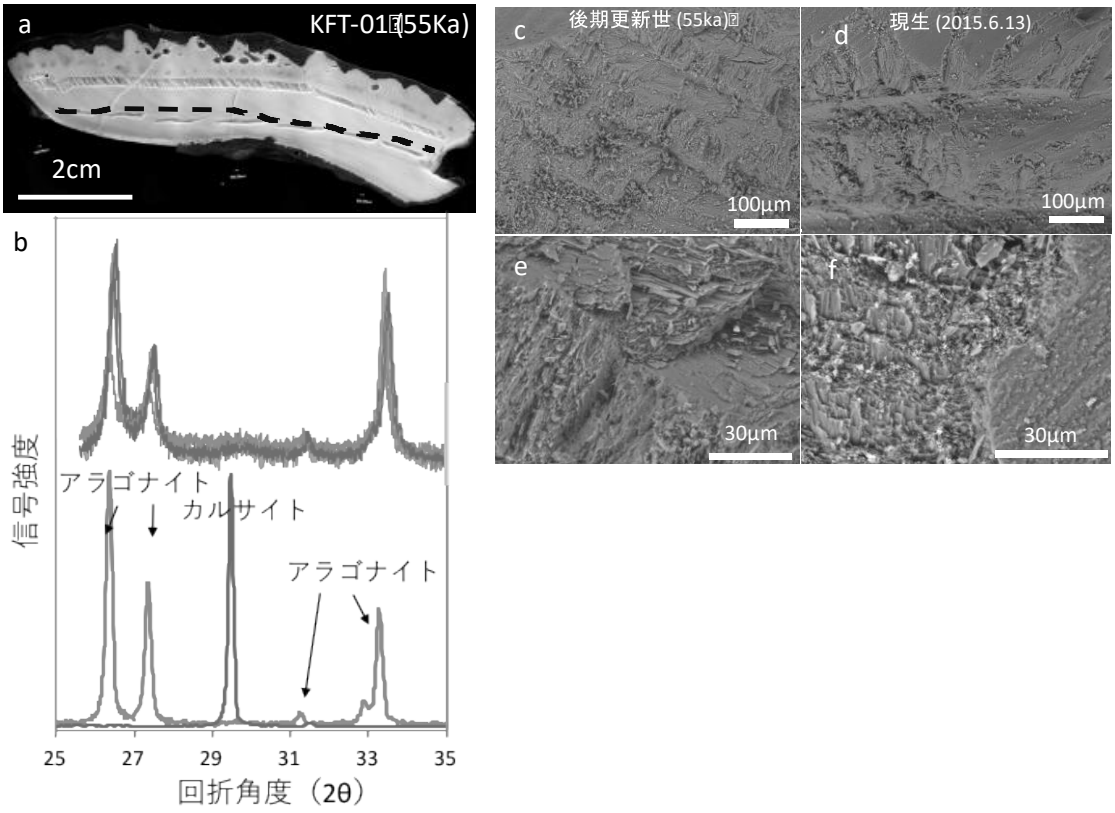

Figure 2 The diagenetic alternation evaluation of late Pleistocene (55 ka) fossil shells

(a) Chemical Analysis Surface of Fossil Sediments. Powder was taken from the broken line and X-ray diffraction was performed.

(b) X-ray diffraction results. Peaks at the bottom of the graph are peaks of aragonite and calcite for comparison.

(c) Observation of cross section of late Pleistocene fossil shells with electron microscope.

(d) Observation of the cross section of the reptilian shell in an electron microscope.

(e) Enlarged image of (c).

(f) Enlarged image of (d).

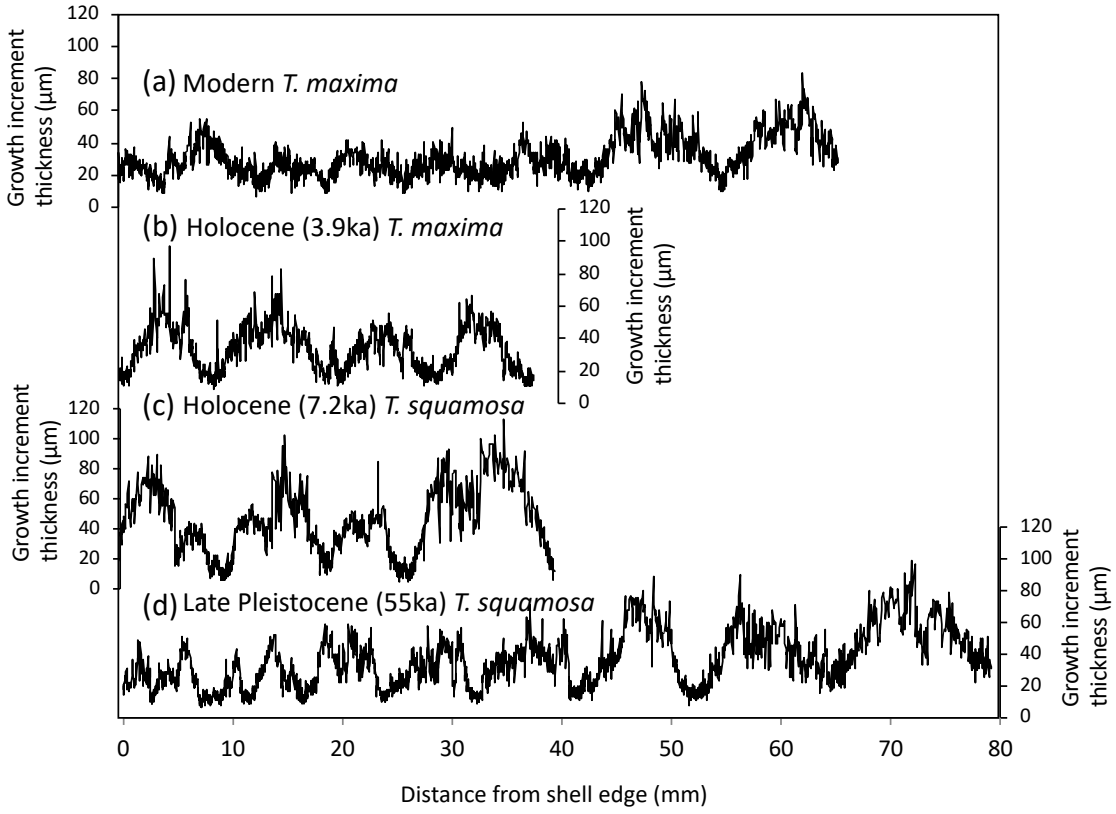

Figure 4-3. Growth increment in Holocene and MIS-3 giant clam samples.

(a), (b), (c), and (d) showed the growth increments thickness in modern T. maxima, Holocene (3.9ka) T. maxima, Holocene (7.2ka) T. squamosa, and late Pleistocene (MIS-3, 55ka) T. squamosa specimens respectively.

	Modern	3942 yr. B.P.	7203 yr. B.P.	55000 yr. B.P.
Growth increment (μm)	*T. maxima*	*T.maxima*	*T. squamosa*	*T.squamosa*
Average	26.82	28.98	34.47	29.49
Maximum	83.32	96.91	113.82	92.03
Minimum	5.86	8.44	5.47	6.8

Table 4-1 Sample species and growth increments

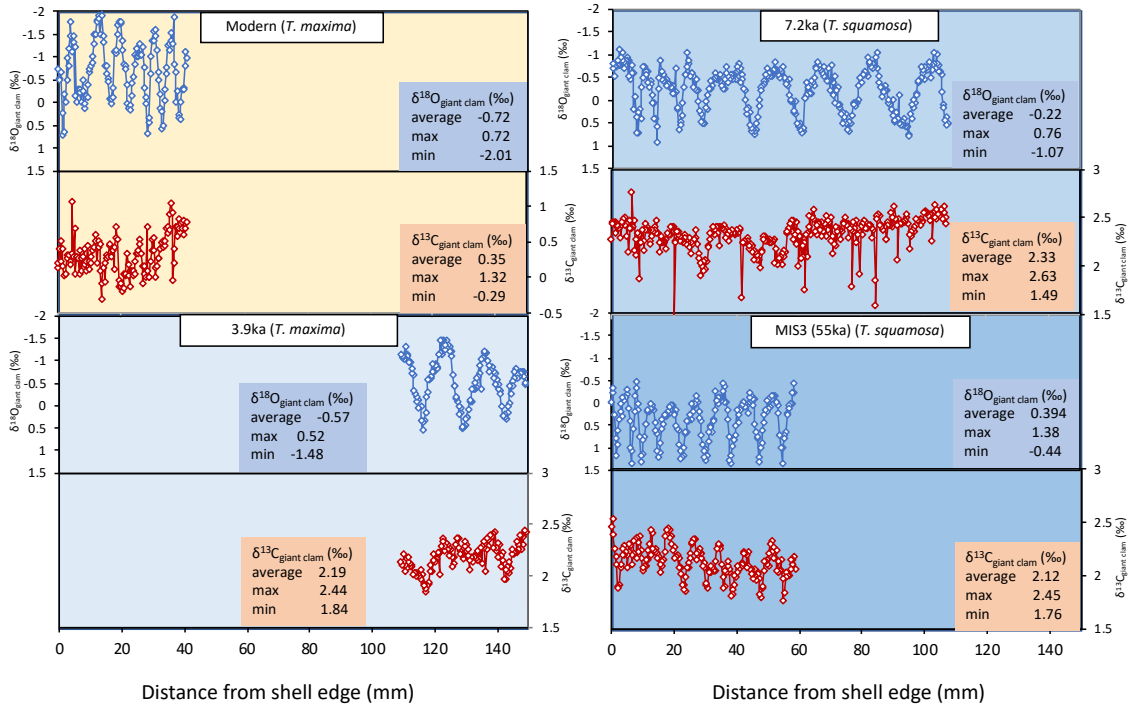

Figure 4-4. Isotopic signature of Kikai island fossil giant clams.

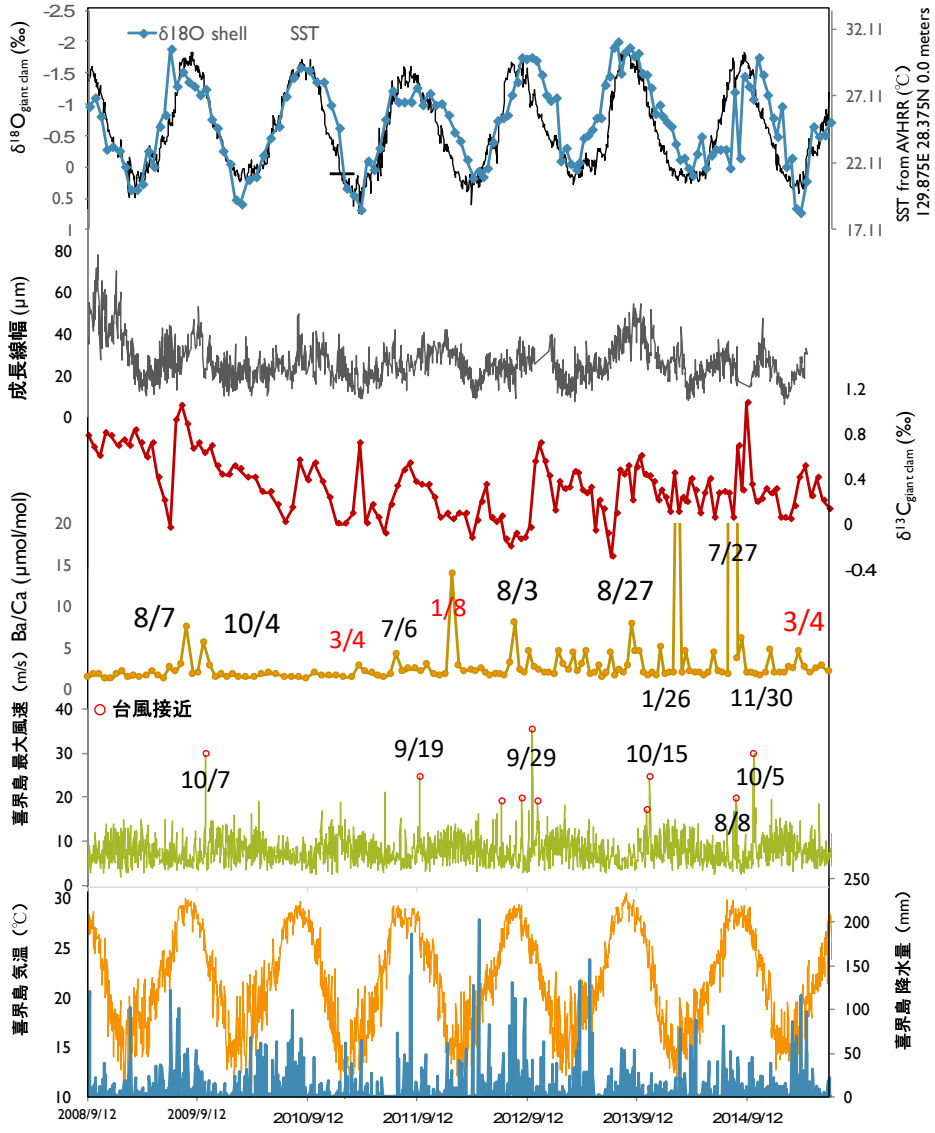

Figure 4-5. Time series of modern giant clam geochemical data and meteorological data in Kikai island. Vertical line showed approaching typhoons in Kikai island.

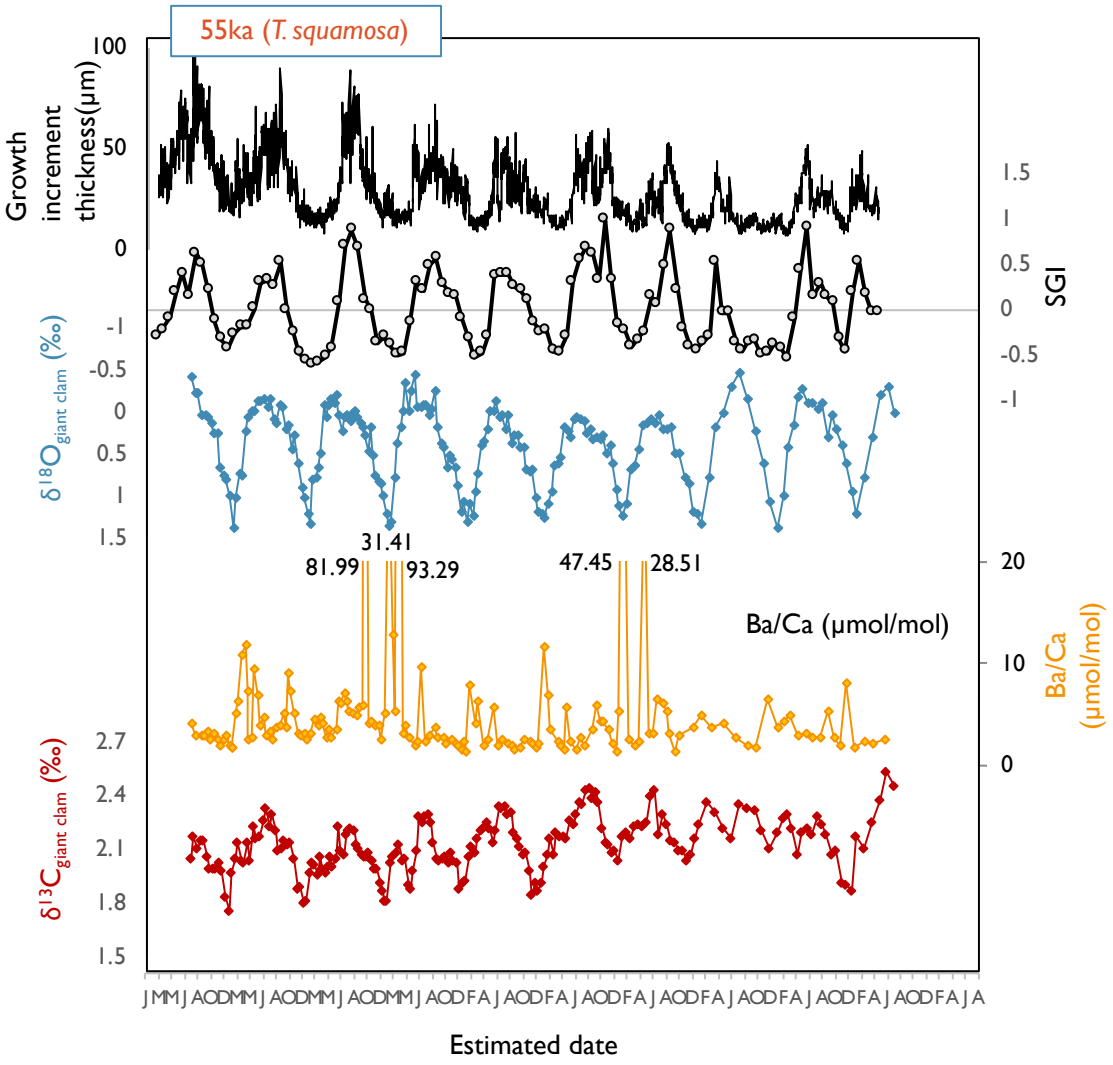

Figure 4-6. Time series of MIS-3 fossil giant clam geochemical data and meteorological data in Kikai island.

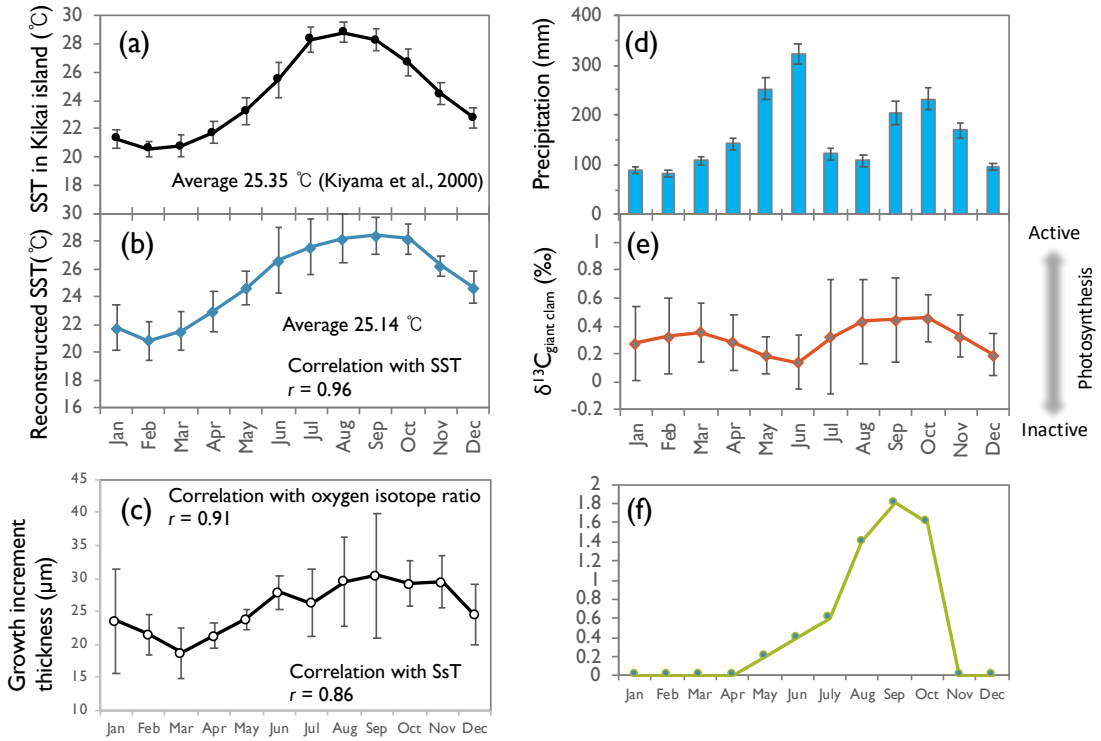

Figure 4-7. The comparison between modern giant clam geochemical data seasonality and meteorological data in Kikai island.

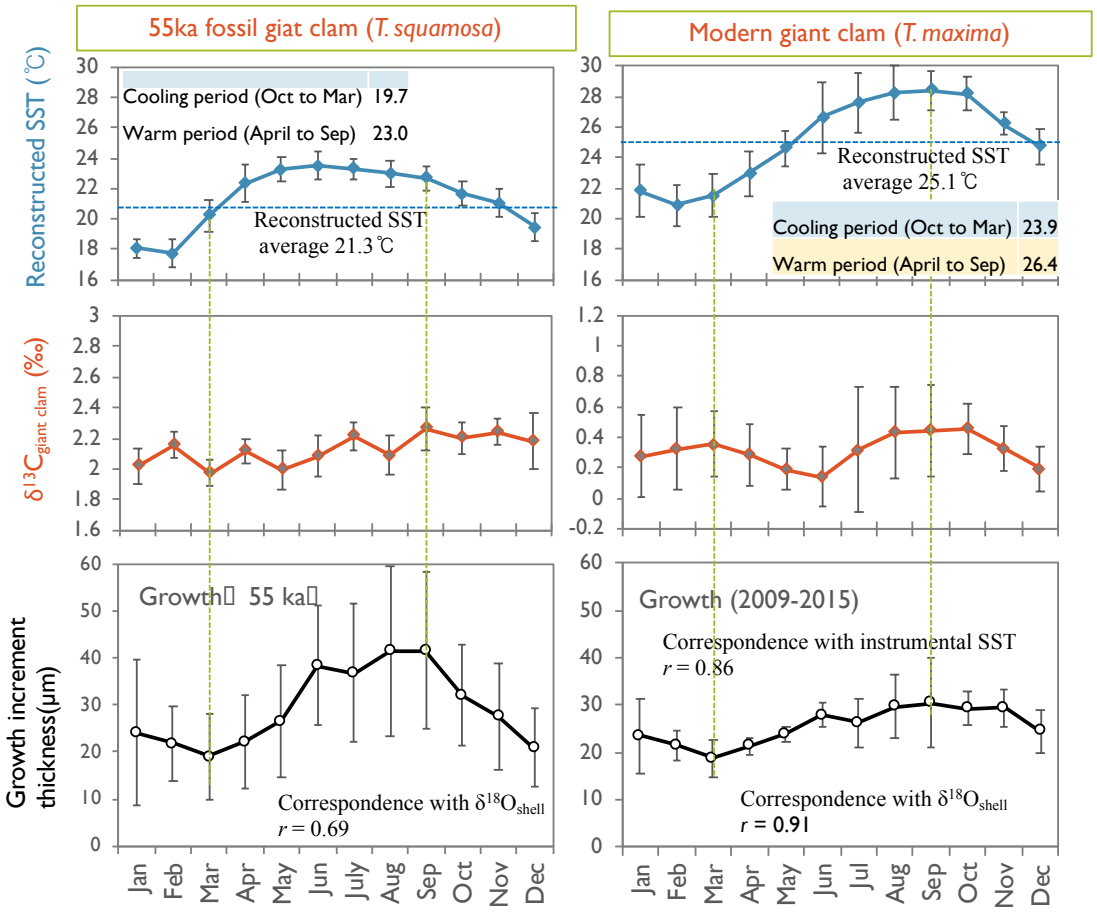

Figure 4-8. The comparison between modern and MIS-3 fossil giant clam geochemical seasonality.

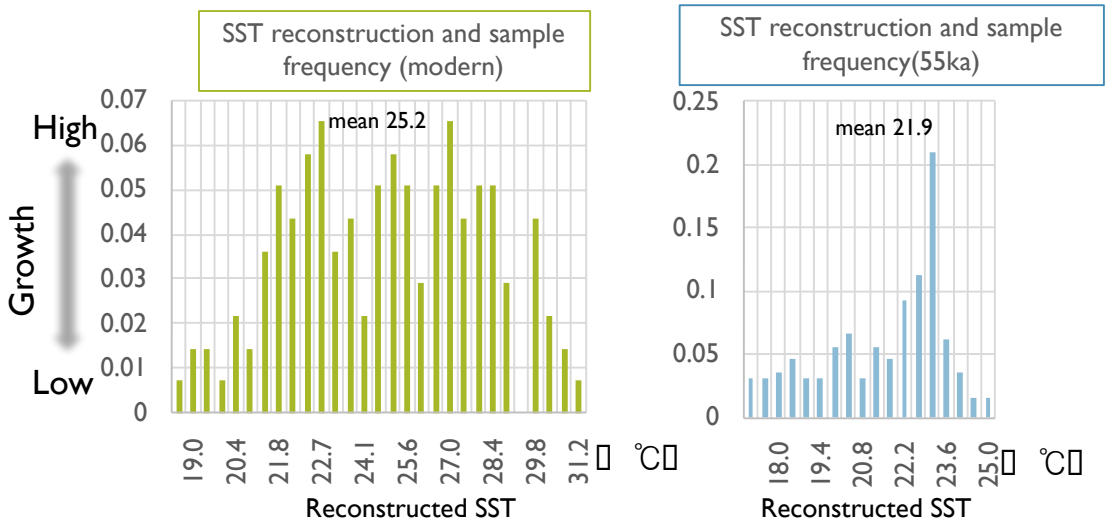

Figure 4-9. SST reconstruction and growth pattern in modern and MIS-3 giant clams.

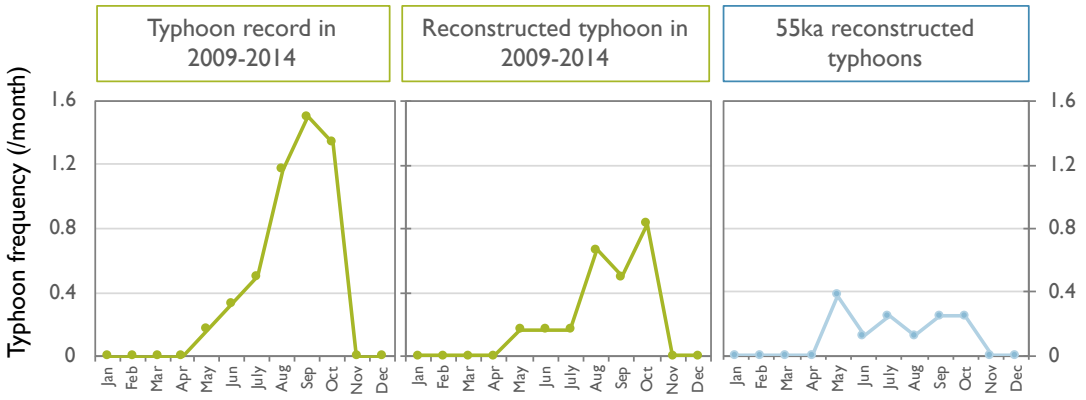

Figure 4-10. The comparison of reconstruction frequency and seasonality from modern and MIS-3 giant clams.

Chapter 5: **A Late-Miocene climate reconstruction from fossil *Tridacna gigas* in Java island, Indonesia**

1. Introduction

Cenozoic is the age range of the next Mesozoic, from the K / Pg boundary extinction has occurred of dinosaurs to the present day, and it was divided into Cenozoic Paleogene, Neogene, and Quaternary periods. Miocene was 23,030,000 to 5,333,000 years ago (23.03-5.333Ma), it corresponds to the Neogene of the first era (Fig. 3-1). Neogene period is tectonics progressed colder compared to Paleogene, a time when such expansion of Strait of formation and back-arc basin has been actively. The warmer climate in Oligocene was sharply getting cooler and glaciers developed, referred to as the Miocene first ice age (Mi-1 Glaciation) Miocene begins from at that period. Miocene first Aquitanian period (23.03-20.44 Ma) was relatively cold in a dry climate. The next Burdigalian period (20.43-15.97 Ma) was a warm period and had Mid-Miocene Climatic Optimum (17-15 Ma). After 15 million years ago (15Ma) the climate had been cooler again, and monsoon climate in Asia had been remarkable (Zachos*et al*., 2001). The reconstruction of the high temporal resolution environment when was warmer period will be important information to predict future greenhouse Earth.

Contemporary species of giant clams appeared in late Miocene (Fig. 1-3), thus high temporal resolution paleoclimate reconstruction using giant clam shell was conducted (Batenburg *et al*., 2011, Warter *et al*., 2015, Warter *et al*., 2017). Since giant clam had thick and dense aragonite shell, the shell contents were well preserved even if

it was late Miocene fossils. However, these prior studies used relatively short life span giant clam specimen, thus more long record needed for reconstructing interannual to decadal climate variability in late Miocene.

2. Material and methods

2-1. Sample description and meteorological data in Java island

The two late Miocene fossil giant clam shells (THL8-1 and THL8-2, *Tridacna gigas* identified in Kase *et al*., 2015) was obtained from Nyalindung layer, Titalahab valley, Pelabuhanratu, west Java island, Indonesia (7°01′16.3″S, 106°56′35.2″E) (Fig. 5-1). Nyalindung layer is a stratum of the the beginning of the Miocene by Oostingh (1938), and Bemmelen (1972) decided the formation as in the Middle Miocene. In recent years, Batenburg *et al*. (2011) suggested that the Nyalindung layer was 10-13Ma (Serravallian, 13.82-11.62 Ma to Tortonian, 11.6-7.2 Ma) as the Tiiangsana layer close to Nyalindung layer contained large foraminifera. There were no index fossils in Nyalindung layer, but Kase *et al*., 2015 found index fossil *Discoaster hamatus* (about 10 Ma, eary late Miocene) in a lower to middle layer of Titalahab valley. Thus, the giant clam fossils estimated as about 10 Ma.

Indonesia is divided into a tropical climate. West Java where was a sample collected point is a tropical rain forest climate, the east is the monsoon climate characterized dry and rainy season. Sea surface temperature (SST) surrounding west Java island (106.875E, 7.875S) data set was obtained from Advanced Very High-Resolution

Radiometer: (AVHRR)（IRI/LDEO Climate Data Library : http://iridl.ldeo.columbia.edu）(Fig. 5-1)

2-2. Sclerochronological analysis of the giant clam shell and evaluation of diagenetic alternation

Fossil Giant clam shell samples cut into 5mm-thick sections with rock cutter along the maximum growth axis. The one of the shell sections were processed into thin section (~100 μm thickness) and took panoramic photos using digital microscope (KEYENCE VHX-2000). The growth increment thicknesses were measured using image processing software ImageJ [Abramoff *et al*., 2004]. The surface of each 5 mm-thick sections were polished using alumina polishing powder (#800#2000#6000).

It is important to evaluate the fossil preservation when reconstruct paleo environment using fossil biogenetic carbonates. In fossil giant shell specimen, the pristine shell aragonite sometimes altered to calcite, and or secondly aragonite precipitation occurred [Faylona *et al.*, 2011] . Powder samples for evaluation of diagenetic alternation were taken next to the sampling spots for geochemical analysis. Mineral phase of fossil specimens was checked using X-ray diffraction machine (MiniFlex II) in Hokkaido University Institute for the Advancement of Higher Education. In order to evaluate diagenetic alternation, the shell thin section observation by optical microscope and scanning electron microscope (SEM) observation were performed.

2-3. Stable oxygen and carbon isotope analysis

Powder samples for isotope analysis were taken from the pair of shell sections. The position for powder sampling was selected due to avoid diagenetic altered part in the shell inner layer. Each sample was obtained from the parallel to the growth increments using a hand drill (HP-200S, Toyo associates Co., Ltd., Japan) with a 0.4-mm drill bit (model BS1201, Minitor Co. Ltd., Japan) (Figure 2.6). The sampling grooves were taken discretely. Hand drill sampling provided an average width of 400 μm providing 20 - 40 μg powder samples for isotope analysis. The microsampling stage provided an average width of 300 μm, length of 1000 μm, and ~200 μm depth groove providing 200~300 μg powder samples for isotope analysis. The 20- to 40-μg powder samples were reacted with 100% phosphoric acid at 70 °C in a carbonate preparation device (Kiel IV Carbonate preparation device), and the produced CO2 was analyzed using a stable isotope ratio mass spectrometer (Thermo Scientific MAT 253). Isotopic values ($\delta^{18}O$ and $\delta^{13}C$) were one-point calibrated against National Bureau of Standards (NBS) 19 and reported in standard δ notation relative to Vienna Pee Dee belemnite (VPDB) and confirmed the calibration using NBS 18. The standard deviations (1σ) for 22 replicate measurements of NBS 19 are 0.03‰ and 0.02‰ for $\delta^{18}O$ and $\delta^{13}C$ as external long-term reproducibility throughout this study, respectively.

2-4. Trace element analysis

(1) LA-ICP－MS

Magnesium /Calcium (Mg/Ca), Magnesium /Calcium (Mg/Ca), Strontium/Calcium (Sr/Ca), and Barium and calcium (Ba/Ca) concentrations were analyzed by Laser Ablation Inductively Coupled Plasma Mass Spectrometry (LA-ICP-MS) (Agilent 7700 ICP-MS coupled with New Wave Research NWR193 laser ablation system: 193 nm ArF excimer laser (pulse width <5 ns)) along the same sampling line used for isotopic analysis sampling. The laser conditions were below; irradiance 0.82 GW/cm^2, repetition rate 10 Hz, and 40 second of laser duration. The sample surface was cleaned by 5 seconds of pre-ablation. The shell sample was ablated using a 100-μm laser spot, and each spot was adjacent to its neighbor, without overlap. There were 2 to 6 growth increments in each ablated spot. The calibration of the signal intensity to the Ba/Ca ratio was performed using glass standard materials: NIST 612 standard grass distributed by the National Institute of Standard and Technology [*Shirai et al*., 2008]. ^{43}Ca was used as an internal standard.

(2) ICP-AES

Strontium Calcium ratio (Sr/Ca), and Magnesium Calcium ratio (Mg/Ca) were measured with an Inductively Coupled Plasma Atomic Emission Spectrophotometer (ICP-AES) installed at Hokkaido University. Approximately 132 ± 15 μg of giant clam powder sample was dissolved in 4 mL of HNO_3. The sampling grooves for ICP-AES were independent from stable isotope and LA-ICP-MS sampling spots. The sample solution for the measurement of trace elements was prepared via serial dilution with 2% HNO3 for a Ca concentration of ca. 9 ppm. Analytical precision of the Sr/Ca, Mg/Ca, and Ba/Ca determinations were 0.06, 0.4, and 5.5 RSD (%, n = 23, 1σ, JCt-1) respectively.

3. Results

3-1. Sample preservation and sclerochronological data in the Miocene giant clam shell

It is important to avoid altered biogenetic aragonite sample to precise paleo environment reconstruction. X-ray diffraction for THL8-1 and THL8-2 showed no significant calcite peaks (Fig. 5-2)

In addition, there were less secondary or dissolved aragonite in two fossil samples by SEM observation. Thus, thick giant clam inner layer of THL8-1 and THL8-2 was well preserved though these were 10 Ma fossils.

Growth curve of the Miocene giant clam was established using growth increments in the shell thin sections (Fig. 5-3). Pair of transparence and translucent growth increments were assumed as annual growth ring and there were 25 and 7 annual rings observed in THL8-1 and THL 8-2 respectively. The shape of the growth curve was similar to the growth curve of same species in Holocene optimum reported in Watanabe *et al*., 2004, but the amount of growth was about 50% of Holocene one. There were 4479 and 2284 of micro growth increments observed in THL8-1 and THL8-2 respectively. The thickness of the increments in THL8-1 ranged 4.66 to 43.70 μm and 15.77 for the average. In THL8-2 the thickness ranged 7.29 to 67.13 μm, and the average thickness was 19.83 μm (Fig. 5-3).

3-2. Stable oxygen and carbon isotope ratio in the shell specimens

The average of stable oxygen isotope ratios ($\delta^{18}O_{shell}$) was -2.85 and -2.91 ‰ for THL8-1 and THL8-2 respectively (THL8-1; n=143, THL8-2; n=90). The maximum of stable oxygen ratios was 2.08‰ and -2.39‰, and the minima was -3.42‰▪-3.34‰ for THL8-1 and THL8-2 respectively. In THL8-1, $\delta^{18}O_{shell}$ profile showed annual like cycles in earlier growth (0 to 55 mm from the shell edge), but unclear cycles in later growth (50 to 55mm from the shell edge.) In THL8-2, $\delta^{18}O_{shell}$ profile showed annual like cycles and suddenly $\delta^{18}O_{shell}$ increased in 19 to 35 mm from the shell edge.

The average of stable oxygen isotope ratios ($\delta^{13}C_{shell}$) was 2.15 and 1.88 ‰ for THL8-1 and THL8-2 respectively (THL8-1; n=143, THL8-2; n=90). The maximum of stable oxygen ratios was 9.27 ‰ and 2.37 ‰, and the minima was 0.87 ‰ and 1.25 ‰ for THL8-1 and THL8-2 respectively. There was annual like cycles in $\delta^{13}C_{shell}$ of each sample. Watanabe *et al*., 2014 showed the two possible sources of carbon for shell carbonates. There were dissolved inorganic carbon (DIC) in ambient seawater, and metabolic CO_2 passing through the respiration and photosynthesis pathways, which includes symbiotic zooxanthellae within Tridacna tissue.

3-4. Trace elements in the shell specimens

LA-ICP-MS

Trace element concentrations using LA-ICP-MS were below.

Manganese /Calcium（Mn/Ca）

Mn/Ca in THL8-1 ranged 0.002 to 169.14 μmol/mol and the average was 1.24 μmol/mol（n=753）. The standard error was 7.15 μmol/mol of replicated measurement

of NIST 610 (n = 123). Mn/Ca in THL8-2 ranged 1.18 to 16.22 μmol/mol and the average was 4.05 μmol/mol（n=468）. The standard error was 5.01 μmol/mol of replicated measurement of NIST 610 (n = 75). The concentration of Mn/Ca in THL8-2 was about three times bigger than THL8-1 and showed clear cycles.

Magnesium /Calcium（Mg/Ca）

Mg/Ca in THL8-1 ranged 0.29 to 1.53 mmol/mol and the average was 0.66 mmol/mol（n=753）. The standard error was 0.033 mmol/mol of replicated measurement of NIST 610 (n = 123). Mg/Ca in THL8-2 ranged 0.36 to 1.28 mmol/mol and the average was 0.69 mmol/mol（n=468）. The standard error was 0.015 mmol/mol of replicated measurement of NIST 610 (n = 75).

Strontium/Calcium（Sr/Ca）

Sr/Ca in THL8-1 ranged 1.68 to 3.28 mmol/mol and the average was 2.13 mmol/mol （n=753）. The standard error was 0.0048 mmol/mol of replicated measurement of NIST 610 (n = 123). Sr/Ca in THL8-2 ranged 1.81 to 2.91 mmol/mol and the average was 2.25 mmol/mol（n=468）. The standard error was 0.0035 mmol/mol of replicated measurement of NIST 610 (n = 75).

Barium/Calcium（Ba/Ca）

Ba/Ca in THL8-1 ranged 0.99 to 14.25 μmol/mol and the average was 2.41 μmol/mol（n=753）. The standard error was 3.40 μmol/mol of replicated measurement of NIST 610 (n = 123). Ba/Ca in THL8-2 ranged 1.81 to 2.91 μmol/mol and the average was 2.25 μmol/mol（n=468）. The standard error was 2.56 μmol/mol of replicated measurement of NIST 610 (n = 75).

ICP-AES

Trace element concentrations using ICP-AES were below.

Magnesium /Calcium（Mg/Ca）

Mg/Ca in THL8-1 ranged 0.37 to 1.20 mmol/mol and the average was 0.67 mmol/mol（n=130）. Mg/Ca in THL8-2 ranged 0.43 to 2.05 mmol/mol and the average was 0.69 mmol/mol（n=77）. The standard error of Mg/Ca measurements in ICP-AES were 0.0055 mmol/mol of replicated measurement of JCt-1 (n = 23).

Strontium/Calcium（Sr/Ca）

Sr/Ca in THL8-1 ranged 1.81 to 2.43 mmol/mol and the average was 2.02 mmol/mol（n=753）. Sr/Ca in THL8-2 ranged 1.84 to 2.55 mmol/mol and the average was 2.17 mmol/mol（n=77）. The standard error of Sr/Ca measurements in ICP-AES were 0.0067 mmol/mol of replicated measurement of JCt-1 (n = 75).

4. Discussions

4-1. Sample preservation and growth of Miocene giant clam *Tridacna gigas*

There were no significant calcite peaks in THL8-1 and THL8-2 (Fig.5-2). McGregor *et al*., 2002 showed Sr/Ca, $\delta_{18}O$, and $\delta_{13}C$ in hermatypic coral skeleton decreased due to diagenetic precipitated calcite or secondary aragonite. In this study, the range of $\delta^{13}C$ in THL8-1 and THL8-2 were similar to that of $\delta^{13}C$ in 6 ka *Tridacna gigas* reported in Watanabe *et al*., 2004. In addition, Sr/Ca and Mg/Ca in THL8-1 and THL8-2 were almost similar to the modern *Tridacna gigas* (Table 5-1). Thus, THL8-1 and THL8-2 were well preserved fossil specimen and showed the resistance of the *Tridaca gigas*

thick inner layer to diagenetic alternation.

In the thin sections of THL8-1 and THL8-2, there were growth bands which were characterized with translucent and transparence growth lines. Bonham, 1965 first found that growth bands observed in the giant clam shell section were annual growth bands. After that discovery, it is considered that black (translucent) growth band grows in winter season and lighter colored (transparence) growth band growth in summer season respectively (Aharon and Chappell, 1986, Aharon, 1991, Patzold, 1991, Watanabe *et al* 2004, e.g.). The shape of the growth curve was similar to the growth curve of same species in Holocene optimum reported in Watanabe *et al*., 2004, but the amount of growth was about 50% of Holocene one. Also, there were micro growth increments, which was considered daily growth increments of Tridacnidae (Aharon and Chappell, 1986, Watanabe and Oba, 1999 e.g.). In THL8-1, there were 25 pair of translucent and transparence growth band and there were about 160~365 micro growth increments. After 5th growth bands, the width of the growth band gradually decreased and about 200 micro growth increments were observed. In THL8-2, there were 7 pair of translucent and transparence growth band and there were about 365 micro growth increments in each growth band. The width of micro growth increments also decreased along the growth stage (Fig. 5-3). $\delta^{18}O$ and Sr/Ca cycles in THL8-1 and THL8-2 were corresponded with the growth bands, thus the growth band was supposed as annual growth bands. Although Miocene *Tridacna gigas* THL8-1 and THL8-2, the dark colored (translucent) growth bands were corresponded lower SST season. It was useful to reveal the growth pattern in fossil giant clam to use growth bands, stable oxygen ratio.

4-2. Seasonality delivered from trace element and stable isotope ratio

Growth increment thickness, trace elements, and stable isotope ratio in THL8-1and THL8-2 were arranged along the growth increments (Fig. 5-6). The positions of translucent growth banding observed in the shell thin sections were corresponded with maxima $\delta^{18}O$ and minima of Mg/Ca of the shell. These features agreed with prior Miocene giant clam studies, Batemburg *et al*., 2011 and Warter *et al*., 2015. In addition, there were significant correlation between $\delta^{18}O$ and $\delta^{13}C$ of THL8-1 and THL8-2 (Table 5-2). Although THL8-1 had no clear correlation between $\delta^{18}O$ and Mg/Ca, THL8-2 had significant correlation between $\delta^{18}O$ and Mg/Ca. It is not clear why $\delta^{18}O$ and the Mg/Ca records agree well in case of THL8-2, while this does not apply for the corresponding records of THL8-1. Warter et al., 2015 suggested Mg/Ca in the giant clam shell was controlled by the incorporation of environmental signals, species-specific effects, which partly control biomineralization. Elliot *et al*., 2009 showed Mg/Ca in modern *Tridacna gigas* shell increased along the giant clam maturity. THL8-1 was older than THL8-2 and it might be one of the causes that THL8-1 had no clear correlation between $\delta^{18}O$ and Mg/Ca.

Warter *et al*., 2015 presented the comparison of late Miocene *Tridacna gigas* $\delta^{18}O$ record and reconstructed SST. To compare this study's *Tridacna gigas* $\delta^{18}O$ record, the comparison was presented in Table 5-3. THL8-1 and THL8-1 had lower $\delta^{18}O$ values and reconstructed average SST was approximately 1 ~ 2 ℃ higher than other studies (Table 5-3). The amplitude of SST seasonality in THL8-1 and THL8-2 was slightly

smaller than other late Miocene *Tridacna gigas* records. Warter et al., 2015 suggested the high standard deviation of LGS1 might reflect high and low ENSO periods within the 15 years of growth of this specimen. Thus, ENSO variability in late Miocene might be a cause of differ SST seasonality amplitude in late Miocene *Tridacna gigas* because of short term giant clam SST records.

4-3. ENSO like Inter annual variability in 10Ma Late Miocene

Assuming that the maxima of oxygen isotope ratio is September, time axis was determined as the result of geochemical analysis. Thus, stable oxygen isotope ratio anomaly was calculated using the same way of Driscol *et al*, 2014 (Fig. 5-7). Arias-Ruiz *et al*., 2017 showed stable oxygen isotope ratio anomaly in the giant clam shell caught in Sulawesi island gained in La Niña Phase and decreased in El Nino Nino. When anomalies of the oxygen isotope ratio of the late Miocene giant clam shell value shifted to the negative, and the carbon isotope ratio in the giant clam increased (Fig. 5-8). Thus, it was suggested that the amplitude of annual SST decreased, and the precipitation increased same as in the current La Niña in Indonesia (Fig. 5-8). In addition, the lowest $\delta^{13}C$ was April in La Niña and Jun in El Niño conditions (Fig. 5-8). The observed inter annual variability of the fossil giant clam $\delta^{18}O$ record suggested that an ENSO-like inter annual variability existed 10 Ma late Miocene Java island and demonstrated that fossil giant clam shells could record past ENSO-like inter annual climate variability.

Reference

Aubert, A., C. Lazareth, G. Cabioch, H. Boucher, T. Yamada, Y. Iryu, and R. Farman (2009), The tropical giant clam *Hippopus hippopus* shell, a new archive of environmental conditions as revealed by sclerochronological and $\delta^{18}O$ profiles, *Coral Reefs*, *28*(4), 989–998, doi:10.1007/s00338-009-0538-0.

Aharon, P., and J. Chappell (1986), Oxygen isotopes, sea level changes and the temperature history of a coral reef environment in New Guinea over the last 105 years, *Palaeogeogr. Palaeoclimatol. Palaeoecol.*, *56*(3–4), 337–379, doi:10.1016/0031-0182(86)90101-X.

Arias-ruiz, C., M. Elliot, A. Bézos, K. Pedoja, L. Husson, S. Yudawati, E. Cariou, E. Michel, C. La, and F. Manssouri (2017), Geochemical fi ngerprints of climate variation and the extreme La Niña 2010 – 11 as recorded in a Tridacna squamosa shell from Sulawesi , Indonesia, *Palaeogeogr. Palaeoclimatol. Palaeoecol.*, (August), 0–1, doi:10.1016/j.palaeo.2017.08.037.

Batenburg, S. J., G. J. Reichart, T. Jilbert, M. Janse, F. P. Wesselingh, and W. Renema (2011), Interannual climate variability in the Miocene: High resolution trace element and stable isotope ratios in giant clams, *Palaeogeogr. Palaeoclimatol. Palaeoecol.*, *306*(1–2), 75–81, doi:10.1016/j.palaeo.2011.03.031

Kelshaw Bonham, Growth Rate of Giant Clam Tridacna gigas at Bikini Atoll as Revealed by Radioautography, Science, New Series, Vol. 149, No. 3681 (Jul. 16, 1965), pp. 300-302

Schwartzmann, C., G. Durrieu, M. Sow, P. Ciret, C. E. Lazareth, and J.-C. Massabuau (2011), In situ giant clam growth rate behavior in relation to temperature: A one-year coupled study of high-frequency noninvasive valvometry and sclerochronology, *Limnol. Oceanogr.*, *56*(5), 1940–1951, doi:10.4319/lo.2011.56.5.1940.

Romanek, C. S., and E. L. Grossman (1989), Stable isotope profiles of Tridacna maxima as environmental indicators, *Palaios*, 402–413.

Driscoll, R., M. Elliot, T. Russon, K. Welsh, Y. Yokoyama, and A. Tudhope (2014), ENSO reconstructions over the past 60 ka using giant clams (Tridacna sp.) from Papua New Guinea, *Geophys. Res. Lett.*, *41*(19), 6819–6825.

Elliot, M., K. Welsh, C. Chilcott, M. McCulloch, J. Chappell, and B. Ayling (2009), Profiles of trace elements and stable isotopes derived from giant long-lived Tridacna gigas bivalves: Potential applications in paleoclimate studies, *Palaeogeogr. Palaeoclimatol. Palaeoecol.*, *280*(1–2), 132–142, doi:10.1016/j.palaeo.2009.06.007.

McGregor, H. V., and M. K. Gagan (2003), Diagenesis and geochemistry of Porites corals from Papua New Guinea: Implications for paleoclimate reconstruction, *Geochim. Cosmochim. Acta*, *67*(12), 2147–2156, doi:10.1016/S0016-7037(02)01050-5.

McGregor, H. V., and N. J. Abram (2008), Images of diagenetic textures in Porites corals from Papua New Guinea and Indonesia, *Geochemistry, Geophys. Geosystems*, *9*(10), 1–17, doi:10.1029/2008GC002093.

Faylona, M. G. P. G., C. E. Lazareth, A.-M. Sémah, S. Caquineau, H. Boucher, and W. P. Ronquillo (2011), Preliminary study on the preservation of giant clam (Tridacnidae) shells from the Balobok Rockshelter archaeological site, south Philippines, *Geoarchaeology*, *26*(6), 888–901, doi:10.1002/gea.20377.

Welsh, K., M. Elliot, A. Tudhope, B. Ayling, and J. Chappell (2011), Giant bivalves (Tridacna gigas) as recorders of ENSO variability, *Earth Planet. Sci. Lett.*, *307*(3–4), 266–270, doi:10.1016/j.epsl.2011.05.032.

Duprey, N., C. E. Lazareth, C. Dupouy, J. Butscher, R. Farman, C. Maes, and G. Cabioch (2014), Calibration of seawater temperature and δ 18Oseawater signals in Tridacna maxima's δ 18Oshell record based on in situ data, *Coral Reefs*, *34*(2), 437–450, doi:10.1007/s00338-014-1245-z.

Sano, Y., S. Kobayashi, K. Shirai, N. Takahata, K. Matsumoto, T. Watanabe, K. Sowa, and K. Iwai (2012), Past daily light cycle recorded in the strontium/calcium ratios of giant clam shells, *Nat. Commun.*, *3*, 761, doi:10.1038/ncomms1763.

Schone, B. R., Z. Zhang, D. Jacob, D. P. Gillikin, T. Tutken, D. Garbe-Schonberg, T. McConnaughey, and A. Soldati (2010), Effect of organic matrices on the

determination of the trace element chemistry (Mg, Sr, Mg/Ca, Sr/Ca) of aragonitic bivalve shells (Arctica islandica)-Comparison of ICP-OES and LA-ICP-MS data, *Geochem. J.*, *44*(1), 23–37.

Schöne, B. R., Z. Zhang, P. Radermacher, J. Thébault, D. E. Jacob, E. V. Nunn, and A.-F. Maurer (2011), Sr/Ca and Mg/Ca ratios of ontogenetically old, long-lived bivalve shells (Arctica islandica) and their function as paleotemperature proxies, *Palaeogeogr. Palaeoclimatol. Palaeoecol.*, *302*(1–2), 52–64, doi:10.1016/j.palaeo.2010.03.016.

Watanabe, T., T. Oba, and V. Dee (1999), Daily reconstruction of water temperature from oxygen isotopic ratios of a modern Tridacna shell using a freezing microtome sampling technique was recorded monthly to seasonal sea surface to reconstruct using Jones maturity of Tridacna maxima resolution f, , *104*.

Watanabe, T., A. Suzuki, H. Kawahata, H. Kan, and S. Ogawa (2004), A 60-year isotopic record from a mid-Holocene fossil giant clam (Tridacna gigas) in the Ryukyu Islands: Physiological and paleoclimatic implications, *Palaeogeogr. Palaeoclimatol. Palaeoecol.*, *212*(3–4), 343–354, doi:10.1016/j.palaeo.2004.07.001.

Watanabe, T. *et al*. (2011), Permanent El Niño during the Pliocene warm period not supported by coral evidence., *Nature*, *471*(7337), 209–211, doi:10.1038/nature09777.

Warter, V., W. Mueller, F. P. Wesselingh, J. A. Todd, and W. Renema (2015), Late Miocene seasonal to subdecadal climate variability in the Indo-West Pacific (East Kalimantan, Indonesia) preserved in giant clams, *Palaios*, *30*(1), 66–82.

Warter, V., and W. Müller (2017), Daily growth and tidal rhythms in Miocene and modern giant clams revealed via ultra-high resolution LA-ICPMS analysis — A novel methodological approach towards improved sclerochemistry, *Palaeogeogr. Palaeoclimatol. Palaeoecol.*, *465*, 362–375, doi:10.1016/j.palaeo.2016.03.019.

Yan, H., D. Shao, Y. Wang, and L. Sun (2013), Sr/Ca profile of long-lived Tridacna gigas bivalves from South China Sea: A new high-resolution SST proxy, *Geochim. Cosmochim. Acta*, *112*, 52–65, doi:10.1016/j.gca.2013.03.007.

Yan, H., D. Shao, Y. Wang, and L. Sun (2014), Sr/Ca differences within and among three Tridacnidae species from the South China Sea: Implication for paleoclimate reconstruction, *Chem. Geol.*, *390*, 22–31, doi:10.1016/j.chemgeo.2014.10.011.

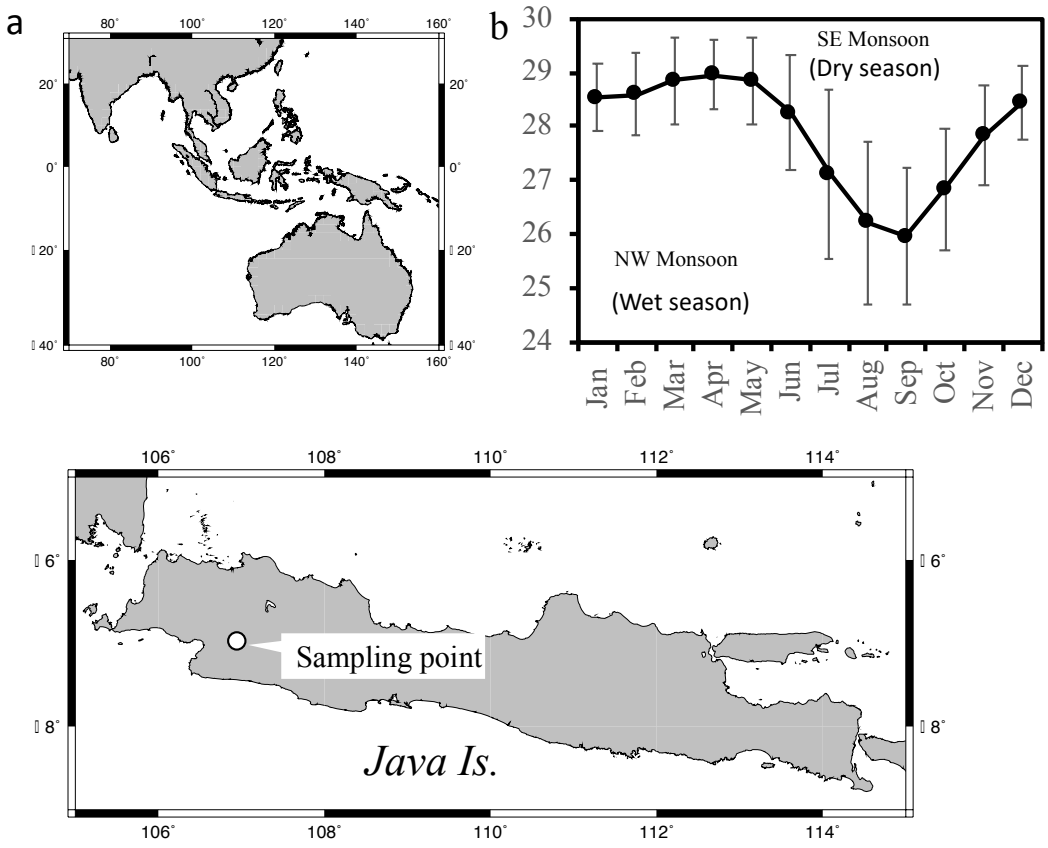

Figure 5-2 (a) Map of Indnesia with sampling location.

(b) SST in Sep-81 - May16 averaged SST in 106.875E 7.875S.

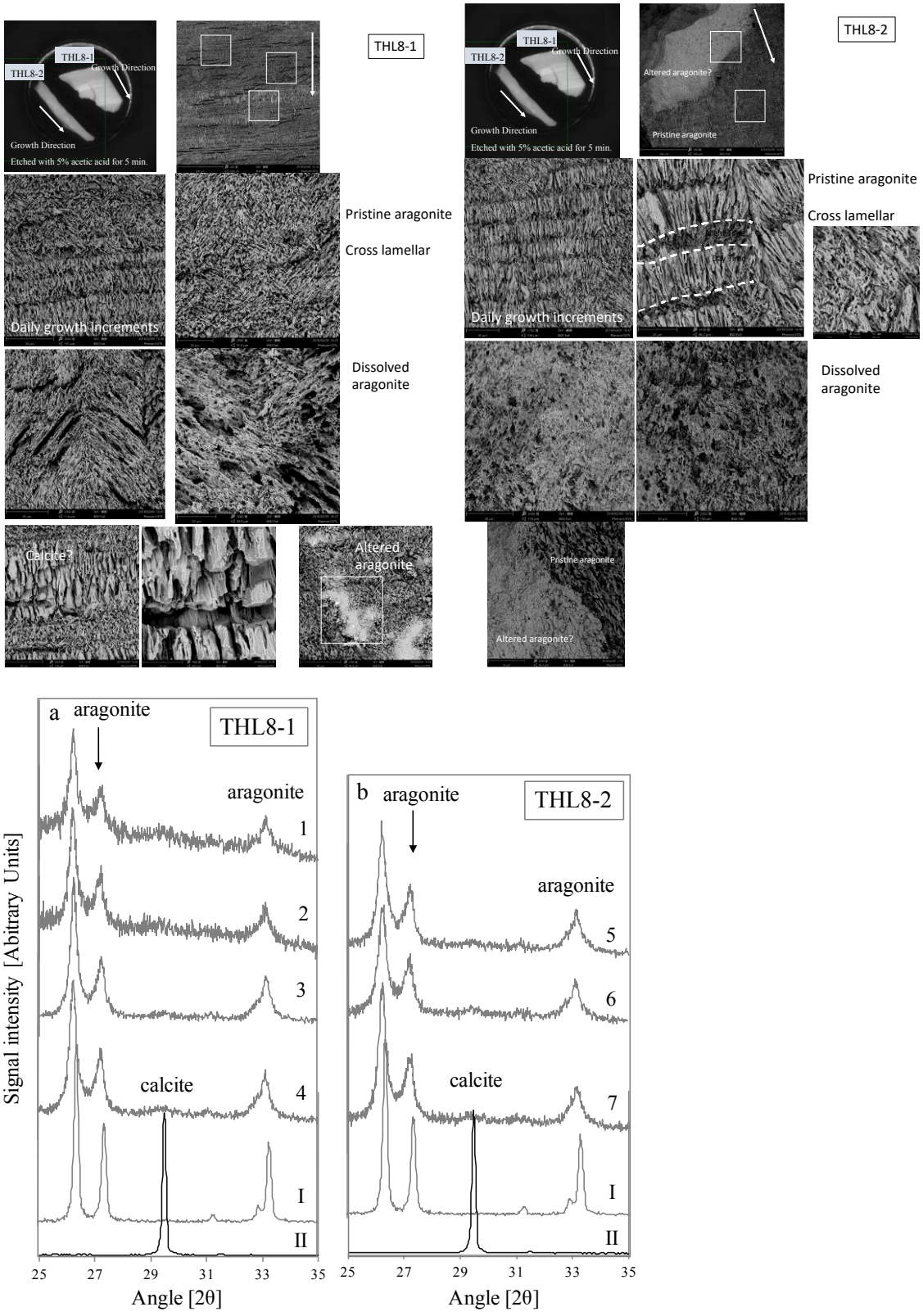

Figure 5-3. SEM observation and X-ray diffraction in Miocene giant clam samples.

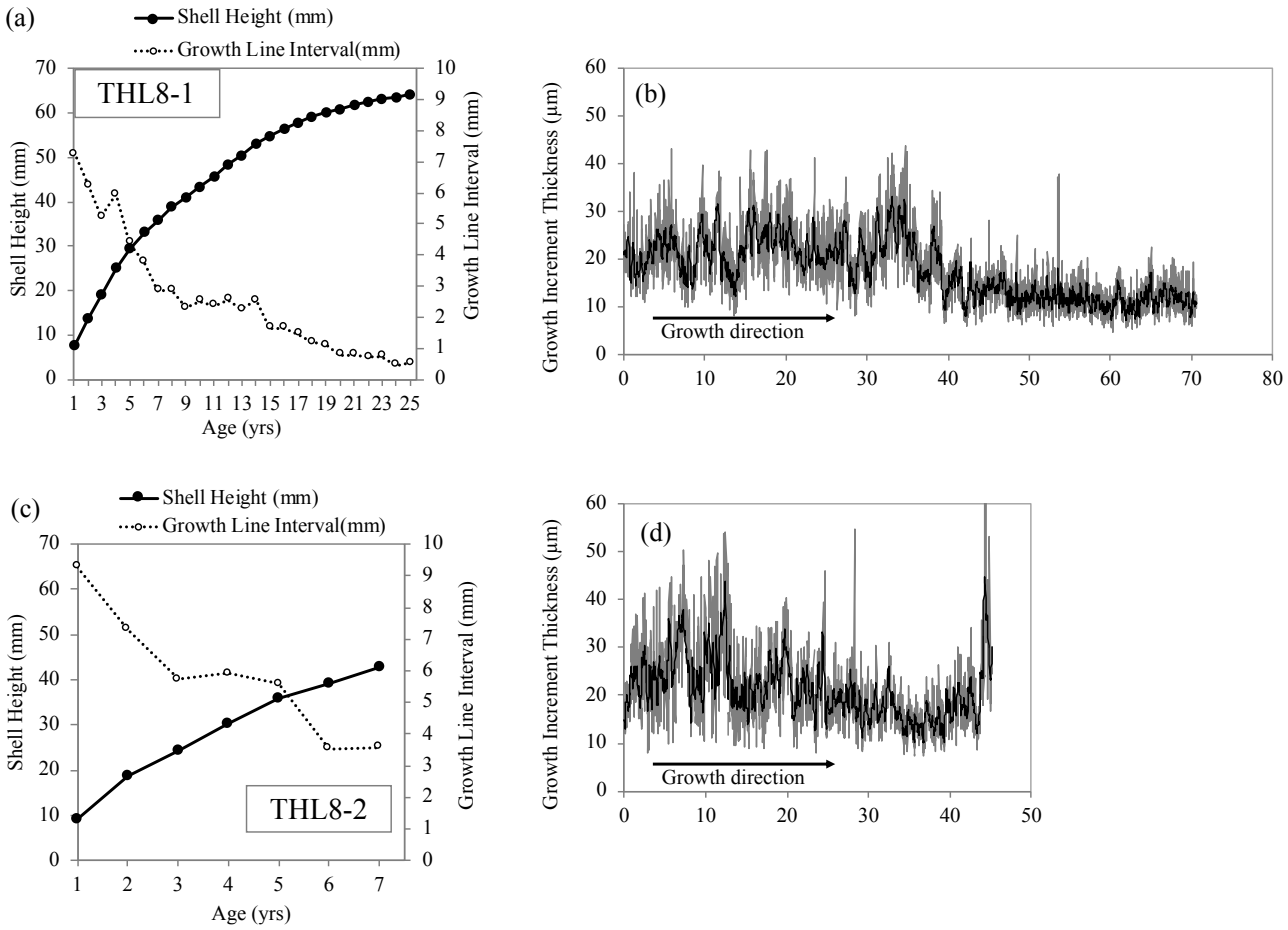

Figure 5-4.

(a), and (c) Growth curve for Miocene *Tridacna gigas* THL8-1 and THL8-2 respectively; closed circles represent the shell height and open circles the growth-line interval. (c), and (d) growth increment thickness of THL8-1 and THL8-2 respectively.

Vertical grey lines showed the position of translucent growth lines observed in the shell specimen thin sections.

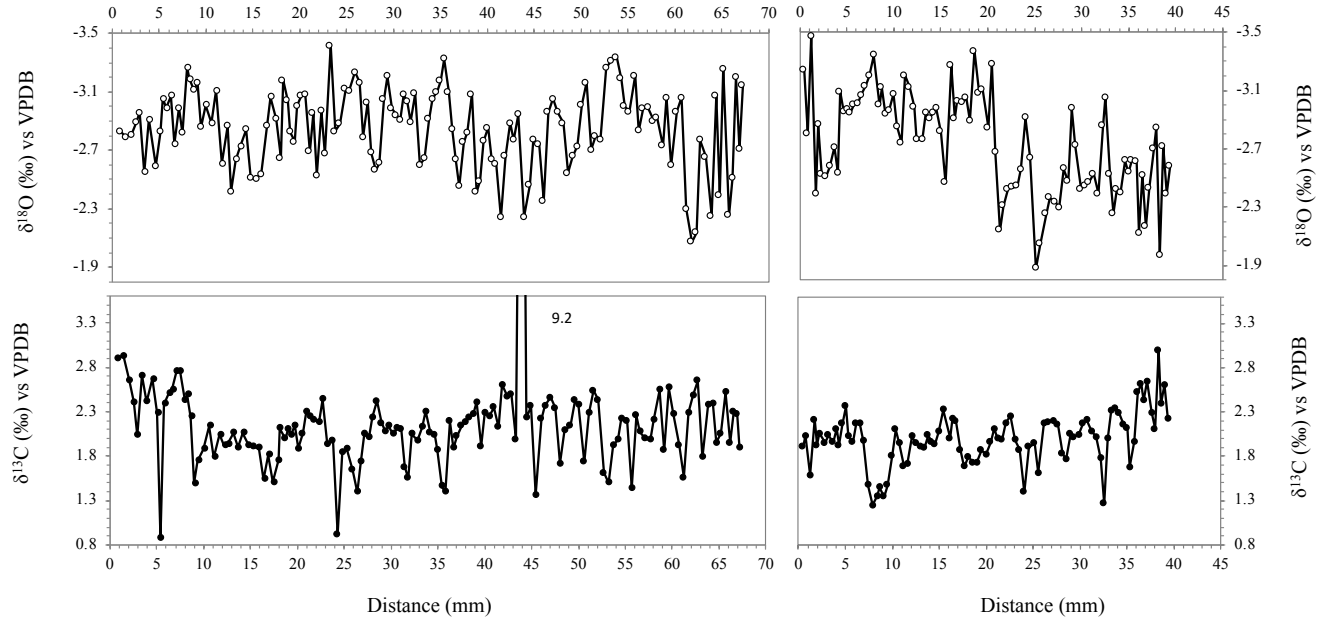

Figure 5-5. Stable isotope ratio from two *Tridacna gigas* shell THL8-1(left) and THL8-2 (right). Horizontal line is sampling point distance from the shell oldest part.

Vertical grey lines show the position of annual growth bands

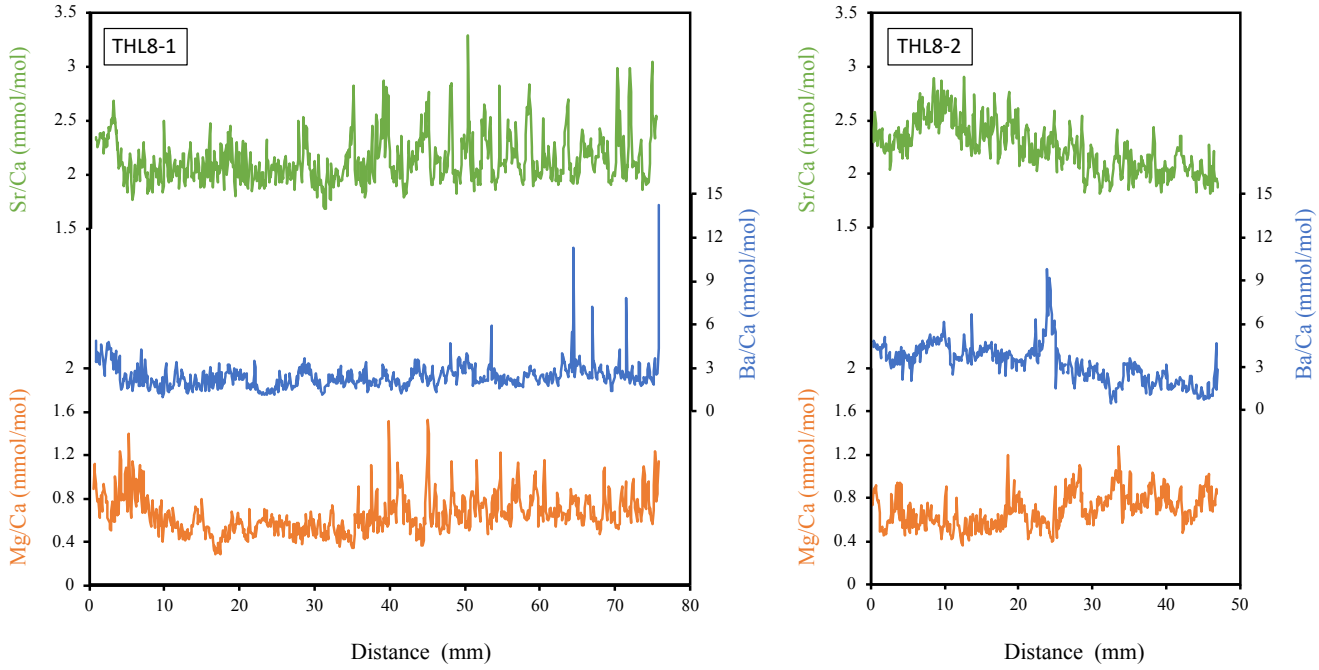

Figure 5-5. Trace element profile of two Miocene *Tridacna gigas* shell THL8-1 and THL8-2.

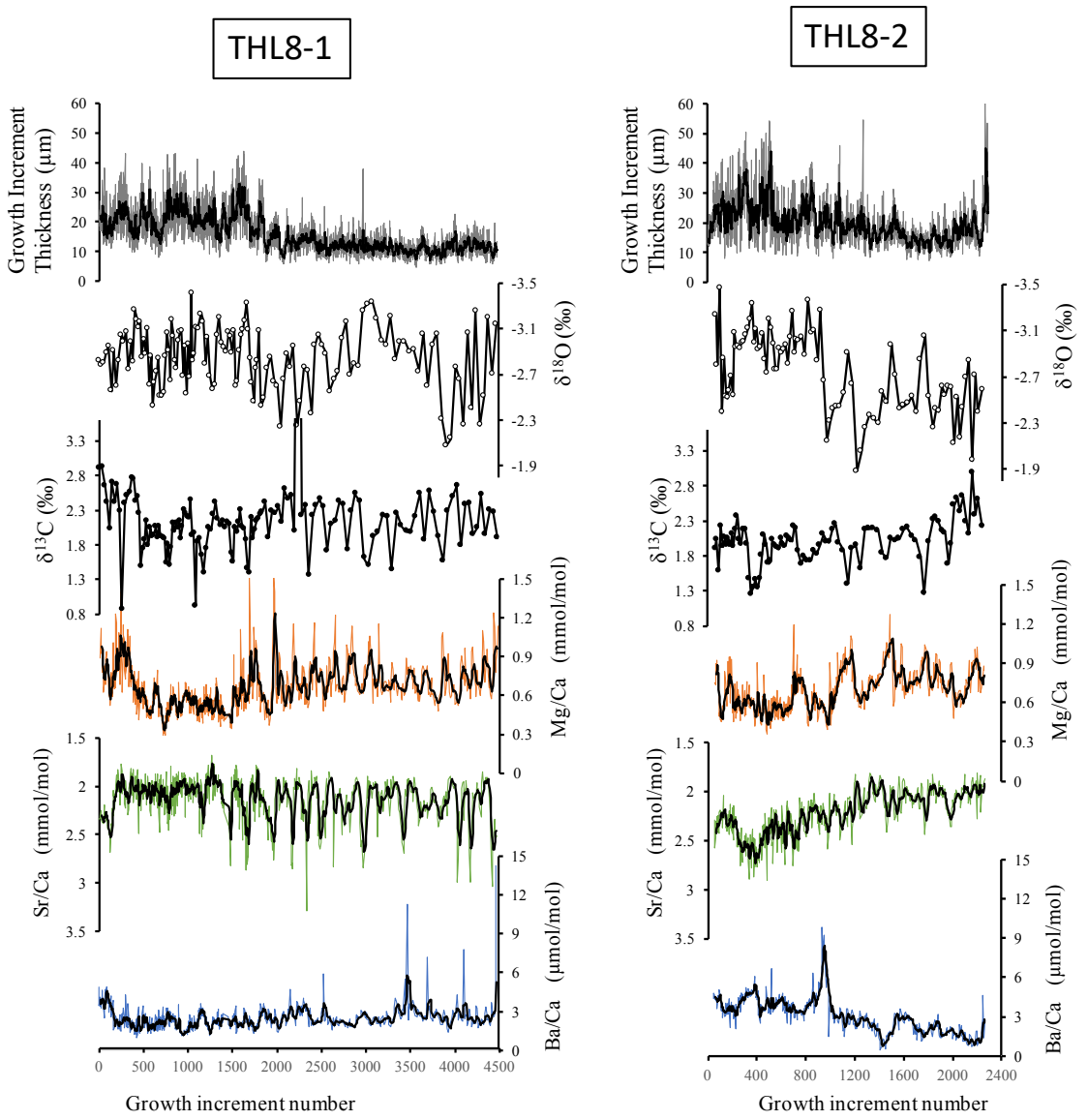

Figure 5-7. Geochemical and microstructural signals in Miocene giant clam fossils. Vertical grey lines showed the position of translucent growth lines observed in the shell specimen thin sections. Back lines showed in growth increment thickness, Mg/Ca, Sr/Ca, and Ba/Ca were 10 points moving average.

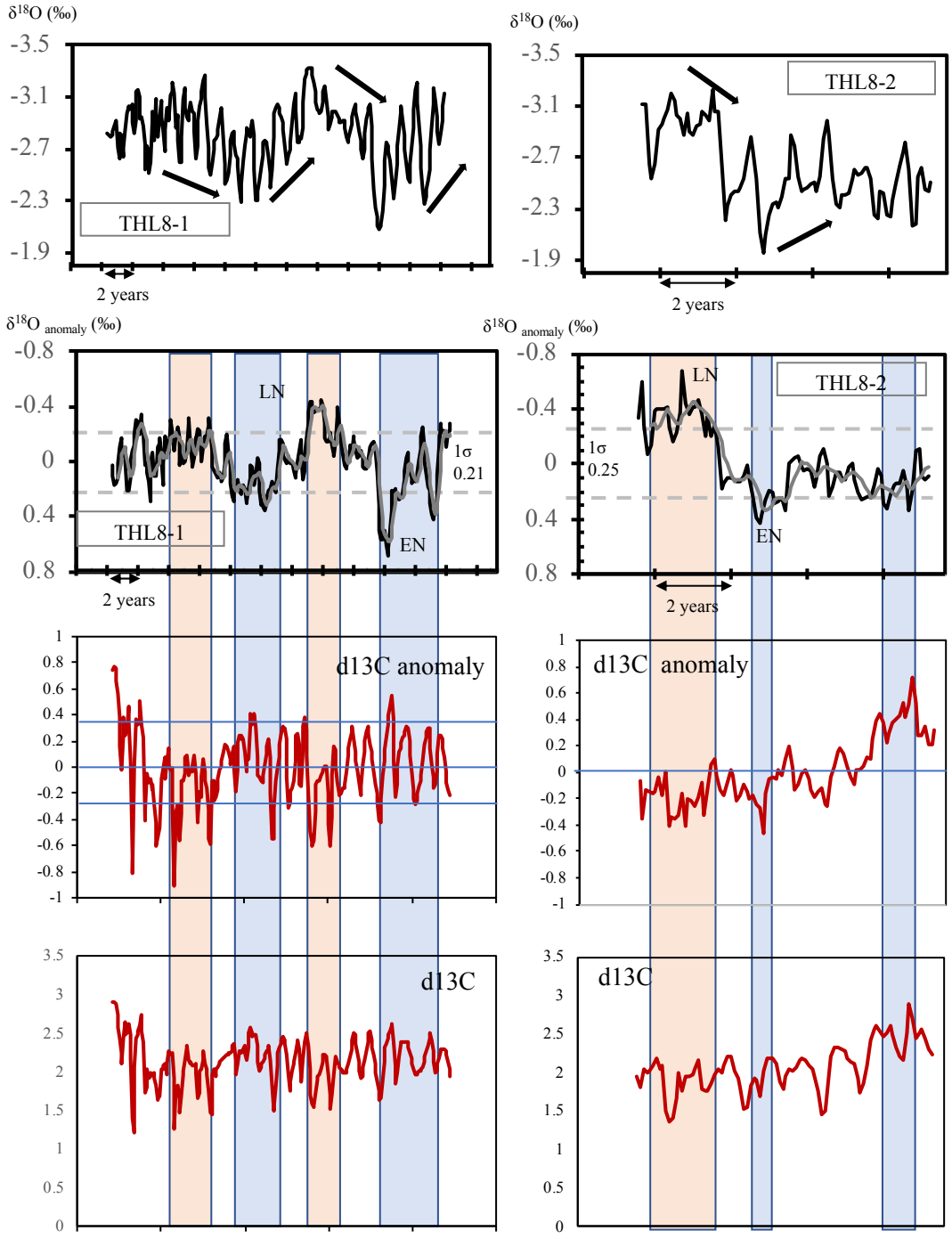

Figure 5-8. Stable oxygen and carbon isotope ratio anomalies in Miocene giant clam fossils. The method for ENSO detection based on Driscoll *et al.*, 2014.

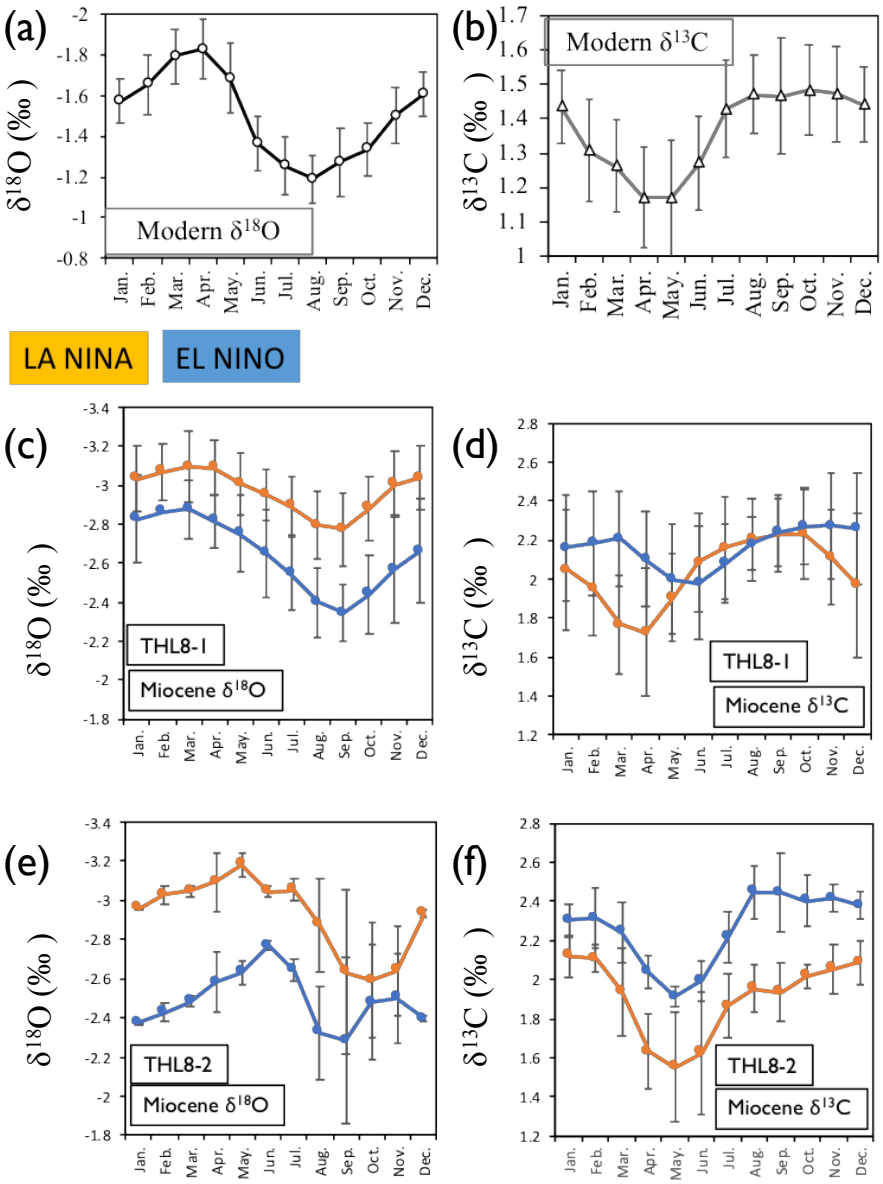

Figure 5-9. The comparison of stable oxygen and carbon isotope ratio seasonality in modern (a, b; *T. Squamosa* from Sulawesi island, Arias-Ruiz *et al*., 2017) and Miocene

(c, d ,e ,f) giant clam fossils. Orange and Blue colored profiles showed the seasonality of La Nina and El Nino phase respectively.

	LA-ICP-MS		ICP-AES	
	Sr/Ca (mmol/mol)	Mg/Ca (mmo/mol)	Sr/Ca (mmol/mol)	Mg/Ca (mmo/mol)
Elliot et al., 2009 Modern *T. gigas*	1.4 – 1.8	0.8 – 1.2 (Early growth) 2.4 – 5.4 (After maturity)	-	1.4 – 4.4
Yan et al., 2013 Modern *T. gigas*	1.23 – 2.04 Ave. 1.69 ±0.14	-	2.04 – 2.40 Ave. 2.24±0.10	-
Batenburg., et al., 2011 Late Miocene *T. gigas*	1000 - 2500	25 - 75	-	-
Warter et al., 2015 Late Miocene *T. gigas*	1.7 – 2.9	0.4 – 1.4 0.4 – 1.0	-	-
This study Late Miocene *T. gigas*	1.68 - 3.28, 1.89 - 2.91 Ave. 2.13, 2.25	0.29 - 1.53, 0.36 - 1.28 Ave. 0.66, 0.69	1.81 - 2.43 1.84 - 2.55 Ave. 2.02, 2.17	0.37-1.20 0.43-2.05 Ave. 0.67, 0.69

Table 5-1. The comparison between Sr/Ca and Mg/Ca in modern and fossil *Tridacna gigas* shell.

THL8-1 n=142

	$\delta^{18}O$	$\delta^{13}C$	Mg	Sr	Ba
$\delta^{18}O$		0.256086178	0.100989145	0.043070941	-0.080754735
$\delta^{13}C$	0.256086178	1	0.149472178	0.102530857	0.278502661
Mg	0.100989145	0.149472178	1	0.163441532	0.051037559
Sr	0.043070941	0.102530857	0.163441532	1	0.532675681
Ba	-0.080754735	0.278502661	0.051037559	0.532675681	1

THL8-2 n=93

	$\delta^{18}O$	$\delta^{13}C$	Mg	Sr	Ba
$\delta^{18}O$		0.538973182	0.432408573	-0.458387448	-0.583069344
$\delta^{13}C$	0.538973182	1	0.159786645	-0.271655189	-0.276745584
Mg	0.432408573	0.159786645	1	-0.450845068	-0.618538726
Sr	-0.458387448	-0.271655189	-0.450845068	1	0.67756206
Ba	-0.583069344	-0.276745584	-0.618538726	0.67756206	1

Significant correlation $p < 0.01$ $p < 0.05$ $p < 0.10$

No correlation

Table 5-2. The correlation of each geochemical signals in Miocene giant clam fossils.

Trace element was obtained using LA-ICP-MS.

	$\delta^{18}O_{shell}$ min (‰)	$\delta^{18}O_{shell}$ max (‰)	average $\delta^{18}O_{shell}$ (‰)
THL8-1	-3.42	-2.08	-2.85
THL8-2	-3.47	-1.88	-2.73
Water *et al*., LGS1	-2.90	-1.46	-2.15
Water *et al*., BW4B	-3.00	-1.59	-2.31
Batenburg *et al.*	-2.97	-1.72	-2.30
	T (°C) max	T (°C) min	T (°C) average
THL8-1	33.70	27.41	31.04
THL8-2	33.95	26.50	30.49
Water *et al*., LGS1	31.28	25.54	27.78
Water *et al*., BW4B	31.75	25.13	28.52
Batenburg *et al.*	31.60	25.74	28.50
	average $\delta^{18}O_{shell}$ min (‰)	average $\delta^{18}O_{shell}$ max (‰)	
THL8-1	-2.96	-2.59	
THL8-2	-2.87	-2.38	
Water *et al*., LGS1	-2.66	-1.69	
Water *et al*., BW4B	-2.62	-2.05	
Batenburg *et al.*	-2.53	-2.09	
	average T (°C) max	average T (°C) min	average seasonality T (°C)
THL8-1	31.58	29.81	1.77
THL8-2	31.15	28.82	2.34
Water *et al*., LGS1	30.17	25.60	4.57
Water *et al*., BW4B	29.96	27.27	2.69
Batenburg *et al.*	29.54	27.47	2.07

Table 5-3. $\delta^{18}O_{shell}$ maxima, minima, and averaged values and respective calculated paleotemperature data of THL8-1 and THL8-2. For comparison, published data of Miocene Tridacna gigas (Batenburg *et al*. 2011; Warter *et al*., 2015) and corresponding paleotemperature and paleoseasonality estimates are presented. Paleotemperature/paleoseasonality was assessed using the aragonitic oxygen isotope temperature equation by Grossman and Ku (1986) and assuming δ18Osw = 0.88%.

Chapter 6: Summaries and Future perspective of giant clam paleo recorder

It is useful and important tool for reconstructing tropical-subtropics paleoenvironment to use giant clam shell and harmatypic coral skeleton. The paleoenvironmental information obtained from the coral skeleton lasts for several hundred years, but the giant clam has a short life span of several decades to one hundred years. However, the shell composed of precise aragonite is resistant to the sequential action [Watanabe *et al*., 2004]. The microstructure of the shell such as annual growth bands and daily growth increment is preserved well even if it had been altered diagenetic effects.

Microstructure in the shell is an advantage to the another paleoenvironment proxies. Dairy growth increment and trace element in the giant clam shell have several hours to 1day, very high temporal resolution information [Watanabe and Oba, 1999, Sano *et al*., 2012, Hori *et al*., 2015, Warter *et al*., 2017]. Thus, the giant clam shell is also frequently found in the tropical zone ruins [Faylona *et al*., 2011], we can clarify the meteorological phenomena experienced by the past human beings on the same time scale as human life.

Giant clam has not only interesting ecology such as having zooxanthella, but they are an important signpost to forecast future Earth environment to reconstructing paleo environments. The researches using the giant clam shell will become more sophisticated to handle high temporal resolution geochemical and microstructure analysis. Also,

calibration researches to reveal the correspondence among giant clam shell geochemical signals, its surrounding environment, and its ecological responses will be subjected.

Reference

Sano, Y., S. Kobayashi, K. Shirai, N. Takahata, K. Matsumoto, T. Watanabe, K. Sowa, and K. Iwai (2012), Past daily light cycle recorded in the strontium/calcium ratios of giant clam shells, *Nat. Commun.*, *3*, 761, doi:10.1038/ncomms1763.

Hori, M., Y. Sano, A. Ishida, N. Takahata, K. Shirai, and T. Watanabe (2015), Middle Holocene daily light cycle reconstructed from the strontium/calcium ratios of a fossil giant clam shell, *Sci. Rep.*, *5*(8734), 5, doi:10.1038/srep08734.

Warter, V., and W. Müller (2017), Daily growth and tidal rhythms in Miocene and modern giant clams revealed via ultra-high resolution LA-ICPMS analysis — A novel methodological approach towards improved sclerochemistry, *Palaeogeogr. Palaeoclimatol. Palaeoecol.*, *465*, 362–375, doi:10.1016/j.palaeo.2016.03.019.

Watanabe, T., and T. Oba (1999), Daily reconstruction of water temperature from oxygen isotopic ratios of a modern Tridacna shell using a freezing microtome sampling technique, *JGR-Oceans*, *104*(C9), 20,667, doi:10.1029/1999jc900097.

Watanabe, T., A. Suzuki, H. Kawahata, H. Kan, and S. Ogawa (2004), A 60-year isotopic record from a mid-Holocene fossil giant clam (Tridacna gigas) in the Ryukyu Islands: Physiological and paleoclimatic implications, *Palaeogeogr. Palaeoclimatol. Palaeoecol.*, *212*(3–4), 343–354, doi:10.1016/j.palaeo.2004.07.001.

Acknowledgements

In the research, I was able to collect fossil giant clam shell sample on corporation of many people in Kikai-town. In addition, I received the ideas from Dr. Sowa for improving the powder sampling methods.

Mr. Hideo Nomura and Mr. Akira Nakamura of Hokkaido University Graduate School of Engineering Department of Thin section Engineering gave cooperation in the creation of shell thin sections. Dr. Kentaro Tanaka of the University of Tokyo Atmosphere and Ocean Research Institute and member of Dr. Shirai laboratory helped LA-ICP-MS measurement and analysis. I would like to express my gratitude to the people involved in this research and CREES members.

And Professor Suzuki and Professor Sawada of the Earth Evolution Group got a lot of guidance at the seminar. In the MAT 253 analysis of the oxygen-carbon stable isotopic ratio, the measurement was successfully carried out while being watched by assistant professor Tomohisa Irino of the Global Environmental Science Institute, Hokkaido University. In case of trouble, we got guidance accurately and promptly.